UNIVERSITY OF SOUTHAMPTON

Faculty of Engineering and Physical Sciences
Department of Physics & Astronomy / Electronics & Computer Science

Exploring and Decoding Theories of New Physics at Colliders and Beyond

by

Daniel Locke
MPhys

A thesis for the degree of
Doctor of Philosophy

October 2021

University of Southampton

Abstract

Faculty of Engineering and Physical Sciences
Department of Physics & Astronomy / Electronics & Computer Science

Doctor of Philosophy

Exploring and Decoding Theories of New Physics at Colliders and Beyond

by Daniel Locke

A qualitatively new approach is taken in building Minimal Consistent Dark Matter (MCDM) models, which facilitate the interpretation of complementary experimental results for Dark Matter (DM). These models offer broader applicability than EFTs and greater consistency with the symmetries of the SM than Simplified Models. Although many of these models have been studied in the literature, we offer a complete systematic classification of possible MCDM models before discussing the phenomenology of such models. We perform extensive numerical studies of the phenomenology of a simple but novel representative MCDM model at NLO, which gives rise to two-component DM.

We present a model independent method to measure the mass of a DM particle (D) if it appears alongside a charged partner ($D^{\pm}$) at e^+e^- colliders. This takes advantage of kinematic features of the energy distribution of charged leptons emitted from a $W^{\pm}$ lepton emitted in cascade decays $D^{\pm} \to W^{\pm}D$. We apply this to consistent models of both Dirac fermion and scalar thermal DM, at benchmark points which produce the observed DM density and evade direct detection experimental bounds. Realistic simulations are performed to detector level, and an optimised analysis cut-flow is proposed. Mass resolution for D,$D^{\pm}$ in this analysis was found to be better than 20% for the benchmarks considered. Furthermore, we explore a method to distinguish the spin of the DM particle using the angular distribution of $W^{\pm}$ reconstructed from di-jets.

Precision electroweak data, a light higgs and LHC searches for new spin one particles are all very constraining on technicolor models. We use a holographic model of walking techicolor (WTC) gauge dynamics, tuned to produce a light higgs and low S parameter, to estimate the range of possible vector(ρ) and pseudo-vector(A) resonance masses and couplings as a function of the number of colours and the number of flavours of techni-singlet and techni-doublet quarks. The resulting models predict techni-hadron masses and couplings above the current limits from dilepton resonance searches at the LHC because their masses are enhanced by the strong coupling extending into the multi-TeV range, while couplings to Standard Model fermions are partly suppressed. The

models emphasize the contortions needed to continue to realize technicolor, the need to explore new signatures beyond dilepton for LHC and also motivate a 100 TeV proton collider.

Contents

List of Figures

List of Tables

Declaration of Authorship

I declare that this thesis and the work presented in it is my own and has been generated by me as the result of my own original research.

I confirm that:

1. This work was done wholly or mainly while in candidature for a research degree at this University;
2. Where any part of this thesis has previously been submitted for a degree or any other qualification at this University or any other institution, this has been clearly stated;
3. Where I have consulted the published work of others, this is always clearly attributed;
4. Where I have quoted from the work of others, the source is always given. With the exception of such quotations, this thesis is entirely my own work;
5. I have acknowledged all main sources of help;
6. Where the thesis is based on work done by myself jointly with others, I have made clear exactly what was done by others and what I have contributed myself;
7. Work contained in this thesis has been published in [7], with work included from [8], [9] to be published.

Signed:..... Date:.....

UNIVERSITY OF Southampton

Copyright Declaration

Acknowledgements

Thanks to my supervisor, Sasha Belyaev, for fielding my application and being receptive to my ideas and ambitions. Thank you for pushing me to study a wide range of models and methods, and mostly for teaching me to recognise when I am fooling myself that I truly understand something. I would also like to thank the many collaborators A.Pukhov, G.Cacciapaglia, I.Ginzburg, A.Freegard, A.Coupe, N.Evans, who have inspired me along the way in my research, and provided amiability in addition to expertise.

I would not have had such an enriching experience in Southampton without the loving support of my partner Kate. Her sacrifices are greatly appreciated, and hopefully rewarded with a doorstop made from this thesis.

I must also thank my family and friends, who have given me ample distraction from physics, as and when needed.

Chapter 1

Introduction

The Standard Model (SM) of particle physics has proved to be robust to precise observations at energy scales probeable in laboratories. However when confronted with the distribution and behaviour of matter in the cosmos, and especially in the early universe at energy scales unachievable at colliders, the SM proves lacking. Increased efforts to systematically explore the electroweak scale at colliders may still provide answers to some of these important questions.

Two of the biggest mysteries, which this thesis attempts to tackle, are connected by the weak interaction. One of which, Dark Matter (DM), has been posited to explain the motion of galaxies and large scale structures in the universe, under the sensible assumption that Newtonian gravity is an effective description at those scales. The introduction of Weakly Interacting Massive Particles (WIMPs) are viable candidates for DM. The other mystery addressed in this work, the hierarchy problem, states that quantum corrections to the mass of fundamental scalars are highly sensitive to the scale of new physics. Technicolor addresses this by removing fundamental scalars from the theory and providing an alternative mechanism to break the electroweak symmetry.

The strategy to understand DM includes both the discovery and subsequent identification of the DM properties and its interactions in order to narrow the field of candidate models. Although the former would be a huge achievement, to understand the candidates character is a highly non-trivial task. In this thesis, strategies to survey and characterise models of new physics are presented.

Other pivotal shortcomings of the SM not explored here include neutrino oscillations and a mechanism to generate masses, flavour physics anomalies, matter/antimatter asymmetry, strong CP, muon g-2 and quantum gravity. In order to answer these questions, we must go Beyond the Standard Model (BSM). In this work, I will study BSM models which address DM, the hierarchy problem and EWSB, in addition to the techniques, tools and problems employed in experimental searches for such models.

The task to decode new physics may be tackled in a "top-down" approach, whereby fast simulations of complete models and comparison with experiments would allow construction of composite likelihoods over their respective parameter spaces. This would allow a Bayesian interpretation of which models offer the greatest possibility to describe new data as it becomes available. Although a full realisation of this approach is currently beyond the computing and man power available, steps towards this goal are being taken by the community. This includes development and public release of codes to implement [10, 11, 12] and simulate the phenomenology [13, 14, 15, 16, 17] for generic models of particle physics, and the ability to store and catalogue these models [18]. Codes to make use of such packages to enable rigorous statistical interpretation [19, 20, 21] rely on experiments providing re-interpretable results [22], which may be published on [23, 24]. The alternative is the "bottom up" approach by which details about new physics are gleaned from the data with minimal assumptions about the complete theory. Although there have shown to be problems associated with interpreting new physics [25, 26, 27, 28] in simplified model frameworks [29], the observation of a signal could permit the characterisation of mass,spin, cross-section or branching ratios associated with new particles by analysis of distributions in kinematic observables (see [30, 31, 32, 33, 34], Chapter 3).

1.1 The Standard Model of Particle Physics

The SM describes strong, electromagnetic and weak interactions using a renormalisable quantum field theory based on local (or gauge) symmetries. There are eight strong charges of QCD ("colour" charges) and four electroweak charges. The gauge structure may be expressed as $SU(3)_C \otimes SU(2)_L \otimes SU(1)_Y$, where C,L,Y are the respective gauge charges of colour, isospin and hypercharge.

The fermionic matter fields interactions are mediated by the exchange of gauge bosons (or the Higgs boson). These interactions depend on the gauge numbers of the matter fields. These are expressed in table 1.1, where matter fields are described by Weyl fermions (or scalar for Higgs), with left(right) chirality expressed by subscript L(R). In this table Q describes the doublet containing up (u) and down (d) type quarks, and L is the doublet containing charged lepton e and neutrinos. The index i runs over three flavours. When the electroweak symmetry is intact, the gauge bosons are vector bosons appearing in the adjoint representation of their respective gauge group.

Field	Representation/Charge			Spin
	$SU(3)_C$	$SU(2)_L$	$U(1)_Y$	
$Q_{L,i}$	3	2	1/6	1/2
$u_{R,i}$	3	1	2/3	1/2
$d_{R,i}$	3	1	-1/3	1/2
$L_{L,i}$	1	2	-1/2	1/2
$e_{R,i}$	1	1	-1	1/2
Φ	1	2	1/2	0

TABLE 1.1: Table of matter fields and their charges in the SM.

1.1.1 EWSB

The 2013 discovery of the Higgs boson [35, 36], cemented the understanding of the key mechanism in the SM by which the breaking of electroweak symmetry gives mass to fundamental particles such as charged leptons, quarks, gauge bosons and the Higgs itsef. Here, a brief overview of this mechanism is given.

The Higgs field is a weak isospin doublet constituting four components. The electroweak symmetry is spontaneously broken, when the Higgs acquires a vacuum expectation value (VEV). This is shown below, where the right hand side is given in unitary gauge, where the missing degrees of freedom are "eaten" by the W and Z bosons, in order to give these massive gauge bosons the required longitudinal components.

$$\Phi = \frac{1}{\sqrt{2}} \begin{pmatrix} \phi_1 + i\phi_2 \\ \phi_3 + i\phi_4 \end{pmatrix} \rightarrow \frac{1}{\sqrt{2}} \begin{pmatrix} 0 \\ v + h \end{pmatrix} \tag{1.1}$$

$$SU(2)_L \otimes U(1)_Y \rightarrow U(1)_{EM} \tag{1.2}$$

Fermion masses are then generated through Yukawa terms, which are gauge invariant before EWSB occurs, for example quark masses

$$\mathcal{L} \supset -Y_d \bar{Q}_L \Phi d_R - Y_u \bar{Q}_L \widetilde{\Phi} u_R + h.c. \tag{1.3}$$

This leads to mass terms $-m_u \bar{d}_L d_R + h.c$ when $Y_d = \frac{m_d \sqrt{2}}{v}$, and similarly for the down quarks [1].

Masses for the W and Z bosons are generated through the Higgs kinetic term, as shown in equation 1.4.

[1] Here, $\widetilde{\Phi} \equiv i\tau_2 \Phi^*$, with τ_2 being the second Pauli matrix

$$
\begin{aligned}
(D^{\mu}\Phi)^{\dagger}(D_{\mu}\Phi) &= \frac{v^2}{8}\left[g_2^2(W_1^2+W_2^2)+(g_1 Y B_{\mu}-g_2 W_3)^2\right] \\
&= \frac{v^2}{8}\left[2g_2^2 W^+W^- + (g_1^2+g_2^2)Z_{\mu}^2 + 0A_{\mu}^2\right]
\end{aligned} \tag{1.4}
$$

Where, the second line is expressed in terms of the mass basis gauge bosons as defined by equation 1.5.

$$
\begin{aligned}
W^{\pm} &= \frac{(W_1 \mp W_2)}{\sqrt{2}} \\
A_{\mu} &= \frac{(g_1 W_3 + g_2 B^{\mu})}{\sqrt{g_1^2+g_2^2}} \\
Z_{\mu} &= \frac{(g_1 W_3 - g_2 B^{\mu})}{\sqrt{g_1^2+g_2^2}}
\end{aligned} \tag{1.5}
$$

1.1.2 The hierarchy problem and naturalness

If the SM, a theory defined at the electroweak scale ($\mathcal{O}(100GeV)$) is assumed to be a valid effective field theory up to the Planck scale ($\mathcal{O}(10^{18}GeV)$, then why are these two scales so different? The introduction of new physics at intermediate scales may be required to solve some of the puzzles and anomalies in particle physics.

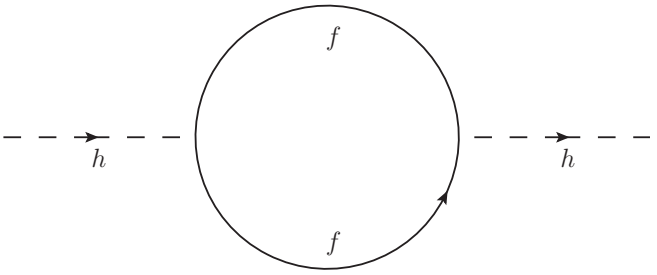

FIGURE 1.1: NLO fermion correction to Higgs mass

However, the introduction of an intermediate scale of new physics incites naturalness issues [37] generated by the presence of a fundamental scalar particle in a theory, such as the Higgs boson. The one-loop fermionic corrections to the Higgs propagator (see figure 1.1) are sketched in equation 1.6, assuming zero external momentum.

$$i\Pi_{hh}(0) \sim -g_f^2 \int^{\Lambda} d^4k Tr\left[\frac{1}{(k-m_f)^2}\right]$$
$$\sim -g_f^2 \Lambda^2 \tag{1.6}$$

This quadratic dependence on the scale of new physics Λ, presents the fine-tuning problem.

Two of the most interesting and studied solutions to this problem are Supersymmetry and Technicolor. In Supersymmetry, a superpartner is introduced for every particle (scalar superpartner of fermion and vice versa). These superpartners generate an equal and opposite contribution to the Higgs mass correction, leaving a freedom in introducing new particles at higher scales. The non-observation of these superpartners at low scales in experiments leads to the renormalised Higgs mass in SUSY not being completely natural as exact cancellations are not possible - this is the so-called "little hierarchy" problem. In technicolor, the Higgs boson is no longer a fundamental scalar which causes spontaneous EWSB. Instead, the Higgs is a bound state of new technifermion particles coupled by an additional strong gauge group, in anology with the pion of QCD. EWSB is generated dynamically by the formation of a technifermion condensate (see section 1.4 for details).

1.2 The Standard Model of Cosmology

Prior to describing the behaviour of DM in the universe, a review of the history of the matter content in the universe is essential.

The ΛCDM model, often called the SM of cosmology, is a parameterisation of the big bang model in which the universe comprises of three components; a cosmological constant (Λ), cold dark matter (CDM) and ordinary matter.

The Hubble constant, $H = \dot{r}/r$, describes the expansion of the universe; objects move apart with velocity proportional to their spatial separation. The cosmological constant, Λ which describes the dark energy density (the majority of the energy content in the universe) may be defined through the Einstein-Hilbert action. It is convenient to define dimensionless quantity $\Omega_\Lambda = \Lambda/(3H_0^2)$, which describes the fraction of energy in the universe due to the cosmological constant.

The matter densities of the universe evolve with time, this may be separated non-relativistic matter density ρ_m and relativistic matter (or radiation) density ρ_r. The critical density, ρ_c, is the threshold energy density which bisects the cases of an expanding or collapsing universe. It is again useful to define dimensionless quantities $\Omega_m = \rho_m/\rho_c$ and $\Omega_r = \rho_r/\rho_c$. An additional delineation is also possible, by separating baryonic and non-baryonic (or DM) matter; $\Omega_= \Omega_m - \Omega_b$.

To describe the history of the universe, and ultimately DM in the ΛCDM paradigm, the line element in curved spacetime may be described using the Friedmann–Lemaître -Robertson–Walker (FLRW) metric, given by equation 1.7. The FLRW metric is an exact solution of general relativity which describes a homogeneous, isotropic and expanding universe.

$$ds^2 = dt^2 - a(t)^2 \left[\frac{dr^2}{1 - kr^2} + r^2 d\theta^2 + r^2 \sin^2 \theta d\phi^2 \right] \tag{1.7}$$

Here the time-dependent scale factor $a(t)$ describes expanding distance between objects, $r(t) \rightarrow a(t)r(t)$, and k is the curvature. Hubble's law may be written as $H(t) = \dot{a}(t)/a(t)$, assuming no relative motion other than the expansion of the universe.

$$R_{\mu\nu}(t) - \frac{1}{2} g_{\mu\nu}(t) R(t) + \Lambda(t) g_{\mu\nu}(t) = \frac{T_{\mu\nu}(t)}{M_{Pl}^2} \tag{1.8}$$

Using the FLRW metric and Einstein's equation (1.8), we may deduce the Friedman equation and ultimately the thermodynamic equations of state for the types of matter and energy, which gives the relationship between pressure, p, and density, ρ.

$$p_j(t) = w_j \rho_j(t) \tag{1.9}$$

Where $w_m = 0$, $w_r = 1/3$, $w_\Lambda = -1$. The energy and matter densities dependence on a may also be extracted by expanding $a(t)$ around current value a_0; $\rho_j \propto a^{-3(1+w_j)}$ [38].

$$\rho_j(a) \sim \begin{cases} a^{-4} & \text{relativistic radiation} \\ a^{-3} & \text{non-relativistic matter} \\ const & \text{vacuum energy} \end{cases} \tag{1.10}$$

This evolution of densities describes the epochs which the universe observes as it expands and temperature, T, decreases. A truncated overview of the history of the universe, following [39, 40, 38], is given in order to set the scene for DM and its associated observables. Initially ($T \gtrsim 10^{19} GeV$), the four fundamental forces may be unified, however a theory of quantum gravity is required to understand this period. At $T \sim 10^{15} GeV$, the Grand Unified Theory (GUT) phase transition occurs when the electroweak and strong forces delineate causing quarks and leptons to distinguish themselves. Around this time, baryogenesis and the origin of matter anti-matter asymmetry occurs. A period of inflation begins, driven by the negative pressure associated with a vacuum energy dominated epoch. Inflation offers a solution to the Flatness and Horizon problems of cosmology [39]. At

$T \sim 1 - 100sGeV$, WIMPs could freeze-out (or FIMPs freeze-in) - see section 1.3.3 for details. Around $T \sim 100GeV$ the electroweak phase transition occurs, before hadrons begin to form in the quark-hadron phase transition. At $T \sim 0.1MeV$, Big Bang Nucleosynthesis (BBN) occurs offering concrete mechanisms and measurements, which are well understood. Following from equation 1.10, the epoch of radiation domination ends at matter-radiation equality (around $T \sim 3eV$). At $T \sim eV$, electrons and protons *recombine* to form Hydrogen, CMB photons decouple. The CMB therefore offers a snapshot of this "time of last scattering", when the departure of free electrons causes the universe to be transparent to radiation.

1.3 Dark Matter

It has been observed since the 1930s, from the rotation curves of galaxies, that there is insufficient luminous mass in the universe to account for many complementary observations. Multiple surveys of MACHOs [41, 42] (Massive Compact Halo Objects) via gravitational lensing conclude these objects are incapable of explaining this missing mass. Cyburt [43] showed that this *Dark Matter* cannot be baryonic, by measuring the Deuterium-Hydrogen ratio as produced almost exclusively in Big Bang Nucelosynthesis. COBE [44], WMAP [45] and then Planck [46] surveyed the CMB to accurately measure the baryonic and DM abundance from the anisotropies, with DM composing 83% of the matter in the universe. Simulations of large scale structure disfavour hot dark matter, corresponding to masses for thermal candidates less than a few keV. Particle DM provides fundamental candidates for cold non-baryonic dark matter, with many possible models studied extensively in the literature. Some of the most studied include Supersymmetry, extended higgs sectors and Kaluza-Klein states.

1.3.1 Observations

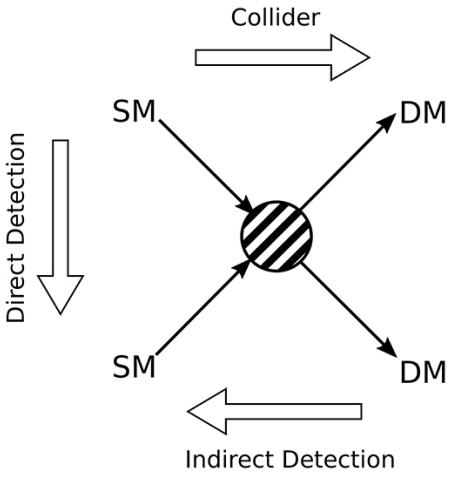

FIGURE 1.2: A schematic to describe the ability to probe the interactions between DM and SM particles in different experiments [1]

The lack of a DM candidate is one of the biggest current problems with the Standard Model (SM) of particle physics. If the solution takes the form of a Weakly Interacting Massive Particle (WIMP), that is light, stable and weakly interacts with standard model (SM) particles then it may be possible to observe at colliders. WIMPs are an attractive solution due to the often-cited WIMP miracle (see section 1.3.3 for further discussion), whereby weak scale interactions reproduce the correct relic abundance for thermal DM masses of order 10-1000GeV; scales which can be probed by current colliders.

The exploration of DM candidates via their fingerprint on the distribution of mass in the universe may be accompanied by experiments which probe the non-gravitational interactions of particle DM. As illustrated by figure 1.2, potential production in a collider (left to right) is complemented by experiments which aim to directly detect DM when they scatter off target nuclei (top to bottom), or indirectly by their impact on other particles arriving from the cosmos as a proxy (right to left). Calculation and measurement of DM relic abundance further can reveal the nature of DM interactions with the SM. If DM annihilates to photons, then the CMB could also show traces of DM through distortions in the anisotropies.

1.3.2 Astrophysical distributions

To measure the distribution of DM in a galaxy, we must rely on the gravitational impact on visible objects. Stars serve as a collisionless tracer for the distribution of DM.

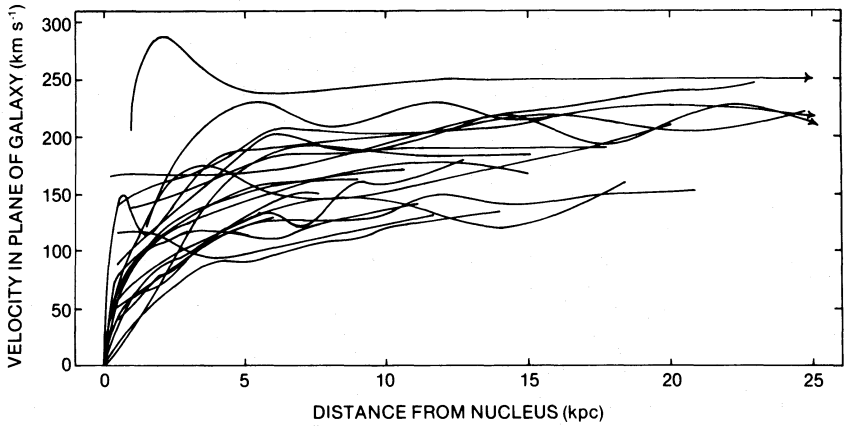

FIGURE 1.3: 21Sc galaxy rotation curves [2]

Using Newtonian gravity, the rotational velocity of stars was anticipated to be proportional to $\sqrt{M/R}$, where M is the enclosed mass at a distance R from the centre of the galaxy (when R is outside the galactic disk). Assuming all mass is concentrated in the disc, M is constant. However, the velocity curve was observed to flatten at such distances, implying $M(R) \propto R$ suggesting an additional 'dark' component of matter. In figure 1.3, we see the 21Sc rotation curves originally presented by Rubin et al. [2].

1.3.3 Relic Density and DM production mechanisms

The standard calculation of WIMP relic density assumes that the entropy of matter and radiation was conserved, that they were produced thermally and decoupled in the radiation dominated epoch, before BBN. In more recent times, alternative production mechanisms have been studied. These mechanisms for non-thermal relics include freeze-in [3] of feebly interacting massive particles or FIMPs, and the misalignment mechanism for Axions or Axion like particles (ALPs) [47]. This section will discuss the strong motivations for thermal DM prior to a review of the freeze-out and freeze-in mechanisms.

After reheating, a thermal DM particle maintains thermal equilibrium with the bath of SM particles through annihilation processes $\chi\chi \to ff$. When thermal decoupling occurs, the DM will **freeze out** with a density. Decoupling occurs when the interaction rate drops below the Hubble expansion, i.e $\Gamma(T_{dec}) = H(T_{dec})$.

$$\Gamma(T_{dec}) = \sigma_{\chi\chi} v n_{\chi} \tag{1.11}$$

By using the Friedmann equation for radiation domination:

$$H(T_{dec}) = \frac{\pi}{3\sqrt{10}M_{Pl}} \sqrt{g_{eff}(T_{dec})} T_{dec}^2 \tag{1.12}$$

Assuming $g = 2$ (Majorana fermion or complex scalar DM candidate) and an weakly interactiong DM (WIMP).

$$\sigma_{\chi\chi} = \frac{\pi\alpha^2 m_\chi^2}{s_W^4 m_W^4} \tag{1.13}$$

then decoupling occurs at $x_{dec} \equiv m_\chi / T_{dec} \approx 28$. Once decoupled, the number density falls like a^{-3} with constant entropy. Taking this into account we arrive at the so-called **WIMP miracle** (equation 1.14), by which a weakly interacting particle with mass around the electroweak scale gives rise to the measured value of DM density (Planck experiment measures $\Omega_\chi h^2 = 0.11$ [46]).

$$\Omega_\chi h^2 \approx 0.11 \left(\frac{100GeV}{m_\chi}\right)^2 \tag{1.14}$$

This simplistic sketch is the result of solving the equations of thermal evolution of DM number density, n. The first term is related to the Hubble expansion (H scales like square root of the current matter density). The last term expresses two related processes - DM annihilation into SM particles and the reverse. When $n = n_{eq}$, these processes are in thermal equilibrium.

$$\frac{dn}{dt} = -3Hn - < \sigma v >_T (n^2 - n_{eq}^2) \tag{1.15}$$

Using the law of entropy (s) conservation, $ds/dt = -3Hs$, this equation is usually written with T, the photon temperature, as the independent variable. This is given by equation 1.16, where $x \equiv m/T$ and $Y \equiv n/s$. In the second line, g_* represents the degrees of freedom [48]. This equation may be solved numerically using the initial condition that $Y \approx Y_{eq}$ at $x \approx 1$ to give the present WIMP abundance.

$$\begin{aligned} \frac{dY}{dx} &= \frac{1}{3H}\frac{ds}{dx} < \sigma v >_T (Y^2 - Y_{eq}^2) \\ &= -\left(\frac{45}{\pi M_{Pl}^2}\right)^{-1/2} \frac{g_*^1/2m}{x^2} < \sigma v >_T (Y^2 - Y_{eq}^2) \end{aligned} \tag{1.16}$$

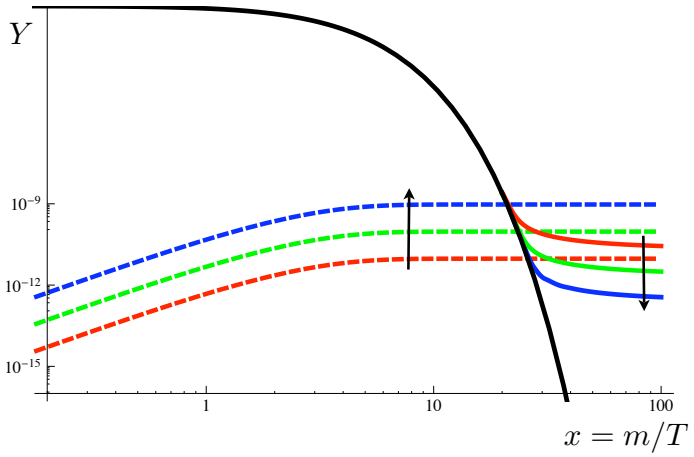

FIGURE 1.4: Typical evolution of DM density for freeze-out (solid) and freeze-in (dashed) with x. [3]

A key focus of the work presented in this thesis involves the calculation of the relic density for dark sectors, which may include unstable sibling particles that may co-annihilate with the DM candidate or additional DM candidates which would contribute to the total DM relic, which could itself reside in its own dark sector. Co-annihilation refers to the process by which dark-sector particles may scatter off DM to produce SM particles, depleting both the number density of DM and associated particles.

Freeze-in is the opposite process to freeze-out, in the sense that as the temperature drops below the DM mass then DM is heading towards thermal equilibrium (freeze-in) or away from it (freeze-out). This is expressed in figure 1.4, where the direction of the two arrows represents the influence of the increase of cross-sections between DM and SM. This demonstrates that as interactions between DM and SM increase, then the relic abundance generated my freeze-in increases and by freeze-out decreases.

When calculating FIMP relics, the assumption is made that at very high temperatures their is negligible initial DM abundance [3]. For a simple FIMP model such as the Higgs portal, the required Yukawa coupling to generate the measured relic abundance would be too small to allow for observation in the laboratory.

1.3.4 Direct Detection

Direct detection (DD) is a key laboratory probe for particle DM which has already generated powerful limits on many DM models. DD experiments search for

events where DM particles could scatter of a target material, as the solar system moves through the Milky Way encountering DM particles with velocities $\sim 10^{-3}$. The current best limits for WIMP masses $> 10GeV$ come from the Xenon1T experiment [49], with the LZ experiment [50] set to begin taking data this year - the sensitivity of these experiments are expressed in figure 1.5.

Typically, DD calculations assume the Standard Halo Model; that DM is distributed in an isotropic, isothermal sphere (DM density $\rho \propto R^{-2}$) implies a truncated Maxwellian velocity distribution (equation 1.17). The $1/R^2$ dependence of the DM density reproduces the observed flat galactic rotation curves. Here, v_c is the average circular velocity at distance R around the galactic centre and v_{esc} is the velocity required for DM to escape the gravitational well of the galaxy. The local expected circular velocity is $v_c(R_0 \approx 8kpc) \approx 220km/s$, with whilst the normalisation $N = erf(z) - 2\pi^{-1/2}ze^{-}z^2$ ($z = v_{esc}/v_c$) results from the Boltzmann equation for collisionless particles.

$$f(\vec{v} < \vec{v}_{esc}) = \frac{1}{N}\exp\left(-\frac{|\vec{v}|^2}{v_c^2(R)}\right)$$
$$f(\vec{v} \geq \vec{v}_{esc}) = 0 \tag{1.17}$$

DM direct detection relies on the detection of a recoiling target particle, at low energy scales (sub-MeV). Whilst early universe observables are calculated at scales similar to the DM mass, DD requires mapping our models to non-relativistic interactions measured by experiments.

DM-nucleon amplitudes may be calculated from the DM-quark amplitudes of a given model by the introduction of form factors which describe the quark content of a nucleon. Typically, DM-quark amplitudes are computed in the $v \to 0$ limit.

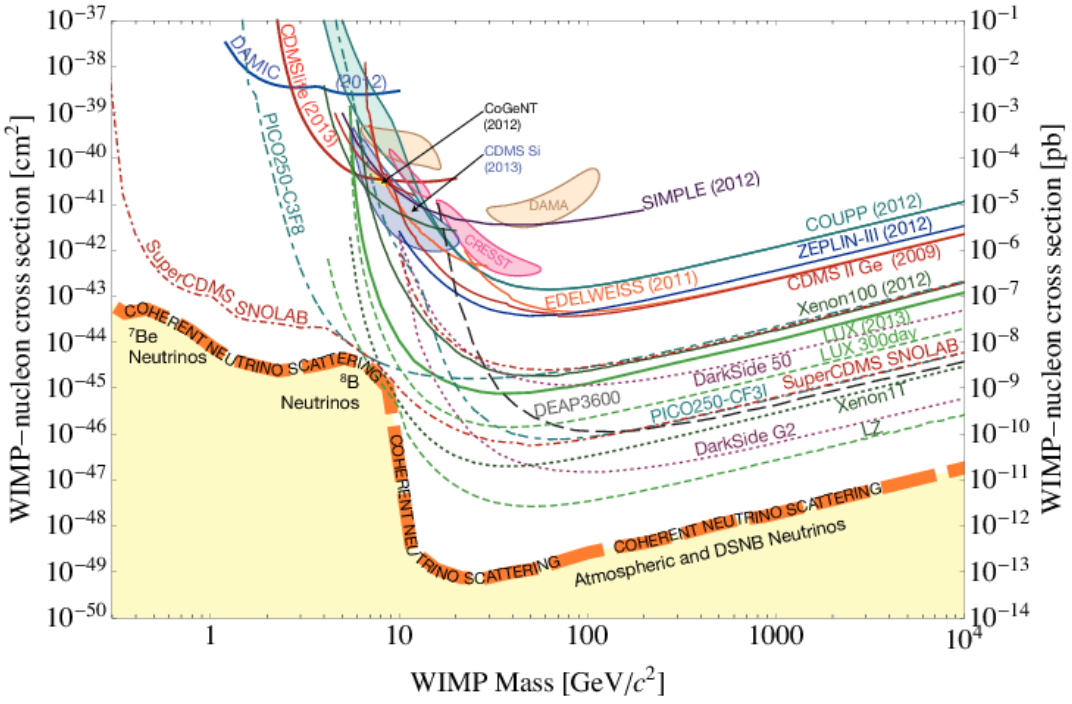

FIGURE 1.5: Limits from DD experiments [4]

1.3.5 Collider

If DM interacts sufficiently strongly with SM particles, and has masses below the energy achievable at a particle collider, then they may be produced and pass invisibly through the detectors, leaving hints only via co-produced visible particles. If a stable neutral particle were detected at a collider (by missing energy in the reconstructed event), there would still remain the difficult task to diagnose that particle as being DM. The interpretation of results has resulted in a fissure between the two types of models employed. The first are the highly specific "complete" models, allowing targeted searches and strong constraining power for that particular model. These models (e.g MSSM) allow robust statements to be made about the likelihood of the various DM observations under the assumption of a given model. The other school of interpretation involves the use of EFTs or Simplified Models, which offer broad classes of signatures and benchmarks for experimentalists to survey. However, the validity of EFTs at such energy scales, and the interpretation of observables at a wide range of energy scales diminishes their utility. Simplified models aim to remedy this, however gauge invariance issues and the presence of additional dark sector partners or mediators can limit their usefulness, especially when connecting the multitude of DM observables from the various experiments.

Searches for DM at the Large Hadron Collider (LHC) typically take the form of direct searches via missing energy signatures or indirect searches for mediators

between DM and SM. The former relies on the production of one or more energetic jets (or H,W,Z bosons) produced in association with large missing transverse momentum (E_T^{miss}), which is carried by the DM. The latter probes potential mediators by dijet or dilepton production. For Higgs portal models, the invisible branching ratio of the Higgs is a key measurement.

Currently, no search for DM has shown a significant deviation from the expected SM backgrounds. This may be interpreted as exclusion limits on models [51].

1.3.6 Indirect Detection

Indirect searches for WIMPs rely on possible self-interactions of DM which can give rise to observable particles in Earth-bound or satellite detectors through DM annihilations into SM particles. Such interactions would only occur in clumps of gravitational matter, such as in the sun or the centre of a galaxy. In these clumpy areas of the universe, efficient annihilation could generate observable photons or pairs of particles or such as electrons and protons or their antiparticles. Whilst many astrophysical backgrounds exist for particles, anti-particles are produced much less copiously. This enables the search for DM annihilations through a "shoulder" in the energy dependence of the antiproton-proton ratio around the DM mass [38]. This relies on the fact that DM moves slowly compared to galactic objects. The approximate energy ranges probed by a selection of indirect detection experiments are shown in figure 1.6 [5].

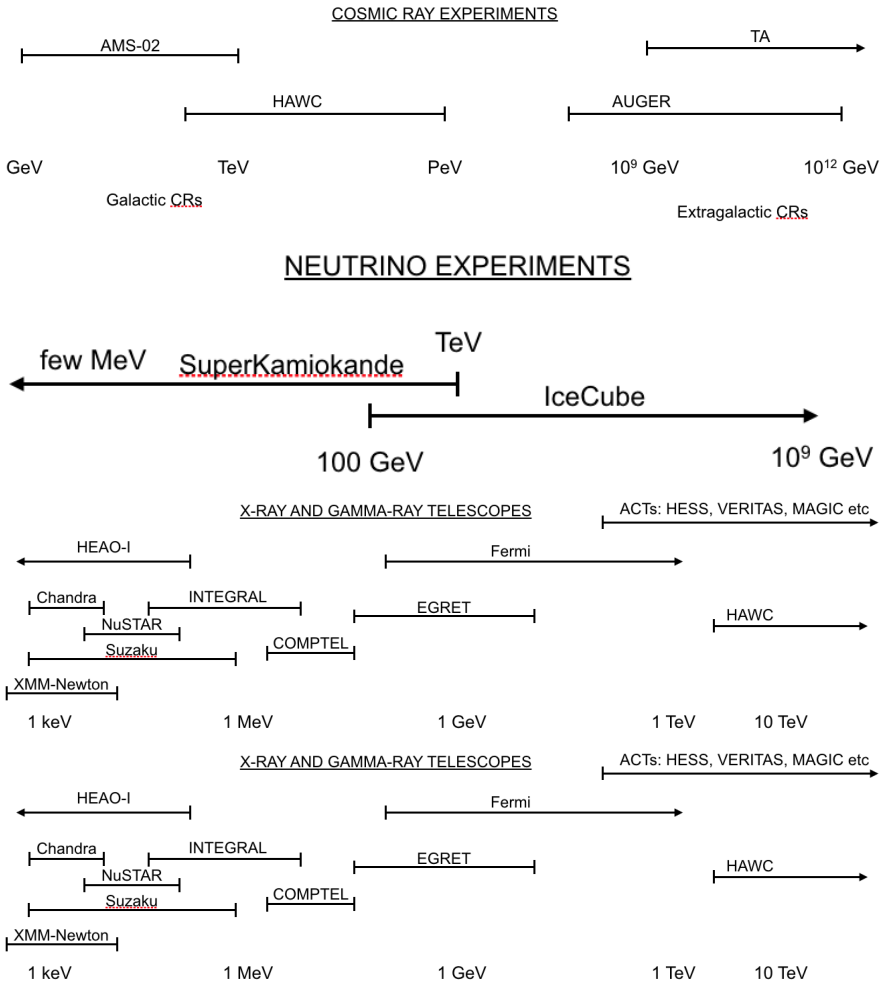

FIGURE 1.6: The energy ranges of SM messenger particles probed by an inexhaustive list of indirect detection experiments [5]

1.4 Technicolor

Technicolor [52, 53, 54] is a model which describes EWSB dynamically. The intoduction of a new strongly interacting gauge group G_{TC} alongside new particles called technifermions charged under G_{TC} and the EW gauge group, allow construction of EWSB mechanism by formation of a bilinear technifermion condensate, analogous to the chiral condensate of QCD. Through this technifermion condensate, masses for the W and Z bosons are generated. In order to generate SM fermion masses however, the model must be extended to models known as Extended Technicolor (ETC) models [55].

The Yukawa terms responsible for fermion mass generation in the SM may be generated if the Higgs is considered a technifermion bound state. However these these non-renormalisable terms appear only in extensions to technicolor where a

second strongly coupled gauge theory G_{ETC} is introduced at higher scales, which the SM fermions and technifermions are charged under.

$$\mathcal{L}_{Yukawa} \rightarrow -y\bar{Q}Qu\bar{d} \tag{1.18}$$

This ETC gauge group would introduce four-technifermion interactions which give masses to the pseudo-Goldstone bosons of the Technicolor sector (those which do not become longitudinal polarizations for the massive SM gauge bosons). Additionally, four-SM fermion interactions would also be generated by ETC, which could give rise to flavour changing neutral currents (FCNCs) which are incompatible with experiment [56]. Assuming an effective coupling of such interactions are $\mathcal{O}(1)$, then $\Lambda_{ETC} > PeV$ [57]. This leads to the generation of the top mass being very difficult in these models.

Walking technicolor (WTC) [58, 59] attempts to remedy these problems. The technicolor condensate responsible for SM fermion mass generation should be evaluated at the ETC scale, which may be related to the condensate at the lower TC scale using the renormalisation group. For Technicolor theories which run similar to QCD, the running of the technifermion condensate is given by equation 1.19, where γ is the anomalous dimension of the technifermion mass operator. Here the logarithmic enhancement to the SM fermion masses is insufficient to solve the puzzle.

$$< \bar{Q}Q >_{ETC} \sim ln \left(\frac{\Lambda_{ETC}}{\Lambda_{TC}}\right)^{\gamma} < \bar{Q}Q >_{TC} \tag{1.19}$$

If instead the technicolor coupling α_{TC} **walks** (runs slowly with energy scale) between Λ_{TC} and Λ_{ETC} then the enhancement to the SM fermion masses may be increased, as may be seen in equation 1.20. This walking regime is near-conformal, the anomalous dimension may be evaluated at α^* (the conformal fixed point). This constant anomalous dimension leads to linear enhancement of the technifermion condensate. This linear enhancement in WTC is sufficient to enable heavy quark mass generation to become feasible whilst limiting FCNCs through the scale of ETC.

$$< \bar{Q}Q >_{ETC} \sim \left(\frac{\Lambda_{ETC}}{\Lambda_{TC}}\right)^{\gamma(\alpha^*)} < \bar{Q}Q >_{TC} \tag{1.20}$$

Technicolor forms a spectrum of techimeson bound states. This spectrum contains a composite scalar meson analogous to the σ in QCD. In WTC, for a technicolor scale of $\Lambda_{TC} \sim 1TeV$, and a technipion decay constant similar to the SM Higgs vev, the mass of σ is naturally found to be close to the measured Higgs mass, $M_\sigma = M_h = 125GeV$ [60]. Therefore in WTC models, the σ can walk and quack like the Higgs.

1.5 Attribution and organisation

Chapter 2 is based on a paper in preparation in collaboration with G.Cacciapaglia and A. Belyaev [8]. The bulk of this work stems from our active discussions at DM conferences in the years prior to COVID-19. My main contribution to this work is the NLO calculations of mass splits and DD cross-sections, and the implementation of models via LanHEP [10]. Additionally, exhaustive numerical simulations which explore the phenomenology of representative models are presented.

Chapter 3 is based on a paper in preparation in collaboration with A.Belyaev, I.Ginzburg, A.Freegard, T.Hosken, A.Pukhov [9]. My contributions include exploration and model-building of the fermion DM model, along with implementation into LanHEP [10], simulation of LHC events to detector level, and subsequent analysis of these events. In order to streamline analysis prototyping, PhenoAnalysis an optimised python framework was developed, which is publicly available at [61].

Chapter 4 is based on work published as [7]. My contribution to this paper is in the statistical analysis of particle physics events, using binned composite likelihood methods.

Section 5.2 is the result of discussions at LHC reinterpretation workshops. The database was developed in collaboration with J.Blandford and A.Belyaev, with a paper in preparation to be submitted to the Computer Physics Communications journal.

Chapter 2

Minimal Consistent Dark Matter models for Collider and Direct detection Characterisation: fermion dark matter

Dark Matter (DM) exploration is becoming an increasingly appealing subject at present, when the LHC, as well as other non-collider experiments, does not indicate any clear signal Beyond the Standard Model (BSM). Indeed DM evidence is the strongest experimental indication of BSM physics. It is well-established from several independent Cosmological and Astrophysical observations, including galactic rotation curves, cosmic microwave background fits of WMAP [45] and PLANCK [46] data, gravitational lensing, large scale structure of the Universe as well as existence of so-called bullet clusters.

While the experimental evidence became more convincing, our knowledge of the nature of DM remains veiled: there are many particle candidates, however no experiment so far was able to probe their properties. Potentially, DM particles can be probed at the LHC by measuring their production in particle collisions, at direct detection (DD) underground experiments which are sensitive to elastic scattering of DM particles in the local galactic Halo, and in the indirect detection (ID) experiments which measure the product of DM annihilation (and/or decay) in the Universe in the form of positrons, gamma-rays, anti-protons and neutrinos from the galactic centre or from the sun. The fact that DM can be probed by a large array of experiments, of differing nature, has resulted in interest in DM rapidly increasing in the particle physics community, especially after the discovery of the Higgs boson.

One of the most important issues behind DM searches is related to how to combine the results of experimental searches, so different in nature, in a consistent

and yet model-independent and general way. Starting from [62] which suggested an Effective Field Theory (EFT) approach in collider and DD searches, the level of sophistication in DM exploration at the LHC and DD experiments has been constantly increasing. Though many ATLAS and CMS papers have been using the EFT approach in Run 1 data analysis and interpretation [63, 64, 65, 66, 67, 68], its limitations soon became clear. The EFT approach uses contact interaction to describe interactions of the DM to ordinary matter: eventually this approximation does not work when the energy scale of the DM interactions is close or above the mass of the mediator(s) probed experimentally. At the next step, the exploration of collider DM phenomenology went beyond the EFT approach towards the approach of *simplified models*, where the dark matter sector is characterised by the dark matter candidate and a mediator which makes the connection with the SM particles [69, 70, 71, 72, 73, 74, 75, 76, 77, 78, 79, 80, 81, 82, 83]. Some of these models have been used in recent ATLAS and CMS experimental interpretation of Run 1 LHC data [84, 85, 86, 87, 88]. In case of simplified models the mass of the mediator, and potentially its width, are non-trivial parameters of the model. In these scenarios, one remains agnostic about the theory behind the dark matter sector and tries to parametrise the interactions in the simplest terms: this often leads to writing interactions which are not invariant under the full SM gauge symmetry but only under the unbroken colour SU(3) and electromagnetic U(1). However, one still needs to know if it is possible to construct viable models that lead to a given scenario, and make this scenario consistent with the symmetries of the Standard Model. The latter point is particularly important at the LHC, a machine which is probing energy scales well above the electroweak symmetry breaking scale, so that for many events the full weak SU(2)$\times$U(1) is a good symmetry. For instance, if a mediator or DM candidate comes in a multiplet of the weak SU(2), its charged partners may play an important role in the LHC phenomenology often being more important that the neutral state itself. It is often the case for the chargino in supersymmetry. In addition, simplified models often violate gauge invariance which is a crucial principle for building a consistent BSM model which incorporates the SM together with new physics. For example, considering simplified model with a new heavy gauge vector boson mediating DM interactions, one should also introduce a mechanism which is responsible for the mass generation of this mediator to provide gauge invariance for the model. Eventually, this necessarily requires introducing a additional particles into the model which may affect the DM phenomenology.

These drawbacks strongly motivate a qualitatively new approach based on building Minimal Consistent Dark Matter (MCDM) models. MCDM models can be still understood as toy models, that however take in full account the consistency with the symmetries of the SM. Furthermore, a particular MCDM model can be easily

incorporated into a bigger, more complete, BSM model and be explored via complementary constraints from collider and direct/indirect DM search experiments as well as relic density constraints as independent and consistent model. The exploration of complementarity of the collider and non-collider constraints within the complete models such as MCDM ones is very appealing especially now as we have a large amount of data from the LHC. Combining searches may shed light on the BSM physics in the form of Dark Matter, which can be near the corner of the combined collider and non-collider searches. Another attractive feature of the MCDM approach is their minimal but self-consistent parameter space which can be potentially mapped to the parameter space of known (and potentially new) BSM models.

Many implementations of MCDM models are known in the literature [89, 90, 91, 73, 81, 75, 74], however there were no attempt, yet, on their systematic classification. This is precisely the aim of this chapter. In this study we shall a) perform a complete classification of MCDM models and b) present the main features for each class of MCDMs constructed using the main building principles we state below. We believe that this classification, and the MCDM approach, will create a solid framework for the exploration of consistent DM models at collider and non-collider experiments for the complementary probe of Dark Matter.

2.1 Classification of MCDM models

The building blocks we will use to construct models are multiplets defined in terms of their spin and electroweak quantum numbers. We will only consider spin-0 (S), spin-1/2 (F for a Dirac fermion or M for a Majorana one[1]), and spin-1 (V). For models with higher spin, we refer the reader, for instance, to Refs [92, 93, 94, 95]. The electroweak quantum numbers will be encoded in the weak Isospin, I, and the hypercharge, Y, of the multiplet. Furthermore, we will denote with a tilde the multiplets that belong to the dark sector, i.e. they cannot decay into purely SM final states. The multiplets we consider, therefore, read:

$$\widetilde{S}^I_Y\,, \quad \widetilde{F}^I_Y\,, \quad \widetilde{M}^I_0\,, \quad \widetilde{V}^I_Y\,,$$

and similarly with un-tilded ones. As some mediator multiplets may carry QCD quantum numbers, we will use a superscript ^{c} to label this feature.

To construct consistent minimal models, we follow the main building principles:

A) we add one Dark multiplet (including the singlet case) and all its renormalisable interactions to SM fields, excluding the ones that trigger the decays

[1]Here, we consider a Majorana fermion a multiplet with zero $U(1)$ charge and in a real representation of the non-abelian gauge symmetries, such that a mass term $M\bar{\psi}^c\psi$ is allowed.

of the multiplet, which is therefore stable. The models will automatically include a Dark symmetry, being $\mathbb{Z}_2$ or $U(1)$ depending on the multiplet. The weak Isospin and hypercharge are constrained by the need of having a neutral component, therefore we will have the following two cases:

- for integer isospin $I = n, n \in N$, then $Y = 0, 1 \dots n$;
- for semi-integer isospin $I = (2n+1)/2, n \in N$, then $Y = 1/2, 3/2 \dots (2n+1)/2$.

Note that the case of negative hypercharge can be obtained by considering the charge conjugate field, thus the sign of Y is effectively redundant, and we will consider $Y \geq 0$.

B) we consider models where only one Dark multiplet is present, and mediators are SM fields. [2] While our principle is to be limited to renormalisable interactions, under the assumption that higher order ones are suppressed by a large enough scale to make them irrelevant for the DM properties, in some cases we will consider dimension-5 operators.

C) in additional to point B), we consider adding just one mediator multiplet, characterised by the respective weak Isospin, I', and hypercharge, Y'. The mediator multiplet can be odd or even with respect to Dark symmetry, and its quantum numbers are limited to cases where renormalisable couplings to the Dark multiplet and to the SM are allowed. This leaves open the possibility of multiplets carrying QCD charges, which we label with a superscript ^{c}. The mediators are labeled as following:
  - $S_{Y'}^{I'(c)}$, $F_{Y'}^{I'(c)}$, $M_0^{I'(c)}$ and $V_{Y'}^{I'(c)}$ for even mediator multiplets;
  - $\widetilde{S}_{Y'}^{I'(c)}$, $\widetilde{F}_{Y'}^{I'(c)}$, $\widetilde{M}_0^{I'(c)}$ and $\widetilde{V}_{Y'}^{I'(c)}$ for odd mediator multiplets.

D) we consider all renormalisable interactions allowed by the QFT. Our basis assumption for MCDM models is that higher-order operators are suppressed by a scale high enough that the LHC is unable to resolve the physics generating the operators. The effect on the DM properties is also considered negligible (except for dim-5 operators generating mass splits).

E) we ensure cancellation of triangle anomalies, so that the MCDM models entails consistent gauge symmetries, and consider minimal flavour violation (MFV) couplings to SM fermion generations.

With the notations above, following the precepts A) to E), we can classify all MCDM models with up to one mediator multiplet using a 2-dimensional Table in Spin(DM)-Spin(mediator) space, as presented in Table 2.1. Each specific DM

[2] Note that this model building approach has been used in [90] to construct models of so-called Minimal Dark Matter, so some of the results we present here can be found in this reference. However, our approach has some differences: in Ref. [90], the symmetry making the DM candidate stable or long lived emerged as at low energy, at the level of renormalisable interactions, while decays could be induced by higher dimensional couplings to the Higgs multiplets. In our case, we assume that a parity or global $U(1)$ symmetry is also respected by higher dimensional operators.

Spin of Mediator \ Spin of Dark Matter	0	1/2	1
no mediator	$\widetilde{S}^I_Y$	$\widetilde{F}^I_Y$	$\widetilde{V}^I_Y$
spin 0 even mediator	$\widetilde{S}^I_Y S^{I'}_{Y'}$	$\widetilde{F}^I_Y S^{I'}_0$	$\widetilde{V}^I_Y S^{I'}_{Y'}$
spin 0 odd mediator	$\widetilde{S}^I_Y \widetilde{S}^{I'}_{Y'}$	$\widetilde{F}^I_Y \widetilde{S}^{I'}_{Y'}$ $\widetilde{F}^I_Y \widetilde{S}^{I'c}_{Y'}$	$\widetilde{V}^I_Y \widetilde{S}^{I'}_{Y'}$
spin 1/2 even mediator			
spin 1/2 odd mediator	$\widetilde{S}^I_Y \widetilde{F}^{I'}_{Y'}$ $\widetilde{S}^I_Y \widetilde{F}^{I'c}_{Y'}$	$\widetilde{F}^I_Y \widetilde{F}^{I\pm1/2}_{Y\pm1/2}$	$\widetilde{V}^I_Y \widetilde{F}^{I'}_{Y'}$ $\widetilde{V}^I_Y \widetilde{F}^{I'c}_{Y'}$
spin 1 even mediator	$\widetilde{S}^I_Y V^{I'}_0$	$\widetilde{F}^I_Y V^{I'}_0$	$\widetilde{V}^I_Y V^{I'}_{Y'}$
spin 1 odd mediator	$\widetilde{S}^I_Y \widetilde{V}^{I'}_{Y'}$	$\widetilde{F}^I_Y \widetilde{V}^{I'}_{Y'}$ $\widetilde{F}^I_Y \widetilde{V}^{I'c}_{Y'}$	$\widetilde{V}^I_Y \widetilde{V}^{I'}_{Y'}$

TABLE 2.1: Classification of the Minimal Consistent Dark Matter (MCDM) Models in Spin(DM)-Spin(mediator) space. When possible, the Dirac fermion can be replaced by a Majorana one, $F \to M$.

model is denoted by a one- or two-symbol notation, indicating the DM multiplet first, followed by the mediator multiplet. One should note that in this case SM particles as well as members of DM multiplet other than DM, could also mediate DM interactions and their interference with the mediator multiplet can be non-trivial. Eventually, the case with no mediator multiplet is denoted by just one symbol labelling the DM multiplet. In this case the role of mediators can only be played by SM particles and members of DM multiplet.

In the remainder of this paper, we will focus on spin-1/2 DM multiplets, leaving the other two cases for a future publication.

2.2 Case of one DM multiplet: $\tilde{F}^I_Y$ and $\tilde{M}^I_0$ models

Models where the DM belongs to a single EW multiplet, while no other light states are present, have been studied in great detail, starting from the seminal paper in Ref. [90]. In this section we briefly review the main properties of these minimal models, and add a detailed discussion of the following novel aspects:

i) We provide an improved formula for the mass splitting induced by EW loops, which is numerically more stable than the one given in Ref. [90].

ii) We discuss in great detail the effect of couplings to the Higgs boson arising as dimension-5 operators. While going beyond the minimality principle, they can be generated by integrating out a single mediator (thus, they can be considered as a limiting case from the models discussed in Section 2.3). Furthermore, a class of these operators have special phenomenological relevance as they can help salvage some of the minimal models with non-zero hypercharge.

iii) We provide a detailed and up-to date discussion of Direct Detection bounds, including loop-induced interactions.

This section also serves to fix the notation we will adopt in the rest of the paper. When writing Lagrangians and interactions we will consistently use $\Psi = \Psi_L + \Psi_R$ for the DM multiplet (where one chirality is absent for a Majorana DM multiplet, i.e. $\Psi_R = 0$), ψ^i for the components of a Dirac multiplet and χ^i for the components of a Majorana multiplet. Furthermore, we only consider $Y \geq 0$, as the case of negative hypercharge is straightforwardly analogous to the corresponding positive value case.

In the "stand alone" case, the most general renormalisable Lagrangian for the DM multiplet Ψ, with isospin and hypercharge $\{I, Y\}$, is

$$\mathcal{L} = i\bar{\Psi}\gamma^\mu D_\mu \Psi - m_D \bar{\Psi}\Psi - \frac{1}{2}\left(m_M\, \bar{\Psi}^C \Psi + \text{h.c.}\right), \tag{2.1}$$

where the superscript ^{C} indicates the charge-conjugate field. We have explicitly added both a Majorana mass m_M, which is only allowed for $Y = 0$ (thus, integer isospin), and a Dirac one m_D, which vanishes for a Majorana multiplet. This simple class of models has well established properties [90], which we list below:

- A gauge coupling $Z\bar{\psi}_0\psi_0$ is always present for Dirac multiplets with $Y \neq 0$, which are thus excluded by Direct Detection even for under-abundant points (for $m_{DM} < m_Z/2$ the invisible width of the Z also excludes the model).
- In absence of Higgs couplings, the mass splitting between the neutral and charged components of the DM multiplet are generated by EW loop corrections and are always small (below 200 MeV). This leads to long lived particles, especially at high mass. The lightest component is not guaranteed to be neutral.
- For $Y \geq 1$, the mass range with the neutral component being the lightest is excluded by the Z width. Thus, these multiplets in isolation cannot provide a DM candidate.

- In absence of Higgs couplings, loop induced couplings to quarks excludes all non-trivial multiplets via Direct Detection, with the exception of a triplet and a quintuplet at high mass. Future experiments will be able to fully cover these models.
- For $Y = 0$ (both Dirac and Majorana multiplets), the relic abundance is determined by co-annihilation with the charged component via the W, or annihilation via the dim-5 Higgs couplings.
- For $Y = 1/2$, a dim-5 operator with the Higgs boson generates a Majorana mass, thus salvaging the model from exclusion via the Z interactions. Blindspots in Direct Detection can occur, via a cancellation between the loops and the dim-5 Higgs coupling.

We should finally note that for DM multiplets with $\{I, Y\} = \{0, 0\}$, $\{1/2, 1/2\}$, $\{1, 0\}$ and $\{1, 1\}$, a linear Yukawa coupling with the SM leptons is allowed by gauge symmetries, while larger isospin multiplets are automatically protected at renormalisable level. However, higher order couplings involving the Higgs can always generate decays of the DM multiplets, and it has been the main motivation of Ref. [90] to find multiplets that are long-lived enough to be Cosmologically stable. In this work we will be more pragmatic and allow for any multiplet by forbidding implicitly all operators that could mediate the decays of the DM candidate. The origin of such a symmetry is to be searched in the more complete model containing the DM multiplet. After reviewing the properties of Dirac and Majorana multiplets in Sec. 2.2.1 and 2.2.2 respectively, in Sec. 2.2.3 we will study in detail the effect of dim-5 couplings to the Higgs field. In Sec. 2.2.4 we provide novel detailed results on current Direct Detection exclusion limits and future projections.

2.2.1 Dirac multiplets ($\tilde{F}^I_Y$)

In the case of Dirac multiplets, i.e. when both chiralities are present, the lowest order Lagrangian in equation (2.1) is invariant under a global $\mathrm{U}(1)_{\mathrm{DM}}$ symmetry, thus an asymmetric contribution to the relic abundance may be present if the complete model preserves this symmetry. In the case $Y = 0$, the presence of a Majorana mass breaks $\mathrm{U}(1)_{\mathrm{DM}} \to \mathbb{Z}_2$. [3]

[3] Note that the Majorana mass is not generated radiatively as long as the $\mathrm{U}(1)_{\mathrm{DM}}$ symmetry is preserved by the complete model.

Except for the singlet case $\tilde{F}_0^0$, the multiplet contains extra charged states:

$$\Psi = \begin{pmatrix} \psi^{n+} \\ \vdots \\ \psi^{+} \\ \psi_0 \\ \psi^{-} \\ \vdots \\ \psi^{m-} \end{pmatrix}, \qquad \text{with} \quad n = I + Y\,, \ \text{and} \ \ m = I - Y\,. \tag{2.2}$$

The Dirac mass term in equation (2.1) gives equal mass to all components of the multiplet. This degeneracy can only be lifted by radiative corrections due to the EW gauge bosons. This contribution has first been computed in Ref. [90], and can be written as

$$M_Q - M_{Q'} = \frac{\alpha m_D}{4\pi s_W^2}\left[(Q^2 - Q'^2)\left(f_F(x_W) - c_W^2 f_F(x_Z) - s_W^2 f_F(x_\gamma)\right) + 2Y(Q - Q')\left(f_F(x_Z) - f_F(x_W)\right)\right], \tag{2.3}$$

where $f_F(x)$ is a loop function and $x_V = m_V/m_D$. This expression explicitly shows that in the limit of equal masses for W, Z and photon the mass differences vanish. For the loop function, we found an alternative form that is numerically more stable than the one given in Ref. [90] (see Appendix A.1 for more details). The result, which is exact, reads

$$f_F(x) = \frac{x}{2}\left[2x^3 \ln x - 2x - \sqrt{x^2-4}(x^2+2)\ln\frac{x^2 - 2 + x\sqrt{x^2-4}}{2}\right]. \tag{2.4}$$

This function has been defined in such a way that $f_F(x_\gamma) \equiv f_F(0) = 0$. It is instructive to study how the mass split looks in the limit of DM mass small and large compared to the W and Z masses. For light DM, $m_D \ll m_W$, the leading contribution reads

$$M_Q - M_{Q'}\big|_{m_D \ll m_W} \approx \frac{3\alpha}{2\pi}(Q^2 - Q'^2) m_D \left(\log\frac{m_W}{m_D} + \frac{1}{4}\right). \tag{2.5}$$

This mass split vanishes for small DM masses, and is proportional to the difference in squared charges, as an indication that it is dominated by the photon exchange. Furthermore, in this limit the lightest component of the multiplet is always the neural one. In the opposite limit, $m_D \gg m_W$, the leading term in the expansion reads

$$M_Q - M_{Q'}\big|_{m_D \gg m_W} \approx \frac{\alpha m_W}{2(1+c_W)}\left[(Q^2 - Q'^2) + \frac{2Y(Q-Q')}{c_W}\right]. \tag{2.6}$$

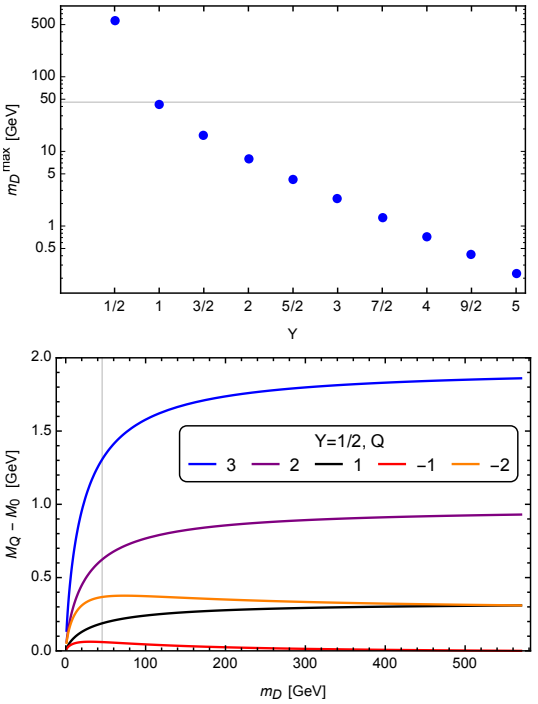

FIGURE 2.1: *Left*: maximum value of m_D above which the lightest component has charge $Q = -1$ for various values of Y. The horizontal line indicates $m_Z/2$, below which decays of the Z exclude the model. *Right*: spectrum for a generic multiplet with $Y = 1/2$, with $m_D < 570$ GeV. The vertical line shows $m_D \approx m_Z/2$, below which the model is excluded by the Z decays.

The second term, which depends on the sign of the charges (we chose $Y > 0$ without loss of generality), does not guarantee that the $Q = 0$ state is always the lightest one. In particular, states with $Q < 0$ are always lighter than the $Q = 0$ one in this limit. Thus, there exists an upper limit on m_D, above which the lightest state in the multiplet is charged, and this value is determined by the $Q = -1$ state. The values of the mass upper bounds for various Y are shown in the left panel of figure 2.1: the highest value is achieved for $Y = 1/2$ which gives $m_D^{\max} = 570$ GeV (we recall that for $Y = 0$ there is no limit), while for $Y = 1$ we find $m_D^{\max} = 42$ GeV, which is already below $m_Z/2$. Thus, multiplets with $Y \geq 1$ are excluded by the Z-width measurement in the region where the lightest state is neutral. For larger Y, the maximal mass value scales exponentially with the hypercharge, with an approximate formula

$$m_D^{\max}|_{Y\gg 1} \approx m_W \left(\frac{m_W}{m_Z}\right)^{\frac{2Y+c_W^2}{s_W^2}} e^{1/4} \approx 21.5 \times (0.32)^{Y-1}\ \text{GeV}\,. \tag{2.7}$$

Note that the issue of lightest charged states does not exist for multiplets that do not feature negatively charged components, i.e. if $Y = I$, and for $Y = 0$.

The analysis of the loop induced mass splitting thus shows that only 3 classes of models are potentially interesting:

a) the singlet $\tilde{F}_0^0$;

b) multiplets $\tilde{F}_{1/2}^I$ (I semi-integer with $Y = 1/2$), with $m_D \leq 570$ GeV for $I \geq 3/2$;

c) multiplets $\tilde{F}_0^I$ (I non-zero integer with $Y = 0$).

As already mentioned, all models with $Y \neq 0$, i.e. a) and c), are excluded by Direct Detection via the Z exchange, in absence of Higgs couplings (see Section 2.2.3.2).

2.2.1.1 Dirac multiplets with a Majorana mass term ($\tilde{F}_0^I$)

In the $Y = 0$ case, a Majorana mass m_M can also be added, which breaks $\mathrm{U}(1)_{\mathrm{DM}}$ to a $\mathbb{Z}_2$. The net effect is to split the multiplet into two Majorana multiplets with masses

$$M_{1,2} = m_D \pm m_M \,. \tag{2.8}$$

This leads to a model with two DM candidates, with the relic density dominated by the lighter one for large mass split. The physics properties will therefore be the same as for the model with a Majorana multiplet, $\tilde{M}_0^I$, that are described in Sec. 2.2.2.

2.2.2 Majorana multiplets

In the case of a Majorana multiplet, $Y = 0$, the multiplet will decompose as

$$\Psi_L = \begin{pmatrix} \chi^{n+} \\ \vdots \\ \chi^{+} \\ \chi_0 \\ (\chi^{+})^C \\ \vdots \\ (\chi^{n+})^C \end{pmatrix}, \qquad \text{with} \quad n = I \,, \tag{2.9}$$

so that the Majorana DM candidate χ_0 is accompanied by I Dirac charged partners. The phenomenology of this multiplet is in large part the same as for a $\tilde{F}_0^I$ Dirac multiplet, in particular the mass split between the various components is given by the same formula given in equation (2.3).

2.2.3 Mass splitting from dim–5 Higgs couplings

In this section we will consider minimal couplings to the Higgs field, which can arise at the level of dim–5 operators. While they may be suppressed by a UV scale, they are relevant because they can induce a mass split between the components of the DM multiplet, potentially competitive with the EW loops. Thus, while they are not renormalisable couplings, we will consider them here as minimal extensions of the single multiplet models. Furthermore, as we will see in Section 2.3, they can arise by integrating out a heavier fermion mediator.

2.2.3.1 Dirac multiplets

The Brout-Englert-Higgs doublet ϕ_H can only couple to the DM multiplet via higher dimensional operators. The lowest order operators have dimension 5 and read:

$$\mathcal{L}_{\text{dim}--5} \supset -\frac{\kappa}{\Lambda}\,\phi_H^\dagger T^a_{1/2}\phi_H\,\bar{\Psi}T^a_I\Psi - \frac{\kappa'}{\Lambda}\,\phi_H^\dagger\phi_H\,\bar{\Psi}\Psi\,, \tag{2.10}$$

where T^a_I are the 3 SU(2)$_L$ generators for the multiplet with isospin I, and Λ is a new scale that we assume being beyond the LHC reach to resolve. The second term generates a common mass contribution for all components, thus it simply shifts the Dirac mass of the multiplet

$$m'_D = m_D + \kappa'\frac{v^2}{2\Lambda}\,, \tag{2.11}$$

and generates a coupling to the Higgs, $-\frac{\kappa' v}{\Lambda}h\,\bar{\Psi}\Psi$, that contributes to Direct Detection.

The first one induces a mass split among the various components, thus it may affect the conclusions about the spectrum we reached in the previous section. We recall that the form of the SU(2) generators for a generic isospin I is

$$T^3_I = \begin{pmatrix} I & 0 & \dots & \dots & 0 \\ 0 & I-1 & \dots & \dots & 0 \\ \vdots & \vdots & \ddots & & \vdots \\ \vdots & \vdots & & -I+1 & 0 \\ 0 & 0 & \dots & 0 & -I \end{pmatrix}, \qquad T^+_I = \frac{1}{\sqrt{2}}\begin{pmatrix} 0 & c_1 & 0 & \dots & 0 \\ 0 & 0 & c_2 & \dots & 0 \\ \vdots & \vdots & \ddots & & \vdots \\ & & & 0 & c_{N-1} \\ 0 & 0 & \dots & 0 & 0 \end{pmatrix} \tag{2.12}$$

with

$$c_k = \sqrt{k(N_I-k)}\,, k = 1,\dots N_I-1, \;\text{ and }\; c_{N_I-k} = c_k\,. \tag{2.13}$$

Once the Higgs field develops its VEV, the only non-vanishing component is

$$\phi_H^\dagger T^3_{1/2} \phi_H = -\frac{1}{2}\varphi_0^* \varphi_0 = -\frac{1}{4}(v+h)^2\,, \tag{2.14}$$

which couples to $\bar{\Psi} T^3_I \Psi$. The resulting term in the Lagrangian reads

$$\mathcal{L}_\kappa = -\mu_D \left(1+\frac{h}{v}\right)^2 \Big(I\, \bar{\psi}^{n+}\psi^{n+} + (I-1)\, \bar{\psi}^{(n-1)+}\psi^{(n-1)+} + \dots \\ -Y\, \bar{\psi}_0\psi_0 - \dots - I\, \bar{\psi}^{m-}\psi^{m-}\Big)\,, \tag{2.15}$$

where $\mu_D = -\frac{\kappa v^2}{4\Lambda}$. In terms of mass splitting, this couplings can be expressed as

$$M_Q - M_{Q'}\big|_{\text{Higgs}} = \mu_D (Q - Q')\,. \tag{2.16}$$

As long as there are components with both positive and negative charges in the multiplet, the lightest state will not be the charged one. For $\{I, Y = I\}$ multiplets with $\mu_D > 0$, however, the lightest neutral state is guaranteed. An interesting situation occurs for $Y = 0$ multiplets, as the Higgs-induced contribution may remain smaller than the loop-induced one. The state that will first turn lighter that the neutral one is the one with charge $Q = +1$ or -1, depending on the sign of μ_D. The mass split, including the EW loops, will read

$$M_Q - M_0 = \delta m_{\text{EW}}\, Q^2 + \mu_D\, Q\,, \tag{2.17}$$

where $\delta m_{\text{EW}} = 166$ MeV for heavy DM masses. The strictest bound comes from the smallest charge states, and it reads

$$|\mu_D| < \delta m_{\text{EW}} \quad \Leftrightarrow \quad \frac{\Lambda}{|\kappa|} > 90 \text{ TeV}\,. \tag{2.18}$$

We can thus see that the presence of a dim–5 coupling to the Higgs does not help salvaging any of the Dirac single-multiplet models of Dark Matter. There is however an exception to this generic statement, that we will study in the following section.

2.2.3.2 Dirac multiplet with Majorana coupling: case $Y = 1/2$

A special case occurs for multiplets with $Y = 1/2$, as an additional coupling to the Higgs can be added:

$$\Delta\mathcal{L}_{dim5} = -\frac{1}{2}\frac{\kappa_M}{\Lambda}\, \phi_H T^a_{1/2} \phi_H\, \bar{\Psi} T^a_I \Psi^C + \text{h.c.} \tag{2.19}$$

The operator above is similar to the Weinberg operators in the SM [96] that gives mass to the left-handed neutrinos. Note also that it preserves a $\mathbb{Z}_2$ symmetry on

the DM candidate, but breaks the U(1). While multiplets with $Y = 1/2$ would be excluded by Direct Detection via the Z coupling, the effect of the operator above is to split the neutral Dirac state into two Majorana states with different mass: the Z now couples to the two states, while the DM candidate is the lightest one. The price to pay is that there is a new direct coupling to the Higgs boson, which will also contribute to Direct Detection. Our goal in this section is to study in detail this scenario.

In the above operator, the only non-vanishing component of the Higgs current is

$$\phi_H T^+_{1/2} \phi_H = \frac{1}{\sqrt{2}} \varphi_0^2 = \frac{1}{2\sqrt{2}} (v+h)^2 \,, \tag{2.20}$$

which couples to $\bar{\psi} T^-_I \psi^C$. The resulting Lagrangian reads

$$\begin{aligned} \Delta\mathcal{L}_{dim5} = -\frac{1}{2}\mu_M \left(1+\frac{h}{v}\right)^2 \Big(& c_1 \bar{\psi}^{(n-1)+} (\psi^{(n-1)-})^C + \cdots + c_k \bar{\psi}^{(n-k)+} (\psi^{(n-k)-})^C + \\ & \cdots + c_{I+1/2} \bar{\psi}^0 (\psi^0)^C + \cdots + c_k \bar{\psi}^{(n-k)-} (\psi^{(n-k)+})^C + \dots \\ & + c_1 \bar{\psi}^{(n-1)-} (\psi^{(n-1)+})^C \Big) + \text{h.c.} \end{aligned} \tag{2.21}$$

where we recall that the neutral state corresponds to $k = n = I + 1/2$, and all states receive a mass correction except the highest charge one, ψ^{n+}. Also, $\mu_M = \frac{\kappa_M v^2}{4\Lambda}$. For the neutral state, the mass matrix can be written in a Majorana form as follows:

$$-\frac{1}{2} \begin{pmatrix} (\bar{\psi}^0)^C & \bar{\psi}^0 \end{pmatrix} \begin{pmatrix} m_D - 1/2\mu_D & c_{I+1/2}\mu_M \\ c_{I+1/2}\mu_M & m_D - 1/2\mu_D \end{pmatrix} \begin{pmatrix} (\psi^0)^C \\ \psi^0 \end{pmatrix} , \tag{2.22}$$

whose eigenstates (Majorana fermions) are

$$m^0_{1/2} = m_D - \frac{1}{2}\mu_D \pm c_{I+1/2}\mu_M \,, \qquad c_{I+1/2} = I + 1/2 \,. \tag{2.23}$$

Note that $c_{I+1/2}$ is the largest coefficient in the generators. This implies that, in the absence of μ_D, the lightest state will always be neutral, independently on the sign of μ_D. For the charged states, the mass matrix can be written as

$$-\frac{1}{2} \begin{pmatrix} \bar{\psi}^{(n-k)+} & (\bar{\psi}^{(n-k)-})^C \end{pmatrix} \begin{pmatrix} m_D + (I-k)\mu_D & c_k \mu_M \\ c_k \mu_M & m_D - (I-k+1)\mu_D \end{pmatrix} \begin{pmatrix} \psi^{(n-k)+} \\ (\psi^{(n-k)-})^C \end{pmatrix} + \text{h.c.} \tag{2.24}$$

The mass eigenstates read

$$m^{(n-k)}_{1/2} = m_D - \frac{1}{2}\mu_D \pm \sqrt{(I-k+1/2)^2 \mu_D^2 + c_k^2 \mu_M^2} \,. \tag{2.25}$$

This implies that there exist a neutral state lighter that the charged ones as long as

$$c_{I+1/2}^2 \mu_M^2 > (I-k+1/2)^2 \mu_D^2 + c_k^2 \mu_M^2 \;\; \forall\, k = 1, \ldots I - 1/2\,. \tag{2.26}$$

The above inequalities imply

$$\mu_M^2 > \xi_I \mu_D^2\,, \quad \xi_I = \text{Max}\left(\frac{I-k+1/2}{k^2 - 2Ik + (I+1/2)^2}\right)\,. \tag{2.27}$$

The largest charge state, which does not receive a mass correction from κ_M, also provides a bound for $\mu_D < 0$, as $m^{n+} = m_D + I\mu_D$, thus

$$|\mu_M| > -\mu_D\,. \tag{2.28}$$

To summarise we have found that a Majorana neutral state is guaranteed to be the lightest for

$$|\mu_M| > \begin{cases} -\mu_D & \text{for } \mu_D < 0\,; \\ \sqrt{\xi_I}\mu_D & \text{for } \mu_D > 0\,; \\ 0 & \text{for } \mu_D = 0\,. \end{cases} \tag{2.29}$$

As a reference, we numerically find:

$$\xi_{1/2} = 0\,, \quad \xi_{3/2} = 1/2\;(k=1)\,, \quad \xi_{5/2} = 2/5\;(k=1)\,, \quad \xi_{7/2} = 1/3\;(k=2)\,,$$
$$\xi_{9/2} = 2/7\;(k=3)\,, \quad \xi_{11/2} = 1/4\;(k=3,4)\,, \ldots \tag{2.30}$$

2.2.4 Direct Detection

Here, we will focus on spin-independent scattering only, as the experimental sensitivity to such operators is far greater than spin-dependent interactions. One loop level direct detection in single (non-chiral) multiplet DM models has been considered by several papers [97, 90, 98]. In [90], only scalar current type interactions were considered, whereas in [97] a sizable suppression was shown through cancellations with Twist-2 operators. Here we will extend these results to include the case of pure Dirac DM ($Y = 0$ only, otherwise tree-level scatterings would rule this out), and also consider the effect of the mass gap between DM and its partners that propogate inside the loops. The relevant interaction Lagrangians are given by

$$\Delta\mathcal{L}_{Dirac} = \left[\frac{g_2}{2\sqrt{2}}\sqrt{n^2-1}\bar{D}^0\gamma^\mu D^- W_\mu^+ + \frac{g_2}{2\sqrt{2}}\sqrt{n^2-1}\bar{D}^0\gamma^\mu D^+ W_\mu^- + h.c\right]$$

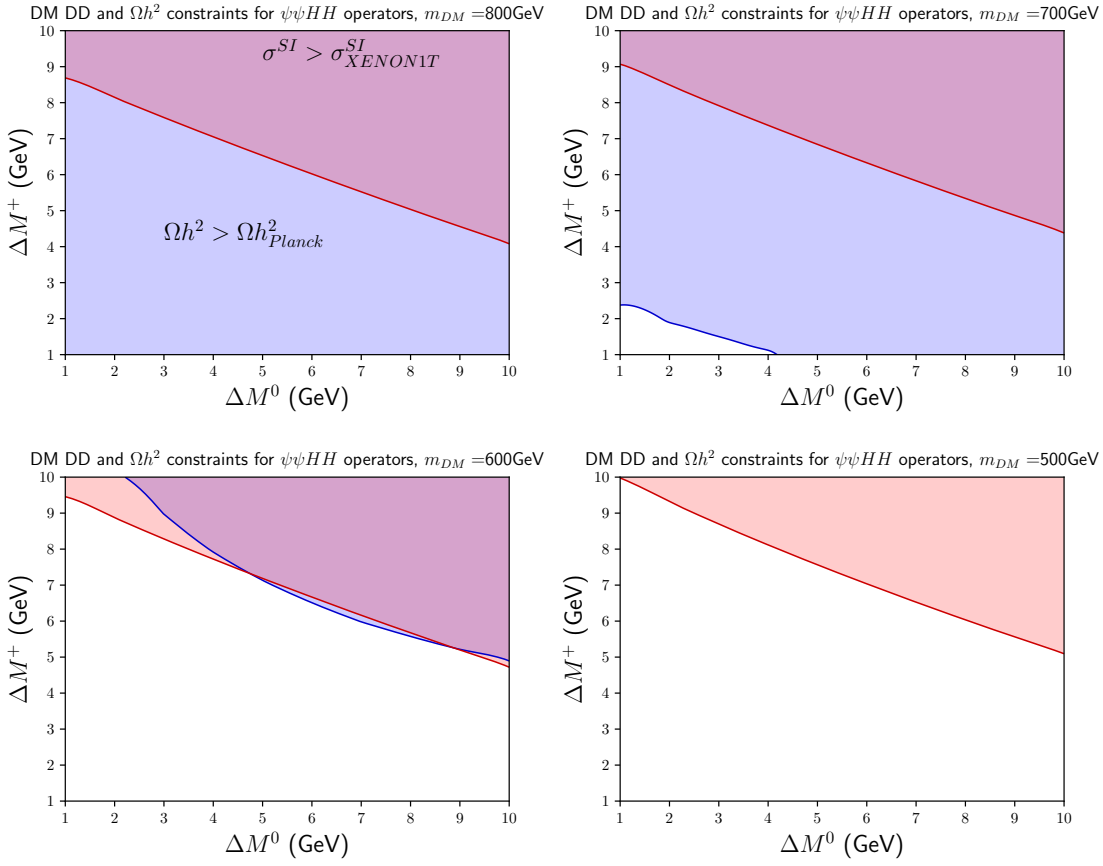

FIGURE 2.2

If a Dirac fermion D^0 is split into two Majorana fermions via some higher scale physics, i.e $D^0 \to (\chi^0_1 + i\chi^0_2)/\sqrt{2}$ such that χ^0_1 is sufficiently lighter to prevent tree-level inelastic scattering via Z boson (when mass split larger than $\mathcal{O}(10)keV$), and is the DM candidate,

$$\Delta\mathcal{L}_{PseudoDirac} = \left[\frac{g_2}{4}\sqrt{n^2-(2Y+1)^2}\bar{\chi}^0_1\gamma^\mu D^- W^+_\mu + \frac{g_2}{4}\sqrt{n^2-(2Y-1)^2}\bar{\chi}^0_1\gamma^\mu D^+ W^-_\mu + h.c\right] + \frac{ig_2(-Y)}{c_W}\bar{\chi}^0_1\gamma^\mu\chi^0_2 Z^0_\mu$$

A pure majorana multiplet is also possible (constructed from a multiplet of single Weyl fermions), in this case Y=0:

$$\Delta\mathcal{L}_{Majorana} = \left[\frac{g_2}{2\sqrt{2}}\sqrt{n^2-1}\bar{\chi}^0\gamma^\mu\chi^- W^+_\mu + \frac{g_2}{2\sqrt{2}}\sqrt{n^2-1}\bar{\chi}^{0^c}\gamma^\mu(\chi^-)^c(W^+_\mu)^c + h.c\right]$$

For the most general, Dirac case, D^+ and D^- are distinct particles ($\bar{D}^\pm$ is used to refer to their respective antiparticles), where D^- disappears for the doublet. As

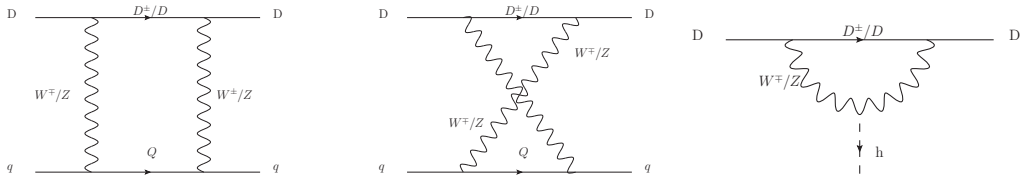

FIGURE 2.3: Loop diagrams for DM direct detection, labelled A,B,C from left to right.

such, a DM particle(antiparticle) will couple to:

(a) up(down)-type quarks via diagram A containing a $D^+(\bar{D}^+)$ or diagram B containing a $D^-(\bar{D}^-)$

(b) down(up)-type quarks via diagram A containing a $D^-(\bar{D}^-)$ or diagram B containing a $D^+(\bar{D}^+)$

(c) all quarks by diagrams A, B (when two Z bosons are exchanged) and C

We will label the particle loop functions, A_q^i and B_q^i where i refers to the charge of the DM partner running in the loop and q to the type of external quark spinor contained within these expressions. After removing the Lorentz structures not relevant to spin independent scattering cross sections, each of these loop functions may be expressed in terms of five Lorentz structures (this may be seen in appendix A.2. Note here that the spinor/antispinors contained within A,B are implicit, and should be chosen such to match the external particle.

In the limit of small quark momenta, assuming that internal quark masses are similar to external we derive the effective Lagrangian 2.31. This Lagrangian coefficients are given for the Pseudo-Dirac case, analogous to the calculation performed in [97], however modification for other cases involves a trivial modification of the couplings and spinors. Spinors for DM here are represented by the first pair of angular brackets in each term, whilst quark spinors are represented by the second pair.

$$\mathcal{L} = X_A < 1 >< 1 > + X_B < p^\mu p^\nu > [\mathcal{O}_{\mu\nu}] + X_C < \gamma^\mu p^\nu > [\mathcal{O}_{\mu\nu}] + f_G < 1 > G^a_{\mu\nu} G_a^{\mu\nu} \tag{2.31}$$

Where these coefficients are given by equation 2.32, where $\Pi^i_\alpha \equiv \Pi_\alpha(a_V^{q,(i)}, a_A^{q,(i)}, x^i, y^i)$ with $x^i \equiv m^2_{V^i}/m^2_D$, $y^i \equiv (m_{D^i} - m_D)/m_D$. The vector and axial couplings for the quarks are given by $a_V^{q,(\pm)} = \frac{1}{2}T_{3q} - Q_q \sin^2\theta_W$, $a_V^{q,(\pm)} = -\frac{1}{2}T_{3q}$, $a_V^{q,(0)} = a_A^{q,(0)} = \frac{1}{2}$.

$$
\begin{aligned}
X_A &= X_{tri} + \frac{\alpha_2^2 Y^2}{4c_W^4}\Pi_A^{0_2} + \frac{\alpha^2}{32}\Big[(n^2-(2Y+1)^2)\Pi_A^- + (n^2-(2Y-1)^2)\Pi_A^+\Big] \\
X_B &= \frac{\alpha_2^2 Y^2}{4c_W^4}\Pi_B^{0_2} + \frac{\alpha_2^2}{64}\Big[(n^2-(2Y+1)^2)\Pi_B^- + (n^2-(2Y-1)^2)\Pi_B^+\Big] \\
X_C &= \frac{\alpha_2^2 Y^2}{4c_W^4}\Pi_C^{0_2} + \frac{\alpha_2^2}{64}\Big[(n^2-(2Y+1)^2)\Pi_C^- + (n^2-(2Y-1)^2)\Pi_C^+\Big]
\end{aligned} \tag{2.32}
$$

where in the limit of zero mass splits between DM and the internal propagating partners we arrive at equation 2.33, which agrees with Ref [97].

$$
\begin{aligned}
X_A &= \frac{\alpha^2 m_q}{4m_h^2}\left[\frac{(n^2-(4Y^2+1))}{8m_W}g_H(w) + \frac{Y^2}{4c_W^4 m_Z}g_H(z)\right] + \frac{m_q}{m_Z^3}\frac{\alpha_2^2 Y^2}{c_W^4}(a_A^2-a_V^2)g_s(z) \\
X_B &= \frac{2}{m_D^2 m_Z^3}\frac{\alpha_2^2 Y^2}{c_W^4}(a_A^2+a_V^2)g_{T2}(z) + \frac{\alpha_2^2}{8m_D^2 m_W^3}(n^2-(4Y^2+1))g_{T2}(w) \\
X_C &= \frac{2}{m_D m_Z^3}\frac{\alpha_2^2 Y^2}{c_W^4}(a_A^2+a_V^2)g_{T1}(z) + \frac{\alpha_2^2}{8m_D m_W^3}(n^2-(4Y^2+1))g_{T1}(w)
\end{aligned} \tag{2.33}
$$

where the contribution from diagram C is given by (see appendix A.2) for details.

$$
X_{tri} = \frac{\alpha^2 m_q}{2m_h^2}\left[\frac{(n^2-(1+2Y)^2)}{16m_W}\Delta^- + \frac{(n^2-(1-2Y)^2)}{16m_W}\Delta^+ + \frac{Y^2}{4c_W^4 m_Z}\Delta^0\right]
$$

The notation Δ^i is used to refer to loop function $\Delta(x^i, y^i)$. In the limit of no mass split, $\lim_{y\to 0}\Delta^i = g_H(x)/2$, in agreement with [97].

The two loop result for coupling to gluons (fG in equation 2.31) is not derived here, but taken from [97] (and given for completeness in appendix A.2). The operator with coefficient X_C is the dominant contribution, and is of opposite sign to other operators. This leads to a cancellation that was not observed in [90], which only computed the scalar-scalar current terms (i.e those proportional to X_A).

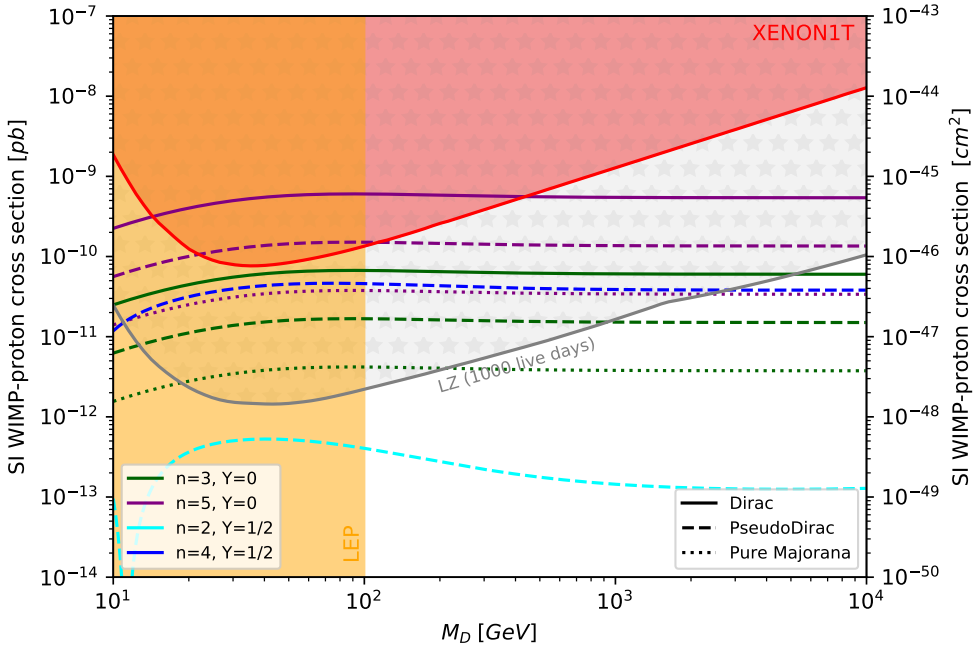

FIGURE 2.4: The spin-independent WIMP-proton cross section for a single fermion multiplet, for surviving cases $n \leq 5$ for which the neutral component is the lightest

In figure 2.4 (calculated assuming internal DM partner masses $= m_D$), we see that although the models plotted evade current limits for the most part, the next generation experiment LZ [50] will severely restrict the possibilities for single multiplet models. There is an additional caveat; DM from this source could not make up 100% of the DM abundance (100% relic is achievable at masses 1-10TeV for the models considered here). Further refinement of this calculation would require consideration of realistic mass splits generated from either electroweak corrections or dim-5 operators to the Higgs. An initial exploration of the loop functions behaviour with this split is given in Appendix A.2.

2.3 Fermionic Dark Matter with one additional multiplet

In this section, we present the classification of the models that contains one additional multiplet (mediator multiplet), in addition to the the DM one. The mediator multiplet can be either odd or even under the symmetry protecting the stability of DM candidate, and its quantum numbers are limited (and defined) by the requirement of the renormalisability and gauge invariance of its interaction with DM multiplet. We use different labels $F/\tilde{F}$ and $M/\tilde{M}$ for Dirac and Majorana fermion multiplets respectively since they could define quite different models when mediator is present as we discuss below.

2.3.1 Even scalar mediator ($\tilde{F}^I_Y S^{I'}_{Y'}$ and $\tilde{M}^I_0 S^{I'}_0$).

The case of a scalar mediator that couples to the SM has been one of the first models considered in simplified scenarios (see e.g. [99, 100, 101]), however it has been by now established that it is not simple nor minimal to achieve phenomenologically relevant models once the simplified case is included in a fully gauge-invariant model [102]. In particular, couplings to SM fermions are hard to obtain without breaking the EW symmetry, while couplings to gauge bosons only arise at dim–5 operator level unless the scalar is allowed to develop a non-zero vacuum expectation value. In the following, we will limit ourselves to the most minimal scenarios and not consider higher dimensional operators in this section.

The models we consider in this section include Yukawa coupling connecting two DM multiplets and (peudo)scalar mediator multiplet. They can be classified as follows (for the sake of minimality we consider multiplets with zero hypercharge, S^I_0, to be real):

D1 - $\Delta\mathcal{L}_{D1} = -y_{\psi 1}\,\Phi\,\bar{\Psi}\Psi$, where the scalar multiplet has $I' = 0, 1, \dots 2I$ and $Y' = 0$. This coupling preserves a U(1) global symmetry acting on the DM multiplet. The scalar multiplet S^I_0 is a real CP-even multiplet.

D2 - $\Delta\mathcal{L}_{D2} = -iy_{\psi 2}\,\Phi\,\bar{\Psi}\gamma^5\Psi$, where the presence of the γ^5 implies simply that Φ is a real CP-odd multiplet.

D3 - $\Delta\mathcal{L}_{D3} = -y_{\psi 3}\,\Phi\,\bar{\Psi}^c\Psi + h.c.$, where the scalar multiplet has $Y' = 2Y$ and $I' = 0, 2, \dots 2I$ for I integer, and $I' = 1, 3, \dots 2I$ for I semi-integer. If $Y \neq 0$, the global U(1) can be extended by giving charge -2 to the scalar multiplet (the latter charge assignment could be forbidden by linear couplings to the SM, thus only a $\mathbb{Z}_2$ acting on the DM multiplet would survive). For $Y = 0$, we can still define a $\mathbb{Z}_4$ under which $\Phi \to -\Phi$ and $\Psi \to i\Psi$ (this can be broken to a dark $\mathbb{Z}_2$ in presence of linear couplings of the scalar, or a concomitant presence of D1/D2 couplings). This coupling is also allowed for a Majorana multiplet.

D4 - $\Delta\mathcal{L}_{D4} = -iy_{\psi 4}\,\Phi\,\bar{\Psi}^c\gamma^5\Psi + h.c.$ is similar to the previous one, except that the CP properties of the scalar are altered. This coupling vanishes for Majorana DM multiplets.

The properties of all the possible models are summarised in Table 2.2, where we identified four template scenarios with distinct properties. In the 4th and 5th columns ("DM sym." and "Ext. sym.", respectively), we list the largest symmetry allowed by the above Yukawa couplings, which could be broken by the couplings of the scalar mediator multiplet Φ to the SM. The last column contains the scalar mediators that can have linear (renormalisable) couplings to the SM.

Model	D1/D2	D3/D4	DM sym.	Ext. sym.	Ext. Charges	Linear to SM
$\tilde{F}_Y^I S_0^{I'}$	$\surd$	-	U(1)	-	-	S_0^0, S_0^1
$\tilde{F}_0^I$=int. $S_0^{I'}$=even	$\surd$	$\surd$	$\mathbb{Z}_2$	-	-	S_0^0
$\tilde{F}_0^I$=int. $S_0^{I'}$=even	-	$\surd$	$\mathbb{Z}_2$	$\mathbb{Z}_4$	$\Phi \to -\Phi$ $\Psi \to i\Psi$	S_0^0
$\tilde{F}_Y^I S_{2Y}^{I'}$	-	$\surd$	$\mathbb{Z}_2$	U(1)	$\Phi \to e^{-2qi}\Phi$ $\Psi \to e^{iq}\Psi$	S_1^1, S_2^0
$\tilde{M}_0^I S_0^{I'}$=even	-	$\surd$	$\mathbb{Z}_2$	-	-	S_0^0

TABLE 2.2: Classification of models with a scalar even mediator multiplet. The extended symmetry in the fifth column refers to charges assigned to the scalar multiplet, as shown in the sixth column. In the last column we highlight scalar multiplets that allow for linear couplings to the SM that break the extended symmetry.

The most general Lagrangians, for the real and complex scalar multiplets, read:

$$\Delta\mathcal{L}_{S_0^I} = \tfrac{1}{2}(D_\mu\Phi)^2 - V(\Phi) - \tfrac{1}{2}\lambda\,(\Phi^2)(\phi_H^\dagger\phi_H) + V_{\text{linear}}\,, \tag{2.34}$$

$$\Delta\mathcal{L}_{S_Y^I} = |D_\mu\Phi|^2 - V(\Phi) - \lambda\,(\Phi^\dagger\Phi)(\phi_H^\dagger\phi_H) - \lambda'\,(\Phi^\dagger T^a\Phi)(\phi_H^\dagger\tau^a\phi_H) + V_{\text{linear}}\,; \tag{2.35}$$

where $V(\Phi)$ is a generic potential for the scalar. Note that for the real case, only one Higgs-portal coupling is allowed due to the fact that Φ has integer isospin and T^a must be anti-symmetric matrix. The term V_{linear} contains eventual linear couplings of Φ to a SM operator, which can be made of the Higgs field or of leptons. Only 5 such cases occur[4]:

$$S_0^0 \;\Rightarrow\; V_{\text{linear}} = -\mu_{00}\,\Phi\,\phi_H^\dagger\phi_H\,,\ \text{(CP-even)}\,; \tag{2.36}$$

$$S_0^1 \;\Rightarrow\; V_{\text{linear}} = -\mu_{10}\,\Phi^a\,\phi_H^\dagger\tau^a\phi_H\,,\ \text{(CP-even)}\,; \tag{2.37}$$

$$S_1^1 \;\Rightarrow\; V_{\text{linear}} = -\mu_{11}\,\Phi^a\,\phi_H^\dagger\tau^a\phi_H^\dagger + \text{h.c.}\,; \tag{2.38}$$

$$S_2^0 \;\Rightarrow\; V_{\text{flinear}} = -\xi_{02}\,\Phi\,\bar{e}_R^c e_R\,; \tag{2.39}$$

$$S_1^1 \;\Rightarrow\; V_{\text{linear}} = -\xi_{11}\,\Phi^a\,\bar{l}_L^c\tau^a l_L\,. \tag{2.40}$$

The linear Higgs portal coupling, allowed only for CP–even S_0^0 and S_0^1 and for the charged iso-triplet S_1^1, necessarily implies that the scalar meditator will acquire a vacuum expectation value via the Higgs one, thus a universal coupling to SM fermions is generated via the mixing with the physical Higgs boson [103, 104]. However, this mixing is strongly suppressed in the triplet cases because of

[4]Note here that subscript L,R refer to the chirality of particle or gauge multiplet it is assigned to

three–level contributions to the ρ parameter, while in the singlet case milder (but still important) bounds derive from the measurement of the 125 GeV Higgs couplings [105]. This shows that the couplings of the scalar mediator to SM fermions and gauge bosons are deemed to be small.

The only exception is due to the direct couplings to leptons: the doubly-charged scalar S_2^0 in equation (2.39) and the triplet S_1^1 in equation (2.40). The latter corresponds to type-II see-saw models [106, 107, 108] for neutrino mass generation, and it has been studied in connection to DM in Refs [109, 110, 111, 112]. The former also contributes to neutrino masses, as it breaks lepton number by two units, and it has been studied in Ref. [113] paired with a scalar DM multiplet.

We finally note that a vacuum expectation value for the scalar mediator can be induced in all cases, in particular via the quartic coupling to the Higgs field, and with all the limitations and bound described above. The phenomenology of such cases follow the analyses done in the simplified models [114, 115].

There is, however, a new class of mediators that arise from our classification: scalar mediators that only have bilinear couplings to the SM Higgs field. Such models have new interesting features that we will study in detail in the next section. For now, we content ourselves to classify the relevant models:

(a) *Accidental stability:* the scalar mediator multiplet can be accidentally stable if all linear couplings to the SM are forbidden, and it is lighter than the fermionic DM multiplet. This case may occur in models $\tilde{F}_Y^I S_0^{I'}$ (U(1) DM) and $\tilde{M}_0^Y S_0^{I'}$ ($\mathbb{Z}_2$ DM) for the case when S_0 is CP-odd or when S_0 is CP-even and $I = 1$ (i.e. DM is the EW singlet). In case, when $I \neq 0$, at one loop level, couplings of $S_0^{I'}$ to the SU(2)$_L$ gauge bosons are generated which makes $S_0^{I'}$ unstable. In addition, the presence of the coupling to the scalar mediator multiplet does not affect the mass spectrum of the DM multiplet: this implies that models with $Y \neq 0$ are excluded by Z-mediated direct detection, while $Y = 0$ models with $I \geq 3$ are ruled out by direct detection experiments due to the loop-induced processes (as we have shown in section 2.2.4 and in particular in figure 2.4) due to the small mass split, which is only induced by the EW loops. The only model that avoids this exclusion is $\tilde{F}_0^0 S_0^0$ with coupling D2 (i.e. CP–odd mediator). [5]

(b) *Stability protected by $\mathbb{Z}_4$:* in models with an extended $\mathcal{Z}_4$ symmetry, i.e. $\tilde{F}_0^I S_0^{I'}$ ith couplings D3/D4, the stability of the mediator is guaranteed by a discrete charge. Like for case α), direct detection bounds cannot be avoided, thus the only surviving case involves gauge singlets, $\tilde{F}_0^0 S_0^0$ with D4.

(c) *Stability protected by U(1):* similarly, stability can be guaranteed by a U(1) symmetry in $\tilde{F}_Y^I S_{2Y}^{I'}$ models. In such cases, however, the fact that $Y \neq 0$ requires that a Majorana mass split is generated in the neutral DM fermionic

[5] For $\tilde{M}_0^0 S_0^0$, the scalar mediator is CP–even, thus linear coupling to the Higgs cannot be forbidden.

candidate. This can only be achieved in models $\tilde{F}^I_{1/2}S^1_1$ with the couplings in equation (2.38) included: this however explicitly breaks the U(1) symmetry and allows decays of the mediator. By integrating out S^1_1, or by a small vacuum expectation value, the same mass split induced by the Higgs operator discussed in Section 2.2.3.2 will arise. The only difference would be the presence of a coupling to a scalar mediator, which can affect the relic density computation.

We note that in all cases, direct detection from the fermionic DM candidate may be avoided if the dominant contribution to the relic density is coming from the stable scalar, however this case will best fit under a scalar DM multiplet study [116].

One should pay a special attention to constraints from the electroweak precision data, in particular from ρ_0 parameter [117] which is one in SM and measured with per-mille precision. In case of arbitrary number of SU(2) scalar multiplets ρ_0 takes the form (see equation(10.58) of in [118]):

$$\rho_0 = \frac{\sum_n [I_n(I_n+1) - I^2_{3n}]|v_n|^2}{2\sum_n I^2_{3n}|v_n|^2} \ , \tag{2.41}$$

where I_n, I_{3n} and v_n are isospin, the third component of the isospin and the vacuum expectation value of the n^{th} scalar multiplet respectively. So besides the cases with doublet and singlet, strong bounds from ρ can be avoided in several other cases, for example, in the model with septet scalar (S^3_2) [119] which would couple to DM quintuplet. The custodial symmetry is a symmetry which remains after EWSB which protects the ρ parameter, by the preservation of $SU(2)_L \otimes SU(2)_R$ (this may be achieved by adding a bimultiplet built from n $n$plets). This may also be achieved in models with custodial combinations like triplets in the Georgi-Machacek model ($S^1_0 + S^1_1$) [120]. This model would rather be the part of less minimal models, but still possibly quite interesting. From equation(2.41) one can see that the case $\tilde{F}^I_{1/2}S^1_1$ described in point (c) can better fit in a Georgi-Machacek scenario, where the triplet VEV is not too constrained. On the other hand for the scenario with a custodial violating triplet only, the coupling may be enough to generate a large enough mass split to avoid constraints from ρ_0.

To summarise this section, we found a new class of relevant minimal models with a scalar mediator that is (accidentally) stable: this includes a models with two singlets, $\tilde{F}^0_0 S^0_0$ with D2 or D4, which we study in more details in Section 2.4.

2.3.2 Odd scalar mediator ($\tilde{F}^I_Y \tilde{S}^{I'}_{Y'}$ and $\tilde{M}^I_0 \tilde{S}^{I'}_{Y'}$)

In this class of models, the DM fermion multiplet Ψ couples to the odd scalar φ and to a SM fermion via a Yukawa coupling: the quantum numbers of the scalar multiplet are, therefore, fixed by the properties of the chosen SM fermion. As the

SM fermions are chiral, one can classify two cases, distinguished by their chirality, a SU(2)$_L$ doublet, f_L, or a singlet, f_R:

- for left-handed SM fermions, the respective interactions read as:

$$\Delta\mathcal{L} = -h^i_{f_L}\ \varphi_{f_L}\bar{\Psi}_R f^i_L + h.c. \tag{2.42}$$

  thus $\varphi_{f_L} = \{I \pm 1/2, Y - Y_f\}$ (and an anti-triplet of QCD colour if f_L is a quark);

- for right-handed SM fermions:

$$\Delta\mathcal{L} = -h^i_{f_R}\ \varphi_{f_R}\bar{\Psi}_L f^i_R + h.c. \tag{2.43}$$

  thus $\varphi_f = \{I, Y - Y_f\}$ (and an anti-triplet of QCD colour if f_R is a quark).

Note that $i = 1, 2, 3$ is a SM family index, and the two types of couplings cannot co-exist with the same multiplet in the minimal models. In other words, the couplings of the mediator necessarily involve one chirality and only one type of SM fermions. The scalar multiplet will also have couplings to the Higgs [91], in the form analogous to that of Eqs (2.34) or (2.36), but with the absence of any linear coupling forbidden by the DM parity. As the cases of quarks and leptons have quite different physics, we will discuss them in detail separately.

2.3.2.1 Quark-type mediators

Firstly, as $\varphi_{q_{L/R}}$ carries QCD charges, the scalars cannot contribute significantly to the DM relic density, thus they are expected to always be heavier than the DM fermion candidate. Therefore, they should be heavier than DM and generically Also, generically, these interactions will not affect DM direct detection bounds since the contribution will come from Z-couplings or loop-induced couplings. Thus the only safe cases involve $\tilde{F}^0_0$ and $\tilde{M}^0_0$, for which the scalar mediator has the same quantum numbers as the corresponding SM fermion. This case is a template of supersymmetry ($\varphi_{q_{L/R}}$ being one of the squarks), and has been studied in detail in the simplified model with φ_{q_L} mediator and Majorana DM [121].

2.3.2.2 Lepton-type mediators

In this case, the scalar multiplet may contain a neutral state which therefore plays the role of DM (this case will be covered in a future work). In the case where the DM arises form the fermionic multiplet, we can apply the same consideration as for the quark case to direct detection, so that the only safe case involves $\tilde{F}^0_0$ and $\tilde{M}^0_0$. This case will also correspond to the supersymmetry template with sleptons, and has been covered in Ref [122].

2.3.3 Even fermion mediator ($\tilde{F}^I_Y F^{I'}_{Y'}$)

This case does not allow for renormalisable couplings between the mediator and the DM multiplet, however we list it here for completeness and because it leads to interesting new models of leptophilic DM. The only allowed coupling involved one mediator multiplet, Σ, and three DM multiplets Ψ. In turn, the even multiplet Σ need to couple to the SM via a Yukawa-type coupling to leptons (quarks are excluded to avoid QCD charged DM).

The DM mediator coupling comes from a dim–6 operator:

$$\mathcal{L} \supset \frac{1}{\Lambda^2}(\bar{\Psi}^c\Psi)(\bar{\Psi}^c\Sigma) + \text{h.c.} \tag{2.44}$$

which preserves a $\mathbb{Z}_3$ DM parity for a complex Dirac multiplet $\tilde{F}^I_Y$. [6] Moreover, the hypercharges are related by:

$$Y' = -3Y\,. \tag{2.45}$$

The last relation imposes a significant constraint on the mediator multiplet, as the hypercharge of the DM one needs to be semi-integer for semi-integer isospin, and integer for integer isospin.

As a consequence, the only allowed cases (with Yukawa couplings to leptons) are:

$$\text{Class A:} \qquad \Delta L = -\xi_L\, \bar{l}_L \phi_H^\dagger \Sigma + \text{h.c.}\,; \qquad \tilde{F}^{I=\text{int.}}_0 F^{0,1}_0\,; \tag{2.46}$$

$$\text{Class B:} \qquad \Delta L = -\xi_R\, \bar{l}_R \phi_H \Sigma + \text{h.c.}\,; \qquad \tilde{F}^{I=\text{semi–int.}}_{1/2} F^{1/2}_{-3/2}\,. \tag{2.47}$$

Due to direct detection constraints, and the role played by gauge interactions in the thermal relic abundance (which would make the mediator irrelevant), the only interesting case appears for a singlet DM, $\tilde{F}^0_0 F^0_0$, which belongs to class A. Note that Σ is effectively a heavy right-handed neutrino. The relic density will thus be determined by the processes:

$$\Psi\Psi \leftrightarrow \bar{\Psi}\nu\,, \quad \Psi\Psi \to \bar{\Psi}\nu h\,. \tag{2.48}$$

If the coupling to SM is very small, being related to neutrino mass generation, then this could be an effective FIMP model.

2.3.4 Odd fermion mediator ($\tilde{F}^I_Y \tilde{F}^{I'}_{Y'}$, $\tilde{M}^I_0 \tilde{F}^{I'}_{1/2}$ and $\tilde{F}^I_{1/2} \tilde{M}^{I'}_0$)

Here we can comment on the general structure, and discuss how integrating out one of the multiplets generates the dim-5 couplings to the Higgs discussed in

[6] For Majorana DM multiplets, the $\mathbb{Z}_3$ would be broken by the mass term. Furthermore, a coupling in the form $(\bar{\Psi}\Psi)(\bar{\Psi}\Sigma)$ does not preserve any DM parity nor U(1) charge.

the previous section. We can classify the matching between models and Higgs couplings.

In the case of the odd fermionc mediators, the only renormalisable coupling is a Yukawa with the Higgs boson. In general, therefore, the DM state will be the lightest mass eigenstate from the neutral components of the two multiplets. Notable examples of this class of models come from SUSY, where the lightest neutralino can be a mixture of bino-Higgsino ($\tilde{M}_0^0 \tilde{F}_{1/2}^{1/2}$) or wino-Higgsino ($\tilde{M}_0^1 \tilde{F}_{1/2}^{1/2}$). Note that in our notation the first multiplet is the one that has the largest component in the DM physical state.

The possible models can be classified based on the form of the Yukawa coupling:

$$\begin{aligned} \Delta\mathcal{L} &= -\lambda\, \bar{\Psi}' \varphi \Psi + \text{h.c.}\,, \\ &\quad \text{with } \; I' = I \pm 1/2 \;\text{ and }\; \begin{cases} Y' = Y + 1/2 \;\text{ if }\; \varphi = \phi_H\,, \\ Y' = Y - 1/2 \;\text{ if }\; \varphi = \tilde{\phi}_H \equiv (i\sigma^2)\phi_H^*\,, \end{cases} \end{aligned} \tag{2.49}$$

where in our convention Ψ' indicates the mediator multiplet. Note that the Higgs field may appear as is, or in the form of the complex conjugate $\tilde{\phi}_H$. Also, either the mediator or the DM multiplet can be of Majorana nature if either $Y' = 0$ or $Y = 0$. In general, this class of mediator models have similar features as the simple DM multiplet cases, with an additional coupling to the Higgs boson that could make direct detection more critical.

One point of interest, though, is the fact that in the case of large mediator mass, i.e. $M' \ll m$, by integrating the mediator multiplet one can generate the dim–5 couplings to the Higgs discussed in Sec. 2.2.3. In the case of Dirac multiplets, the coefficient of equation (2.10) are matched to the Yukawa coupling and mediator mass M' as

$$\frac{\kappa}{\Lambda} = \pm\epsilon \frac{\lambda^2}{M'} \frac{2}{2I+1}\,, \quad \frac{\kappa'}{\Lambda} = \frac{\lambda^2}{M'} \frac{1}{2} \left(1 \pm \frac{1}{2I+1}\right)\,, \quad \text{for } \; I' = I \pm \frac{1}{2}\,; \tag{2.50}$$

where $\epsilon = -1$ if $\tilde{\phi}_H$ appears in the Yukawa in equation (2.49) (and $\epsilon = 1$ otherwise). If the mediator is a Majorana multiplet, then only the coupling in equation (2.19) is generated, with

$$\frac{\kappa_M}{\Lambda} = \pm\epsilon \frac{\lambda^2}{M'} \frac{2}{2I+1}\,, \quad \text{for } \; I' = I \pm \frac{1}{2}\,. \tag{2.51}$$

2.3.5 Even vector mediators ($\tilde{F}_Y^I V_0^{I'}$ and $\tilde{M}_0^I V_0^{I'}$)

Vector mediators are very popular in the simplified model approach to DM phenomenology [123, 124], mainly because they allow for "gauge invariant" couplings to vector current of SM fermions. Nevertheless, it is not a simple task to find a consistent, truly gauge invariant, renormalisable model containing vector

mediator multiplets. As the vector multiplet couples to a current containing the DM multiplet, its isospin and hypercharge are required to be:

$$\Delta\mathcal{L}_V = V_\mu\,\bar{\Psi}\gamma^\mu(g_{VL}P_L + g_{VR}P_R)\Psi\,, \qquad \text{with } I' = 0,\dots 2I\,,\ \ Y' = 0\,; \tag{2.52}$$

where $P_{L/R}$ are chirality projectors. As the hypercharge always vanish (and the isospin is integer), we can always consider real multiplets.

For a generic vector field V_μ, the most general Lagrangian up to renormalisable couplings reads:

$$\begin{aligned}\mathcal{L}_{V_0^{I'}} \;=\;& \frac{1}{2}(D_\mu V_\nu - D_\nu V_\mu)^2 - \frac{1}{2}M_V^2 V^\mu V_\mu + \xi_2\, W^a_{\mu\nu}(V_\mu T^a_{I'} V_\nu) + \text{self int.}\\ &+ \sum_{f\in\text{SM}} V_\mu\,\bar{f}\gamma^\mu(g^f_{VL}P_L + g^f_{VR}P_R)f + g_{VH}V_\mu\,\left(\phi_H^\dagger(D^\mu\phi_H) - (D^\mu\phi_H^\dagger)\phi_H\right)\\ &+\lambda_0\,(V_\mu V^\mu)\phi_H^\dagger\phi_H + \lambda_1\,(V_\mu T^a_{I'}V^\mu)\phi_H^\dagger\tau^a\phi_H\,,\end{aligned} \tag{2.53}$$

where $W^a_{\mu\nu}$ is the energy-stress tensor of $\text{SU}(2)_L$. The second line contains couplings to currents of SM fermions and the Higgs field, compatibly with the quantum numbers of the vector multiplet: they are allowed only for the singlet V_0^0 and a triplet V_0^1. For larger isospin, couplings mediating the decay of the vector multiplet in SM states can only be generated at loop level.

While the Lagrangian in equation (2.53) seems renormalisable and consistent, it needs the presence of additional states. In Ref. [125] it has been shown that the self-interactions of the multiplet can be fixed in order to preserve perturbative unitarity in the scattering amplitude of vector multiplets, however Ref. [126] later showed that violation of perturbative unitarity occur once the vector multiplet couples to massive gauge bosons (i.e. it is charged under a broken gauge group, like $\text{SU}(2)_L$) and/or to the Higgs: thus new states need to be included in order to restore the consistency of the model. They might thus affect the low energy properties of the theory by introducing phenomenologically relevant operators. In theories of this kind, the vector mediator may arise as a composite spin-1 meson of a confining strong dynamics, like in models of composite Goldstone Higgs.

One way to avoid these issues is to introduce the vector multiplet as a gauge field: in general, though, a vector carrying isospin needs to come from a model where the gauge symmetry $\text{SU}(2)_L$ is extended and broken at higher scales. Now, generating the couplings to the SM fermions becomes the challenge, as new fermions are likely to be needed in order to complete multiplets of the extended EW gauge symmetry. Note that here the chiral nature of the SM fermions is the main obstacle, as it may imply the presence of other chiral fermions.

One case that does not suffer from such problem is the singlet, V_0^0, as it could arise from a broken gauged U(1) symmetry under which the SM fermions are charged.

Once again, though, a consistent theory would require an anomaly-free U(1), thus either additional charged heavy states are added, or one has very limited choices.

2.3.6 Odd vector mediators ($\tilde{F}_Y^I \tilde{V}_{Y'}^{I'}$)

In the case of odd vector mediators, the only allowed couplings must involve the DM multiplet and a SM fermion. The classification of mediators, therefore, follows the same as the scalar odd mediators in Sec. 2.3.2:

- for left-handed SM fermions, the coupling reads:

$$\Delta\mathcal{L} = g^i_{Vf_L}\, V^\mu_{f_L} \bar{\Psi}_L \gamma_\mu f^i_L + h.c. \tag{2.54}$$

  thus $V_{f_L} = \{I \pm 1/2, Y - Y_f\}$ (and an anti-triplet of QCD colour if f is a quark);

- for right-handed SM fermions:

$$\Delta\mathcal{L} = g^i_{f_R}\, V^\mu_{f_R} \bar{\Psi}_R \gamma_\mu f^i_R + h.c. \tag{2.55}$$

  thus $V_{f_R} = \{I, Y - Y_f\}$ (and an anti-triplet of QCD colour if f is a quark).

As the mediator typically has non-zero hypercharge, the Lagrangian (2.53) needs to be extended:

$$\begin{aligned}\mathcal{L}_{\tilde{V}^{I'}_{Y'}} \;=\; & |D_\mu V_\nu - D_\nu V_\mu|^2 - M_V^2 V_\mu^\dagger V^\mu + \xi_1\, B_{\mu\nu}(V_\mu^\dagger V_\nu) + \xi_2\, W^a_{\mu\nu}(V_\mu^\dagger T^a_{I'} V_\nu) \\ & + \xi_3\, G^c_{\mu\nu}(V_\mu^\dagger \lambda^c V_\nu) + \text{self int.} + \lambda_0\,(V_\mu^\dagger V^\mu)\phi_H^\dagger \phi_H \\ & + \lambda_1\,(V_\mu^\dagger T^a_{I'} V^\mu)\phi_H^\dagger \tau^a \phi_H\,. \end{aligned} \tag{2.56}$$

Similarly to the case of even mediators, the above Lagrangian cannot be complete because of perturbative unitarity violation or the need to extend the gauge symmetries of the SM to generate $\tilde{V}$ as a gauge boson.

2.4 Phenomenology of a new representative model: $\tilde{F}_0^0 S_0^0$(CP-odd)

We would like to take a closer look at the $\tilde{F}_0^0 S_0^0$(CP-odd) model with a Dirac fermion singlet ($\Psi \equiv \psi$) and a pseudo-scalar (CP-odd) singlet ($\Phi \equiv a$) – probably the simplest two component DM model discussed in section 2.3. The Lagrangian of the dark sector, to be added to the SM one, reads:

$$\Delta\mathcal{L} = i\bar{\psi}\partial_\mu\gamma^\mu\psi - m_\psi\bar{\psi}\psi + \frac{1}{2}(\partial_\mu a)^2 - \frac{m_\Phi^2}{2}a^2 + i\mathcal{Y}_\psi a\bar{\psi}\gamma^5\psi - \frac{\lambda_{aH}}{4}a^2\phi_H^\dagger\phi_H - \frac{\lambda_a}{4}a^4\,, \tag{2.57}$$

Scenario	Y_ψ	λ_{aH}	DM thermal properties
A	$\mathcal{O}(10^{-3}-1)$	$\mathcal{O}(10^{-3}-1)$	ψ and a thermal with SM
B	$< \mathcal{O}(10^{-8})$	$\mathcal{O}(10^{-3}-1)$	ψ non-thermal, a thermal with SM
C	$\mathcal{O}(10^{-3}-1)$	$< \mathcal{O}(10^{-8})$	ψ and a thermal with each other, non-thermal to SM
D	$< \mathcal{O}(10^{-8})$	$< \mathcal{O}(10^{-8})$	ψ and a non-thermal with each other and SM

TABLE 2.3: Table of distinct phenomenological DM scenarios possible in this model.

where ϕ_H is the SM Higgs doublet field. The model contains three new couplings: the Yukawa coupling Y_ψ connecting the scalar mediator a to the fermion DM ψ, the a self-interaction λ_a and the quartic coupling to the Higgs λ_{aH}. The latter is the only coupling connecting the new sector to the SM via a Higgs portal. We recall that a linear coupling of a to the Higgs field is forbidden by CP. Invariance under CP is preserved as long as a does not develop a vacuum expectation value, i.e. if

$$m_a^2 = m_\Phi^2 + \frac{\lambda_{aH} v^2}{8} \geq 0\,, \quad \lambda_a > 0\,, \tag{2.58}$$

where m_a is the physical mass of the scalar particle. We will be working in this region of the parameter space. As ψ couples exclusively and bi-linearly to a, it is a stable fermionic DM candidate protected by a dark $U(1)$ global symmetry. The pseudo-scalar mediator a can only decay into a pair of DM fermions. Hence, if $m_a < 2m_\psi$, a is said to be "accidentally" stable and can contribute to the relic density as a second DM component. Decays of a into SM particles could be mediated by the gauge and CP invariant dimension-5 operator $ia\phi_H \bar{f}\gamma_5 f$ (where f is a SM fermion), which, depending on the size of the coupling, can make a unstable or metastable independently on its mass. However, this operator is not generated in our model at loop level, as it would require CP violation in the dark sector, which is not the case in this model. In fact, a only couples bilinearly to the SM via the Higgs portal and only CP violation can allow for a linear coupling of a to a SM operator. In this sense, it is the CP symmetry itself that prevents a from decaying into SM states.

The interesting dynamics of this model, where a is in touch with the SM via the Higgs portal coupling λ_{aH}, while ψ only interacts with a, leads to four distinct regimes of relevance for DM phenomenology, summarised in table 2.3:

- In scenario A, both fermion and pseudo-scalar can thermalise with the SM states. If $m_a \leq m_\psi$, then a is stable and contributes to the relic abundance. Conversely, if $m_a > 2m_\psi$, then it is unstable and merely acts as a mediator for the interactions of the fermionic DM to the SM.
- In scenario B, the relic abundance of ψ is driven by the freeze-in mechanism, while a contributes as a thermal DM component for $m_a < 2m_\psi$. However, for $m_a > 2m_\psi$, the smallness of Y_ψ can lead to a being metastable and decaying to (possibly warm) ψ.

- In scenario C, both new particles can freeze-in via their couplings to the SM (the coupling of ψ generated at loop level, as we will discuss below), before thermalisation between the two species. Depending on its mass, the pseudo-scalar a can either remain as a DM component, or decay promptly into the fermion DM ψ.
- In scenario D, both particles have very small couplings. While a can freeze-in via its coupling to the Higgs portal, the coupling of the fermion is too small and would lead to a negligible direct production. Depending on its mass, a can be the only significant DM candidate, or decay promptly to the fermion ψ after being produced in the early universe.

Note that any other range of the couplings is excluded by DM over-production (or loss of perturbativity). Furthermore, in scenarios C and D, direct and indirect detection experiments, as well as colliders, would be unable to observe either of these new particles due to the feeble couplings. In contrast, in scenarios A and B, a may be observable due to the sizeable Higgs portal coupling. In scenario A, the fermion may also be directly observables due to a loop-induced coupling to the Higgs, as we will discuss below.

Let us start the discussion of the model by presenting some generic phenomenological features of the new states, ψ and a. If a is stable, its DM fraction can be revealed via direct detection thanks to the following spin-independent (SI) elastic cross section on nuclei:

$$\sigma_a^{SI}(aN \to aN) = \frac{\lambda_{aH}^2 v^2 \lambda_N^2}{8\pi m_H^4} \frac{m_N^2}{(m_a + m_N)^2} \,. \tag{2.59}$$

where the nucleon form factors presented in section 2.2.4 are introduced via a nucleon effective coupling λ_N (N labels the nucleon type), given by

$$\lambda_N = \frac{m_N}{2v} \left[\sum_{q \in \{u,d,s\}} \frac{f_q^{(N)} m_q(\mu)}{m_q(\mu_{LHC})} + \frac{2}{27} f_G^{(N)} \sum_{q \in \{c,b,t\}} \frac{m_q(\mu)}{m_q(\mu_{LHC})} \right] . \tag{2.60}$$

The fermion ψ, which is always stable, couples to the SM only via the mediator a. A direct coupling to the Higgs boson is, however, generated at one loop level. The complete result is given in Appendix A.3.1. Here, we will present this contribution as an effective Yukawa coupling, δY, given by the following expression in the small a mass limit:

$$\mathcal{L}_{1-loop} \supset \delta Y \, H \, \bar{\psi}\psi \,, \quad \delta Y|_{m_a \to 0} \approx -\frac{Y_\psi^2 \lambda_{aH} v}{32\pi^2 m_\psi} \left(\ln \frac{m_\psi}{m_a} - 1 \right) . \tag{2.61}$$

For larger m_a, the loop-induced coupling decreases monotonically, with asymptotically $\delta Y \propto m_a^{-2}$ for large a masses. This coupling is only relevant when both Y_ψ and λ_{aH} are sizeable, and it contributes to direct detection via the following SI

cross section of ψ on nucleons:

$$\sigma_\psi^{SI}(\psi N \to \psi N) = \frac{4\delta Y^2 \lambda_N^2}{\pi m_H^4} \left(\frac{m_\psi m_N}{m_\psi + m_N} \right)^2 . \tag{2.62}$$

As an illustration, we show in figure 2.5 the SI cross section as a function of the masses, rescaled by the tree-level couplings. Knowing that the current direct detection limit is in the range $\sigma^{SI} < 10^{-9 \div 10}$ pb, we can infer that this process provides relevant limits only for relatively small ψ masses and couplings of order unity.

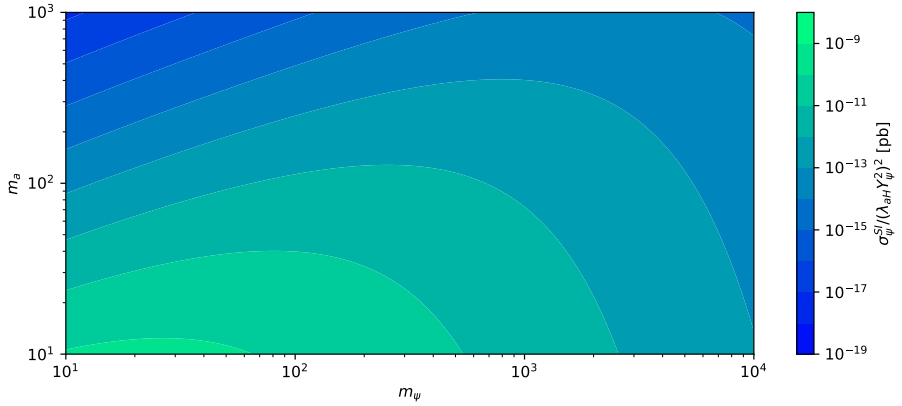

FIGURE 2.5: Loop-induced direct detection cross section for ψ scattering on nucleons σ_ψ^{SI}, scaled by the tree-level couplings $(\lambda_{aH} Y_\psi^2)^2$, as a function of the masses in GeV.

Another important constraint arises if the pseudo-scalar and/or the fermion are lighter than half the Higgs mass, i.e. $m_a,\ m_\psi < m_H/2$, thanks to the LHC limits on Higgs invisible decays. For the pseudo-scalar, the partial decay width is generated at tree-level:

$$\Gamma_{H\to aa} = \frac{\lambda_{aH}^2 v^2}{128\pi m_H} \sqrt{1 - \frac{4m_a^2}{m_H^2}} . \tag{2.63}$$

For the fermion, the decay is induced via the one-loop induced coupling in equation (2.61). Hence, the loop-induced $H \to \psi\psi$ partial decay width is given by

$$\Gamma_{H\to\psi\psi} = \frac{\delta Y_{H\to\psi\psi}^2}{8\pi} \left(1 - \frac{4m_\psi^2}{m_H^2} \right)^{\frac{3}{2}} , \tag{2.64}$$

where the effective coupling $\delta Y_{H\to\psi\psi}$ depends on a loop function Y (see appendix A.3.3)

$$\delta Y_{H\to\psi\psi} = -\frac{Y_\psi^2 \lambda_{aH} v}{32\pi^2} \mathrm{Y}_{H\to\psi\psi} , \tag{2.65}$$

with momenta properly evaluated for the decay process. We recall that a always leads to missing energy, even when it decays promptly.

Finally, the loop induced coupling of ψ can also play a role for the relic density computation (see Appendix A.3.2), and is fully taken into account in our numerical results. This is done by numerically evaluating the loop as a function of the centre of mass momentum using LoopTools [127], applied using the "improveCS.c" routine in MicrOMEGAs [15].

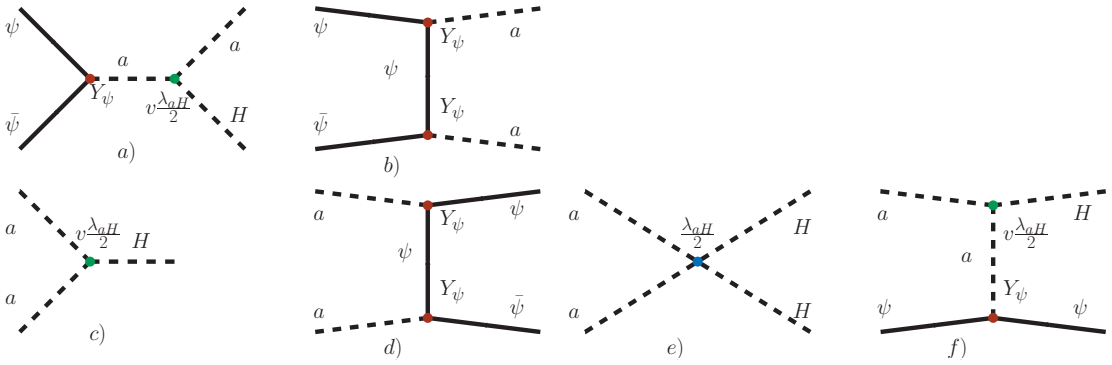

FIGURE 2.6: Feynman diagrams for DM (co)annihilation: a)-b) for $\bar{\psi} - \psi$ annihilation; c)-d) for aa annihilation and d) for $\psi - a$ co-annihilation.

2.4.1 Scenario A: 2-component thermal Dark Matter regime

In this scenario (see table 2.3) both new states couple sizeably to the SM, and will therefore thermalise in the early universe. The relic density in this regime can be evaluated using two coupled Boltzmann equations (see equation(5) of Ref. [128]), which depend on the annihilation and co-annihilation processes illustrated in Figure 2.6. The equations for the two number densities n_a and n_ψ read:

$$\frac{dn_\psi}{dt} = -\sigma_v^{\psi\psi\to aH}(n_\psi^2 - n_a\frac{\bar{n}_\psi^2}{\bar{n}_a}) - \sigma_v^{\psi\psi\to aa}(n_\psi^2 - n_a^2\frac{\bar{n}_\psi^2}{\bar{n}_a^2}) - 3Hn_\psi\,, \tag{2.66}$$

$$\begin{aligned}\frac{dn_a}{dt} = &-(\sigma_v^{aa\to H} + \sigma_v^{aa\to HH})(n_a^2 - \bar{n}_a^2) - \sigma_v^{aa\to\psi\psi}(n_a^2 - n_\psi^2\frac{\bar{n}_a^2}{\bar{n}_\psi^2}) \\ &-\frac{1}{2}\sigma_v^{a\psi\to\psi H}(n_a n_\psi - n_\psi\bar{n}_a) + \frac{1}{2}\sigma_v^{\psi\psi\to aH}(n_\psi^2 - n_a\frac{\bar{n}_\psi^2}{\bar{n}_a}) - 3Hn_a\,,\end{aligned} \tag{2.67}$$

where $\bar{n}_a$ and $\bar{n}_\psi$ denote the equilibrium number densities for the two components, and $\sigma_v \equiv \sigma v$.

We have performed a random scan of the 4-dimensional parameter space of the model by use of MicrOMEGAs [15]. The 4 independent parameters, two masses and two couplings, are probed within the following ranges (the upper value for

the couplings is based on the loss of perturbativity):

$$\begin{aligned} 10\ \text{GeV} < & m_\psi < 10\ \text{TeV}\,, \\ 10\ \text{GeV} < & m_a < 1\ \text{TeV}\,, \\ 10^{-1} < & Y_\psi < 10\,, \\ 10^{-4} < & \lambda_{aH} < 10\,. \end{aligned} \tag{2.68}$$

We determine the allowed regions surviving after imposing the relic density constraint from PLANCK [46] ($\Omega_{\text{Planck}}h^2 = 0.1186 \pm 0.0020$, though we also allow under-abundant model points with $\Omega_h^2 < 0.12$, below PLANCK constraints), DM direct detection constraints from Xenon1T [129, 130] (which are dominant over the DM indirect detection constraints, as we have explicitly checked) and invisible Higgs decay constraints from the LHC from ATLAS [131] (we use $\text{Br}[H \to \text{invis}] < 0.11$). Our results are presented in Figure 2.7, where we show 2D projections of the allowed parameter space for the $\tilde{F}_0^0 S_0^0$ (CP-odd) model after imposing the constraints listed in the top of each frame. The colour map indicates the relic density normalised to the PLANCK value for the two DM components a ($\Omega_a/\Omega_{\text{Planck}}$, shown in green fading to yellow) and ψ ($\Omega_\psi/\Omega_{\text{Planck}}$, shown in Magenta fading to cyan), or their sum ($\Omega_{\text{tot}}/\Omega_{\text{Planck}}$, shown in black fading to red).

In the top row of Figure 2.7 we show the projection in the m_a–λ_{aH} plane, where the colour map corresponds to values of Ω_a/Ω_{Planck} with dark green marking model points that saturate the relic density with a alone. Recall that we keep all points with $\Omega_{\text{tot}}h^2 < 0.12$. In the panel 2.7(a), no other constraint except the relic density is added: it clearly demonstrates the correlation between Ω_a and the value of λ_{aH}, driven by the Feynman diagrams c)/e) and a)/f) of Figure 2.6. One can also see the region of the resonant annihilation through the Higgs boson, $aa \to H$, which takes place for $m_a \simeq m_H/2$. Due to its efficiency, it allows the value of λ_{aH} to go as low as $\simeq 4 \times 10^{-4}$ while being consistent with the Ω_{Planck} constraint. Outside of the resonant region, values of $\lambda_{aH} \lesssim 10^{-1} \div 1$ are excluded by overclosure of the universe. Furthermore, in the panel 2.7(b) we present the same 2D projection with points satisfying DM direct detection constraints from Xenon1T experiment (both on a and on ψ). The plot illustrates how Xenon1T excludes all points for $m_a \lesssim m_H$, except for a sliver close to the Higgs resonance, which has small couplings or small relic density for the a component. The excluded region of the parameter space, in fact, requires relatively large $\lambda_{aH} \gtrsim 0.1$ values in order to provide an effective a annihilation via the virtual Higgs boson. Being consistent with the relic density constraint, therefore, is at odds with the non-observation of a DM direct detection signal. We also superimpose the LHC bound on the Higgs invisible decays ($\text{Br}[H \to \text{invis}] < 0.11$), which excludes the Higgs resonant sliver for $\lambda_{aH} \gtrsim 3 \times 10^{-2}$, as shown by the shaded region above the blue line. Future collider projections are considered as well, showing that the exclusion on λ_{aH}

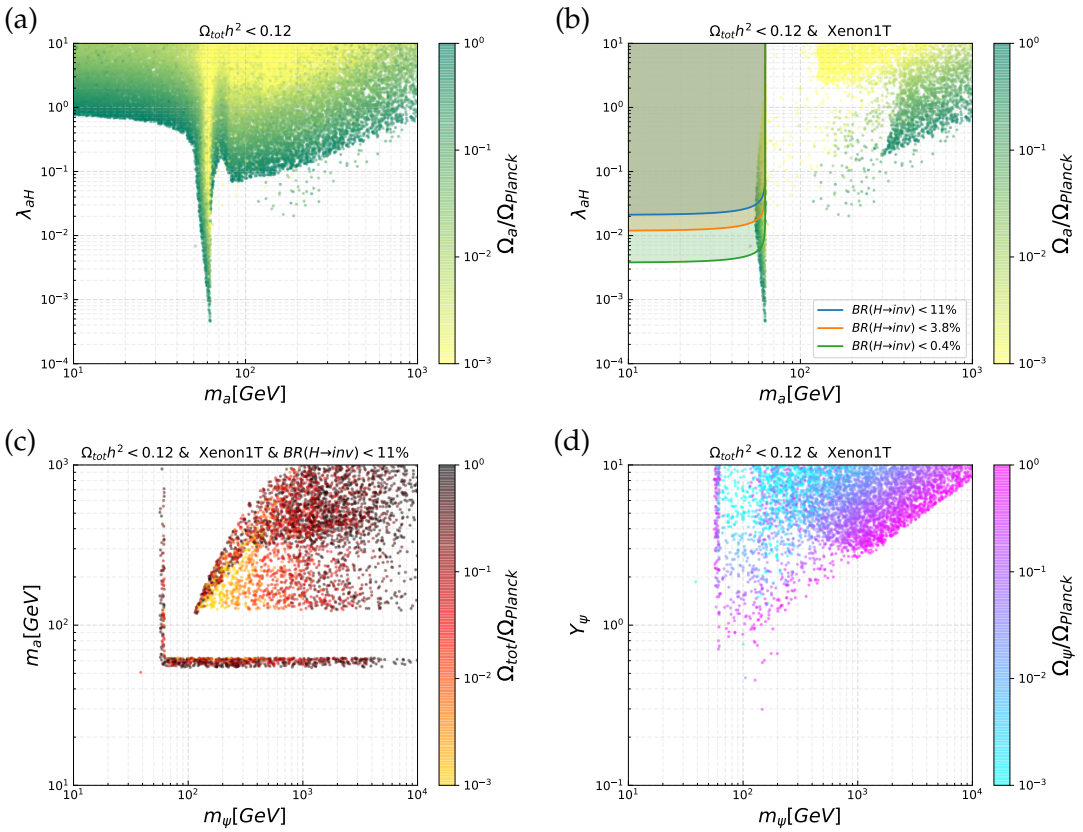

FIGURE 2.7: 2D projections of the allowed parameter space for $\tilde{F}_0^0 S_0^0$ (CP-odd) model (after constraints given at the top of each frame) with the colour map indicating the individual relative relic density of two DM components a ($\Omega_a/\Omega_{\text{Planck}}$), ψ ($\Omega_\psi/\Omega_{\text{Planck}}$) or their sum ($\Omega_{\text{tot}}/\Omega_{\text{Planck}}$). Here, $H \to inv$ curves reflect only tree level contributions from $H \to aa$, and as such are conservative limits in the given projection. In (c) however, one loop $H \to \psi\psi$ is included in exclusion on points.

will improve by a factor of about 3 at the High Luminosity LHC run (HL-LHC) (projected bound of $\text{Br}[H \to \text{invis}] < 3.8\%$ [132]), as shown by the orange line. The International Linear Collider (ILC) running at $\sqrt{s} = 250$ GeV and with an integrated luminosity of 1.15 ab^{-1} will be able to exclude $\lambda_{aH} \gtrsim 4 \times 10^{-3}$, as indicated by the green line, corresponding to a projected exclusion of $\text{Br}[H \to \text{invis}] > 0.4\%$ [133]. One should also note that even the ILC will not be able to fully exclude the Higgs resonant region, since λ_{aH} goes below the ILC sensitivity by one order of magnitude.

Besides the Higgs sliver, a second viable region in the parameter space emerges for $m_a \gtrsim m_H$, as shown in plot 2.7(b). It is defined by the interplay of the semi-annihilation processes $\psi\psi \to aH$ and $a\psi \to H\psi$, involving both new states of the dark sector. This better illustrated by panels 2.7(c–d), in the plane defined by the masses and the ψ mass and coupling, respectively. Panel 2.7(c), showing a colour map corresponding to the total relic density Ω_{tot}, offers the best view of the new region. Besides the Higgs sliver for a, appearing as a horizontal band, the allowed points highlight a vertical band corresponding to the Higgs resonant region for ψ

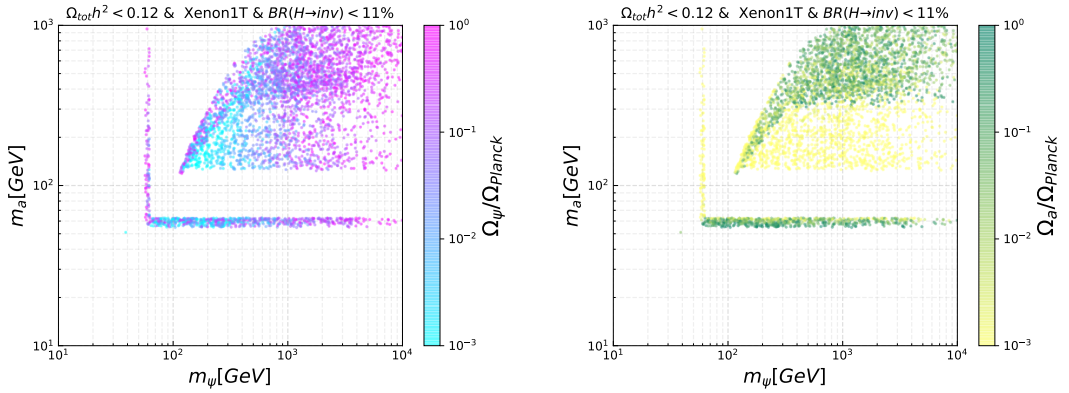

FIGURE 2.8: The distribution of relic density among species in the mass plane.

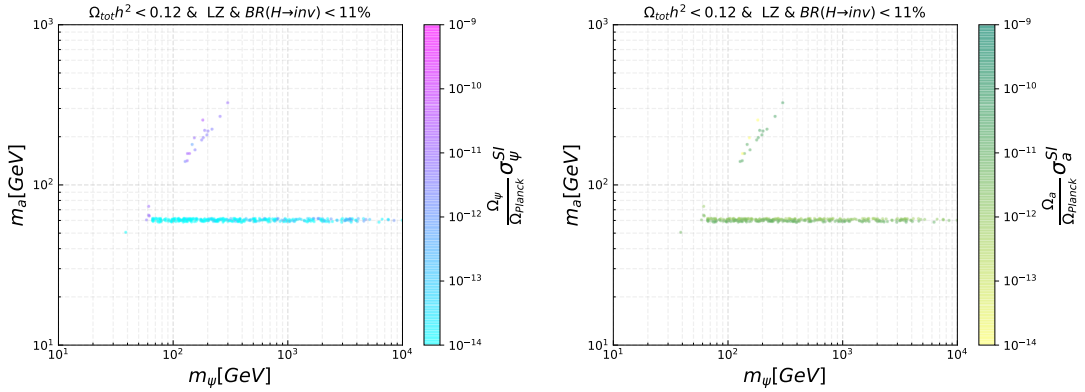

FIGURE 2.9: Direct detection cross-sections (scaled by relevant relic abundance fraction) for the two DM species plotted in the mass plane, with constraints applied from future experiment LZ [6].

via the one-loop induced coupling, and a wedge defined by

$$m_a \gtrsim m_H \quad \text{and} \quad m_\psi \gtrsim m_a \,. \tag{2.69}$$

An interesting feature is the fact that masses below $m_H/2$ are excluded for both DM candidates: while for a this is due to a compbination of relic abundance and direct detection and (more marginally) by the Higgs invisible width. When $m_a < m_H/2$ the coupling λ_{aH} must be $> \mathcal{O}(1)$ in order for efficient annihilation through the Higgs to occur, resulting in the direct detection signals being sufficient for Xenon1T to be exclude them. For ψ this comes from the fact that for low masses the only efficient annihilation channel is $\psi\bar{\psi} \to aa$. This is efficient enough only for $m_\psi \gtrsim m_a$, thus, $m_\psi < m_H/2$ would result in too much relic density due to the limit on m_a. In panel 2.7(d) we show the allowed points projected on the m_ψ–Y_ψ space, with colour map corresponding to the individual relic density of ψ. We can see a clearly defined triangular shape, which emerges from the $\psi\psi \to aa$ annihilation process and which requires the coupling $Y_\psi \gtrsim \mathcal{O}(1)$ to be fairly large to avoid overclosure of the universe. On top of this, there is a "leakage" of points

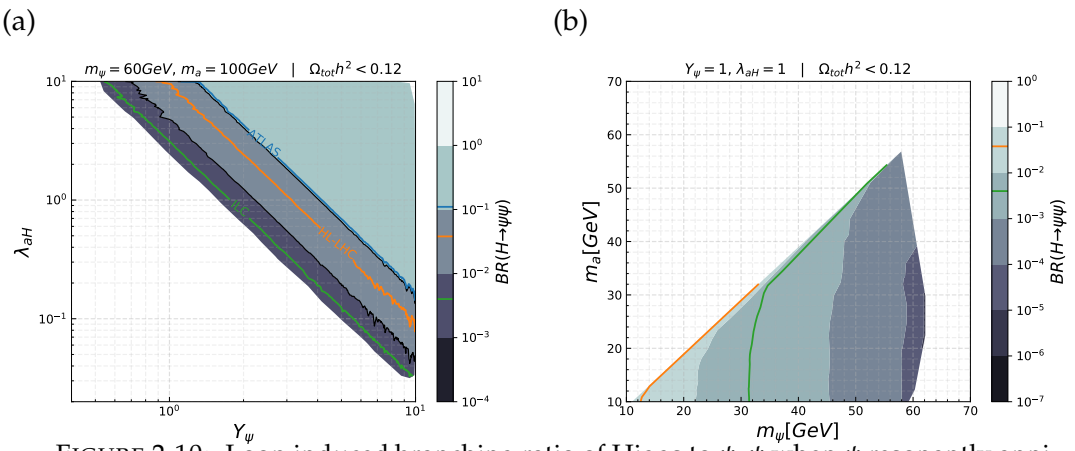

FIGURE 2.10: Loop induced branching ratio of Higgs to ψ, ψ when ψ resonantly annihilates through Higgs.

for $m_\psi \gtrsim m_H$, which emerge from the interplay with the process $\psi\psi \to aH$, which becomes relevant for $m_\psi \gtrsim m_a \sim m_H$. This means that for each value of Y_ψ, one can find a value for λ_{aH} that fixes the relic density below the limit. We also observe a smaller "leakage" of points for masses below m_H: this is due to an interplay between the two processes $aa \to H$ and $\psi\psi \to aH$ and point to masses $m_\psi \simeq \frac{3}{4} m_H$. This value comes from the fact that the first process, $aa \to H$, dominates for $m_a \simeq m_H/2$ in the Higgs resonant region, while the second, $\psi\psi \to aH$, opens up for $m_\psi \simeq (m_a + m_H)/2$.

We remark from panel 2.7(c) that points saturating the measured relic density exist in almost the whole allowed parameter region, thanks to the interplay between the two components a and ψ. In Figure 2.8 we show, in the plane defined by the masses, the contribution of each specie to the total relic (left for ψ and right for a). Interestingly, the region with $m_a \sim m_H/2$ contains points with sizeable and dominant relic from ψ. The remaining parameter space contains a region with $m_a \sim m_\psi$ where both species can receive competitive relic densities, and regions dominated by a for $m_a \gtrsim 300$ GeV and by ψ for $m_\psi \gtrsim 1$ TeV. Future direct detection experiments will be able to probe most of the remaining points, as demonstrated in Figure 2.9, where we impose the projected exclusion by the Lux-Zeplin (LZ) next generation experiment [6]. The surviving points consist on the Higgs sliver for a, with points dominated by the pseudo-scalar relic, and points with $m_a \sim m_\psi$. The latter ones still have sizeable SI cross-sections, discernible from the neutrino floor at future direct detection experiments. However, the Higgs resonance region would prove to be invisible to such experiments and may be probed instead through increased sensitivity to Higgs invisible decays at future colliders.

When $m_\psi \approx 60GeV$ (resonantly annihilates through the NLO coupling to Higgs), and $m_a \approx 100GeV$, the Higgs can decay to a pair of *psi* at NLO. Sensitivity to the couplings in this region are shown in Figure 2.10. In figures 2.7,2.9, we see that although XENON1T cannot fully exclude this region, LZ would have sensitivity. If a signal were to appear at LZ, then future colliders would have sensitivity to

such a scenario also. To fully probe the many DM models which rely on resonant annihilation through the Higgs, future Higgs factory type colliders such as the ILC [134] are critical.

2.4.2 Scenario B: ψ FIMP regime with thermal a

As we have seen, small values of $Y_\psi \lesssim \mathcal{O}(10^{-1})$ are excluded due to an excessive relic density of the fermionic component ψ. However, for extremely small values, $Y_\psi \lesssim \mathcal{O}(10^{-8})$, ψ will not be in thermal equilibrium at early times and it will freeze-in by means of the scattering of a with the Higgs, $aH \to \bar{\psi}\psi$. On the other hand, sizeable values of λ_{aH} would guarantee that a remains thermalised and contribute with a thermal relic component (as a second specie for $m_a > 2m_\psi$ or by decayind into the fermionic DM). To study this regime, we performed a scan of the parameter space, with results shown in Figure 2.11.

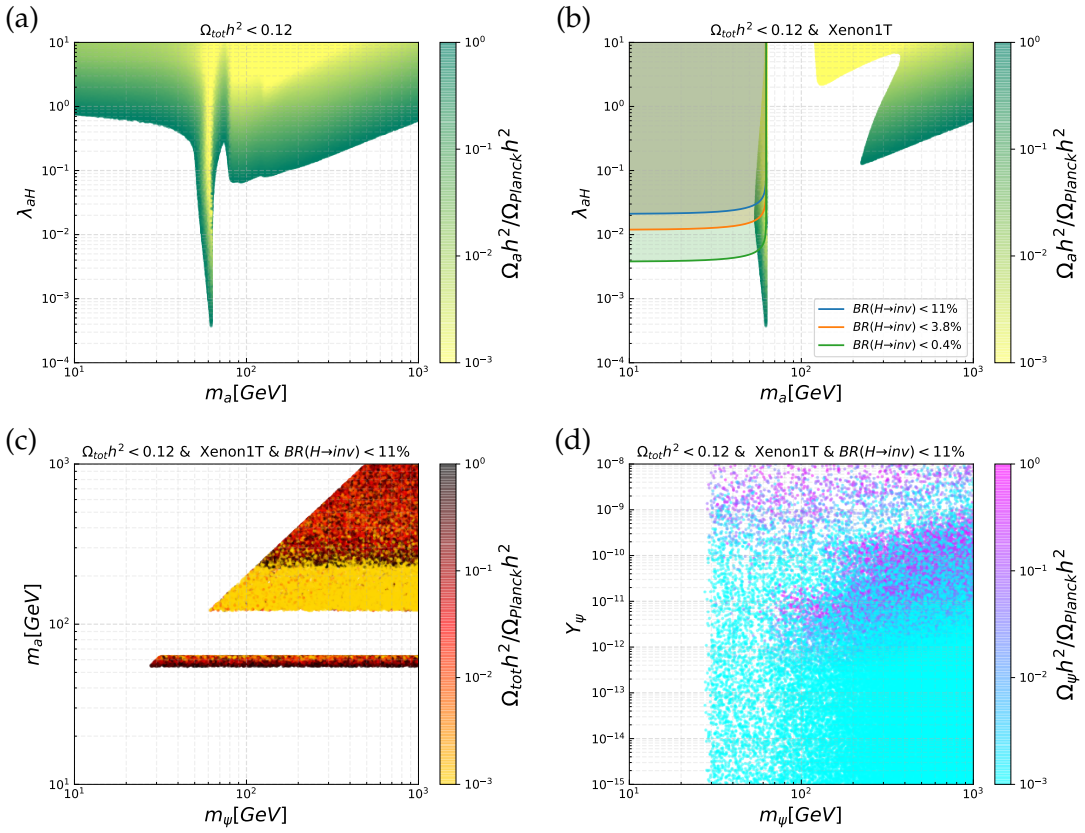

FIGURE 2.11: 2D projections of the allowed parameter space for $\tilde{F}_0^0 S_0^0$(CP-odd) model (after constraints given at the top of each frame) with the colour map indicating the individual relative relic density of two DM components $a(\Omega_a/\Omega_{Planck})$, $\psi(\Omega_\psi/\Omega_{Planck})$ or their sum $(\Omega_{tot}/\Omega_{Planck})$. Here we require that a is totally stable $(m_a < 2m_\psi)$.

The first two plots in the top row of Figure 2.11, showing the parameter space in the m_a–λ_{aH} plane and relic density of a, bear similarity with the top row in Figure 2.7: in both cases, the allowed regions are dominated by the thermal production of a. The only remarkable difference is the absence of "leaking" points,

which were due to the co-annihilation processes involving ψ, which are now suppressed by the small value of Y_ψ. The contribution of ψ via freeze-in is shown in the bottom plots of the figure. In panel 2.11(d), in particular, we show the relic density of ψ in the m_ψ–Y_ψ parameter space. While for most points the relic density is very small, we can identify two distinct regions where sizeable values can be attained (including saturating the whole DM relic density): one for largish $Y_\psi \gtrsim 10^{-9}$ starting from masses $m_\psi \gtrsim 30$ GeV, and another one for lower couplings, $10^{-12} \lesssim Y_\psi \lesssim 10^{-9}$ starting at $m_\psi \gtrsim m_H/2$. These two regions can be better understood in the m_a–m_ψ plane, shown in panel 2.11(c): the former region corresponds to points where a is in the Higgs resonant sliver represented by the horizontal band; the latter region corresponds to triangle region at large a mass, where $m_a > m_H$.

2.4.3 Conclusions

A naive treatment of mediators in such a DM model can overlook some key features, and lead to the underestimation of DM abundance or direct detection cross-sections. Here, this is demonstrated through regions of parameter space where the mediator a can carry a sizeable amount of the DM relic abundance, and also scatter at tree-level off nucleons at direct detection experiments in contrast to the loop level scattering of the fermion candidate it accompanies.

It is demonstrated that although highly constrained by XENON1T experiment, there is a strong sensitivity to discovery for such a model at the next generation direct detection experiment LZ [50]. A non-observation at LZ would push this model to require pseudoscalar masses around half of the Higgs mass, if this is the case then colliders would play a pivotal role in further probing Higgs to invisible decays.

2.5 Conclusions

A systematic classification was presented for MCDM models. The simplest of such models, including only a vector-like multiplet containing DM produce loop-level direct detection signals, calculated here to typically fall directly within the reach of future experiment LZ (for masses less than 10TeV, for which the measured relic abundance is achievable).

The introduction of mediators and their phenomenological impact was surveyed, although a complete treatment of their impact on direct detection signals was not given. This would be a key future work, in order to understand the interplay of mass splittings and generation for fermionic DM (and their respective impact on the DD cross-section through loops) potentially caused by mediators and the associated tree level contributions to DD which they may incur.

Through considering the simple model in section 2.4, we show that the naive treatment of mediators in simplified approaches may lead to the underestimation of relic abundance or direct detection signals. Such a model, along with many other viable EW scale models which rely on resonant (semi)annihilation through the Higgs in order to satisfy the relic abundance would be ideally probed by a combination DD experiments and a future Higgs factory experiment such as ILC, CLIC, LHC-ee.

Chapter 3

Decoding Dark Matter at future e^+e^- colliders

The search for Dark Matter (DM) in High Energy Physics experiments (HEP) has become one of the primary goals of the LHC and future colliders, in addition to non-collider experiments. Indeed it is one of the fundamental problems for the HEP community to discover and decode the nature of DM, the existence of which has been confirmed by several independent cosmological observations. These include galactic rotation curves, cosmic microwave background fits of the WMAP and PLANCK data, gravitational lensing, the large scale structure of the Universe, and interacting galaxy clusters such as the Bullet Cluster. Despite this multitude of observations strongly suggesting the existence of cold non-baryonic particle DM, many of its properties remain a mystery. These properties include the spin, mass, non-gravitational interactions, stabilising symmetry and the nature of mediators between the Standard Model (SM) and DM, plus its potential partner particles in the dark sector.

As one of the most active research areas in HEP, there are many key papers exploring the vast model landscape of DM and the possibilities to disentangle these models experimentally. A selection of important DM models include SUSY [135, 136, 137], non-thermal DM and dark sectors [138], sterile neutrinos [139], general minimal WIMP models [90], Axions [140], Kaluza-Klein DM [141], Universal Extra Dimensions [142] and extended Higgs sectors [143, 144, 145]. Phenomenological investigations into distinguishing the many models of DM via properties such as spin [34, 146, 147] and mass [33, 31] would be key in the event of a discovery.

Traditional searches for DM at the LHC via missing energy signatures through mono-jet [148, 149], mono-V [150, 151, 152, 153, 154, 155], mono-Higgs [156, 157, 158, 159, 160], DM+ top quarks [161, 162, 163] and invisible Higgs decays [164, 165, 154] or through potential mediators [166, 167, 168] expand on constraints

from LEP on DM charged partner masses [169]. DM may also be probed in scenarios where its charged partners are long-lived, providing unique signatures with little background. These scenarios, known as non-prompt searches, include disappearing charged tracks [170, 171] and displaced vertices [172, 173].

On the other hand, in case of generic scenarios where DM is involved in SM $SU(2)$ electroweak (EW) interactions and no additional Beyond-the-Standard-Model(BSM) mediators are present, it is quite challenging for the LHC to probe such a DM even in the 100 GeV range if it does not give rise to non-prompt signatures. For example, in [174] it was shown that even at High Luminosity (HL) LHC, the higgsino-like neutralino DM from the Minimal Supersymmetric Standard Model(MSSM) can be probed only up to about 200 GeV mass with very high transverse momentum mono-jet signature required to reduce large SM background. There are no current constraints on such a scenario from the LHC and the best limits are set up by LEP on charged DM partner (e.g chargino) mass to be above 100 GeV [174].

The most recent global scans of the MSSM [175] plus the neutralino and chargino sector (analogous to split SUSY scenarios) [176] reveal a best fit region consistent with a higgsino-bino DM candidate, which is mostly bino (mostly singlet DM will avoid direct detection constraints). These viable points rely on the so-called "Higgs funnel" annihilation channel (DM mass around half Higgs mass) in order to reproduce the relic density as measured by PLANCK. Such scenarios may be ideally probed by a 500 GeV collider such as the ILC, where the accessible particle spectrum ($<$ 300 GeV) contains the two lightest neutralinos in addition to the lightest chargino.

In this study we explore the potential of a future e^+e^- collider to probe and distinguish two well motivated minimal models with DM of spin-0 and 1/2 embedded into an $SU(2)$ weak doublet with no additional BSM mediator. We assume that the DM sector is represented by an EW doublet without loss of generality and that each model includes DM, D, its charged partner D^+ and heavier neutral partner(s), $D_2(D_3)$ with $M_{D_2}(M_{D_3}) > M_D$, which are odd-particles with respect to a Z_2 symmetry responsible for DM stability. We explore the potential of the 500 GeV e^+e^- collider (which can be ILC, CLIC etc) to measure M_D and M_+ masses and distinguish DM spin using single- and di-lepton signatures from $D^\pm$ decays. The observation of such signature requires a non-vanishing mass gap $\Delta M = M_{D^+} - M_D$ ($\gtrsim$ 10 GeV) which would provide detectable leptons. Our study goes beyond the previous exploration(e.g. [147]) of the ILC potential to discriminate DM models in several principal aspects: a) we explore the signature with leptonic final state which has the advantage of keeping background under better control and more precise determination of the final state energy distributions; b) we make use of the predicted cross-sections for typical parameter points delivering the correct relic abundance; c) we suggest the set of new kinematical

observables and cuts which boost e^+e^- collider potential discrimination of DM models; d) we explore both cases for off-shell and on-shell W-boson decay; e) we use model-independent template based approach to fit kinematic endpoints and determine D and D^+ masses using likelihood methods.

This paper is organized as following. In Section 2 we discuss models and processes under study, in Section 3 we study the signal rate and kinematics, in Section 4 we analyse signal and background separation and find the potential of e^+e^- collider to measure DM properties. Finally in Section 5 we draw our conclusions.

3.1 Models and Processes

3.1.1 Inert doublet model (I2HDM)

The spin-0 or scalar DM (SDM) model which we use as a first case study is the inert Two Higgs Doublet Model [177, 178, 179, 180, 181, 182, 183] which in addition to SM Higgs doublet contains inert scalar Z_2-odd doublet, ϕ_D, that does not acquire a Vacuum Expectation Value (VEV). In our paper we call all particles odd under Z_2 symmetry D-particles, and refer to the Z_2 symmetry as D-parity. The scalar sector of the model is given by

$$\mathcal{L} = |D_\mu \Phi|^2 + |D_\mu \phi_D|^2 - V(\Phi, \phi_D), \tag{3.1}$$

where V is the potential with all scalar interactions compatible with the Z_2 symmetry:

$$\begin{aligned} V &= -m_1^2(\Phi^\dagger\Phi) - m_2^2(\phi_D^\dagger\phi_D) + \lambda_1(\Phi^\dagger\Phi)^2 + \lambda_2(\phi_D^\dagger\phi_D)^2 \\ &+ \lambda_3(\Phi^\dagger\Phi)(\phi_D^\dagger\phi_D) + \lambda_4(\phi_D^\dagger\Phi)(\Phi^\dagger\phi_D) + \frac{\lambda_5}{2}\left[(\Phi^\dagger\phi_D)^2 + (\phi_D^\dagger\Phi)^2\right] . \end{aligned} \tag{3.2}$$

In the unitary gauge, the SM doublet, Φ and the inert doublet, ϕ_D take the form

$$\Phi = \frac{1}{\sqrt{2}}\begin{pmatrix} 0 \\ v + H \end{pmatrix}, \qquad \phi_D = \frac{1}{\sqrt{2}}\begin{pmatrix} \sqrt{2}D^+ \\ D + iD_2 \end{pmatrix}, \tag{3.3}$$

where we consider the parameter space in which only the first, SM-like doublet, acquires a VEV, v. After EW Symmetry Breaking (EWSB), the D-parity is still conserved by the vacuum state, which forbids direct coupling of any single inert field to the SM fields and protects the lightest inert boson from decaying, hence providing the DM candidate in this scenario. In addition to the SM-like scalar H, the model contains one inert charged D^+ and two further inert neutral D and D_2 scalars. The two neutral scalars of the i2HDM have opposite CP-parities, but it is impossible to unambiguously determine which of them is CP-even and which one is CP-odd since the model has two CP-symmetries, $D \to D, D_2 \to -D_2$ and

$D \to -D, D_2 \to D_2$, which get interchanged upon a change of basis $\phi_D \to i\phi_D$. This makes the specification of the CP-properties of D and D_2 a basis-dependent statement. Therefore, following Ref. [145], we denote the two neutral inert scalar masses as $M_D < M_{D_2}$, without specifying which is scalar or pseudoscalar, so that D is the DM candidate.

The model can be conveniently described by a five dimensional parameter space[145] using the following phenomenologically relevant variables:

$$M_D\,, \quad M_{D_2} > M_D\,, \quad M_+ > M_D\,, \quad \lambda_2 > 0\,, \quad \lambda_{345} > -2\sqrt{\lambda_1\lambda_2}, \tag{3.4}$$

where M_D, M_{D_2} and M_+ are the masses of the two neutral and charged inert scalars, respectively, whereas $\lambda_{345} = \lambda_3 + \lambda_4 + \lambda_5$ is the coupling which governs the Higgs-DM interaction vertex HDD. There is a ($\phi_D \to i\phi_D$, $\lambda_5 \to -\lambda_5$) symmetry of the Lagrangian which allows us to chose $\lambda_5 > 0$. The masses of the three inert scalars are expressed in terms of the parameters of the Lagrangian in Eqs. (3.1)–(3.2) as follows:

$$\begin{aligned} M_+^2 &= \tfrac{1}{2}\lambda_3 v^2 - m_2^2, \\ M_D^2 &= \tfrac{1}{2}(\lambda_3 + \lambda_4 - \lambda_5)v^2 - m_2^2, \\ M_{D_2}^2 &= \tfrac{1}{2}(\lambda_3 + \lambda_4 + \lambda_5)v^2 - m_2^2 \; > M_D^2, \end{aligned} \tag{3.5}$$

which represent the only three parameters relevant to our study, since we explore production of D-particles in the gauge interactions at e^+e^- colliders.

Constraints on the Higgs potential from requiring vacuum stability and a global minimum take the following form[145]:

$$\begin{cases} M_D^2 > 0 \text{ (the trivial one)} & \text{for} \quad |R| < 1, \\ M_D^2 > (\lambda_{345}/2\sqrt{\lambda_1\lambda_2} - 1)\sqrt{\lambda_1\lambda_2}v^2 = (R-1)\sqrt{\lambda_1\lambda_2}v^2 & \text{for} \quad R > 1, \end{cases} \tag{3.6}$$

where $R = \lambda_{345}/2\sqrt{\lambda_1\lambda_2}$ and $\lambda_1 \approx 0.129$ is fixed as in the SM by the Higgs mass in equation (3.5). The latter condition places an important upper bound on λ_{345} for a given DM mass M_D. Constraints on the model's parameter space have already been comprehensively explored in a large variety of previous papers [184, 185, 186, 187, 188, 189, 190, 191, 192, 193, 194, 195, 196, 197, 198, 199, 200, 201, 202, 203, 204, 205, 177, 178, 179, 180, 145].

3.1.2 Minimal Fermion DM (MFDM)

The second model we consider here is a minimal model with an EW fermion DM doublet. The model should respect direct DM constraints coming from the most restrictive DM Direct Dtection (DD) searches from the XENON1T experiment [130], and at the same time provide the correct amount (or at least not

over abundant) of relic density. Therefore the model must have a mechanism to suppress DM scattering through intermediate Z-bosons and/or Higgs bosons. Among several candidates for such a mechanism, the most minimal is to introduce Majorana neutral D-odd particles χ_1^0 and χ_2^0 as a part of an EW doublet and split their masses via interactions with the SM Higgs doublet and additional Majorana singlet fermion χ_s^0:

$$\mathcal{L}_{FDM} = \mathcal{L}_{SM} + \bar{\psi}(iD - m_\psi)\psi + \frac{1}{2}\bar{\chi_s^0}(i\partial - m_s)\chi_s^0 - (Y(\bar{\psi}\Phi\chi_s^0) + h.c.) \ , \quad (3.7)$$

where fermion fields are in bispinor form and Φ is the SM Higgs doublet. A DM $SU(2)$ vector-like doublet with hypercharge $Y = 1/2$, may be defined in terms of majorana states χ_1^0, χ_2^0 as:

$$\psi = \begin{pmatrix} \chi^+ \\ \frac{1}{\sqrt{2}}(\chi_1^0 + i\chi_2^0) \end{pmatrix}. \quad (3.8)$$

The model which we suggest and use in our paper has only three new parameters: m_ψ, Y and m_s. This model is more minimal in comparison to the previously studied doublet-singlet model [206, 207] which has four parameters because of *two* Yukawa couplings, distinguishing left- and right-handed interactions of Higgs and DM doublets with χ_s^0. Our choice of the parity conserving $\psi - \Phi - \chi_s^0$ Yukawa interactions adds just one parameter to the model – the Yukawa coupling, which is the same for left and right interactions. We have checked that this scenario is radiatively stable. This parity would be spoiled if the DM sector would directly couple to SM fermions, which is eventually not the case. Therefore our model with just three new parameters is consistent and truly the minimal one.

The Yukawa interaction mixes χ_1^0 and χ_s^0 while χ^+ and χ_2^0 have the same mass m_ψ and remain degenerate at tree-level. This degeneracy is not essential, since χ_2^0 decay is driven by the $\chi_2^0 \to \chi_1^0 Z^{(*)}$ process.

We trade m_ψ, Y and m_s parameters for three physical masses:

$$M_D, m_\psi \equiv M_+ = M_{D_2}, \ \text{and} \ M_{D_3}, \quad (3.9)$$

corresponding to (D, D_2, D_3) mass bases of the neutral DM sector, which one obtains from the diagonalisation of the mass matrix in the $(\chi_s^0, \chi_1^0, \chi_2^0)$ basis:

$$\mathcal{M} = \begin{bmatrix} m_s & Yv & 0 \\ Yv & m_\psi & 0 \\ 0 & 0 & m_\psi \end{bmatrix}, \quad (3.10)$$

where the relation between gauge (χ_1^0, χ_s^0) and mass (D, D_3) eigen-states are given by:

$$\begin{aligned} \chi_s^0 &= D\sin\theta + D_3\cos\theta \\ \chi_1^0 &= D\cos\theta - D_3\sin\theta \end{aligned} \tag{3.11}$$

and the rotation angle θ which diagonalises the mass matrix (3.10) is given by

$$\tan 2\theta = \frac{2Yv}{m_s - m_\psi}. \tag{3.12}$$

One should note that the mass and gauge eigenstate of χ_2^0 coincide and have the mass $m_\psi \equiv M_+ = m_{D_2}$. The relation between the Lagrangian parameters from mass matrix (3.10) and physical mass parameters is given by:

$$m_s = M_D + M_{D_3} - M_+, \tag{3.13}$$

$$Y = \frac{\sqrt{(M_{D_3} - M_+)(M_+ - M_D)}}{v}, \tag{3.14}$$

while the eventual mass order

$$M_{D_3} > M_+ = M_{D_2} > M_D \tag{3.15}$$

follows from the condition for Y to be real. The phase of χ_s^0 may be chosen such that Y is positive. If $Y > 0$ then the sign of $m_s - m_\psi$ $[+,-]$ determines whether θ lies in quadrant $[(0, \frac{\pi}{4}), (\frac{\pi}{4}, \frac{\pi}{2})]$. Likewise, if $Y < 0$ then the sign of $m_s - m_\psi$ $[-,+]$ determines whether θ lies in quadrant $[(\frac{\pi}{2}, \frac{3\pi}{4}), (\frac{3\pi}{4}, \pi)]$. This MFDM model, with singlet-doublet dark sector content can be mapped into the bino-higgsino MSSM model with all other SUSY particles decoupled, including winos.

In this model, DM direct detection rates may be suppressed arising from the fact that D does not interact directly with the Z-boson and couplings to the Higgs may be small depending on scenario. Inelastic up-scatterings arising from the ZDD_2 vertex are kinematically disallowed (which is the case of this study) when the mass split between D and D_2 particles is beyond the recoil energy threshold of direct detection experiments - typically around 1 keV. In such a scenario, the tree level direct detection rate depends exclusively on scattering via the Higgs.

The spin-independent nucleon scattering cross-section depends only on Higgs exchange, where the Higgs couples to DM with strength proportional to g_{DDh}^2. Note here that the sign (resulting from quadrant of θ) does not influence the observable direct detection cross-section.

$$g_{DDh} = -2Y\cos\theta\sin\theta = \pm 2\frac{(M_+ - M_D)(M_{D_3} - M_+)}{v(M_{D_3} - M_D)} \tag{3.16}$$

For cascade decays with sizable cross-sections at colliders we require a relatively large mass gap, $M_+ - M_D$, in order to recoil on-shell (or slightly virtual) W bosons. In this scenario, small couplings may be achieved when $M_{D_3} - M_+$ is small, whilst producing the correct relic abundance through resonant annihilation when $M_D \simeq M_h/2$. $D - D_3$ and $D - D^+$ co-annihilation channels are subdominant in this scenario due to the relatively large mass split between DM and its partners.

3.1.3 Benchmark Points

In our study we chose two benchmarks with different $D^+ - D$ mass gaps: one – providing $D^+ \to DW$ decay with on-mass-shell W-boson in the final state and another – with the off-mass-shell W^*-boson. We choose model parameters providing the right amount of relic density and satisfying the latest DM DD constraint from XENON1T searches to make sure that chosen benchmarks are the realistic ones. The benchmarks are presented in Table 3.1 together with DM observables. One should note that I2HDM model has two more parameters (five versus three) in comparison to MFDM model – λ_{345} and λ_2. First we chose M_D, M_D^+, M_{D_2} to make the relic density consistent with the results from PLANCK for MFDM model, then use additional parameter λ_{345} from I2HDM to make the relic density from this model to be consistent with PLANCK. The other parameter – λ_2 , which controls the self-interaction of DM, is not relevant to collider phenomenology. We keep $\lambda_2 = 1$ without loss of generality[1] since it does not affect any conclusion in this paper. We chose the same D, D^+ and D_3 masses for both models with the aim to explore the ILC potential in distinguishing theories with same mass but different spin of the DM sector.

The relic density, Ωh^2, and spin-independent proton scattering cross-section, σ_{SI}^p, were calculated using the micrOMEGAs package [15].

We have recast an existing SUSY analysis using CheckMATE2 [208] and found that the most sensitive search for BP1 and BP2 is the CMS 13TeV search for electroweak production of charginos and neutralinos in multilepton final states [209] , which gives an r-value [2] of 0.325 and 0.664 respectively. Many of the most stringent LHC constraints on electroweak scale WIMP masses arise from decays mediated by sleptons and sneutrinos of mass $\lessapprox 500GeV$. In the scenarios explored here we assume that all additional SUSY particles (or analogous particles which could appear in the I2HDM extension) are decoupled. It is worth noting that the global scan of electroweakino DM by the GAMBIT collaboration shows favoured parameter points around our benchmarks [176].

[1] The large value of λ_2 could potentially affect the DM density profile and loop-induced DM annhillation into SM particles. These effects are outside the scope of this paper.

[2] $r = \text{Signal}/(95\%\text{CL on Signal})$

Parameters \ Benchmarks		BP1	BP2
M_D		60	60
M_+		160	120
M_{D_3}		160.85	120.85
I2HDM parameters			
λ_{345}		6.5×10^{-4}	7.0×10^{-4}
λ_2		1.0	1.0
DM observables			
Ωh^2	$s_{DM} = 0$	0.111	0.112
	$s_{DM} = \frac{1}{2}$	0.108	0.109
σ^p_{SI}[pb]	$s_{DM} = 0$	6.17×10^{-13}	6.17×10^{-13}
	$s_{DM} = \frac{1}{2}$	1.67×10^{-11}	1.65×10^{-11}

TABLE 3.1: Benchmark points for I2HDM and MFDM with DM observables. All masses are given in GeV.

3.1.4 Analysis setup

In our study we use the following tools to evaluate the ILC potential to probe properties of DM. We use CalcHEP[13] to perform the parton-level signal analysis in section 3.2, including the study of the finite width effects from W-boson decay, and the effects from the Initial State Radiation (ISR) and Beamstrahlung Radiation (BR). We use Pythia8 [210] to simulate final state radiation and hadronisation effects. Events from Pythia are then passed to Delphes [211] fast-detector simulator using the ILC card based on the proposed ILD detector [212]. At this level of simulation we have performed signal and background analysis of the various kinematic distributions to extract D and D^+ masses to distinguish scalar and fermion DM models as discussed in detail in 3.3.

3.2 Exploring DM production via cascade decays at e^+e^- colliders

The neutral and stable DM candidate, D, can be produced and detected via the production of D^+ or D_2 and subsequent decay $D^+ \to DW^\pm$, $D_2 \to DZ$ with either on shell (real) or off shell $W^\pm$ or Z. The off shell W emerges as a $q\bar{q}$ pair (dijet) or $\ell\nu$, having the same quantum numbers as W but with an effective mass $M^*_W < M_W$. From now on, W or Z refers to any of these two cases. We denote maximal value of off shell mass $M^*_W \equiv M_+ - M_D$ as M^*_{max}.

In the text below we denote electron beam energy

$$E = \sqrt{s}/2\,. \tag{3.17}$$

We consider energies E and three-momenta p of particles in different reference systems and use particle name in superscript (W for W^+ and D for D^+) for energy and momentum to indicate their Lorentz frame. For the lab system (cms for e^+e^-) corresponding quantities are written without superscript. The subscript indicates just the name of the particle to which the physical quantity belongs. For example, p_W^D is value of three momentum of W^+ in the rest frame of D^+, and E_μ is energy of muon in the lab. system.

We supply upper superscript by additional sign $(+)$ or $(-)$ to mark upper and lower limits of variation of corresponding energy at value of intermediate parameter mentioned in bracket, subscripts p or k mark values, corresponding to a peak or kink.

3.2.1 Strategy to discover and measure DM properties

To discover particle DM, one needs to specify such processes with a clear signature producing sufficient signal to be distinguishable from SM background. The e^+e^- Collider ILC/ CLIC provides an excellent opportunity for this task (see, e.g., [213], [214]) in the process $e^+e^- \to D^+D^-$ with a clear signature, see Eqs. (3.26) and (3.27) below. The cross section of this process is a large fraction of the total cross section of e^+e^- annihilation, sect. 3.2.2.

The masses M_+ and M_D could be found via the edges of the energy distribution of dijets, originating from W from the decay $D^+ \to DW^\pm$, (see [215, 216] for MSSM and [181, 182, 183] for IDM). However, this method cannot provide a good accuracy in measuring the mass. Indeed, the individual jet energy measurement suffers from a sizable uncertainty. In particular, this uncertainty smoothes the lower edge in the dijet energy spectrum.

On the contrary, the lepton energy can be measured much more precisely. In this chapter we show, first, that the energy distribution of leptons has singular points whose positions are kinematically determined. Measuring positions of these singularities will allow, in principle, to determine the masses M_D and M_+ with good precision. In contrast to [215, 216], [181, 182, 183], our prescription is suitable for different models.

Moreover, we present a simple method for measuring spin of DM particles in these very experiments.

The discussed problem differs strongly from that for the case when the lightest charged D-odd particle is a slepton (which is possible for a different set of parameters of MSSM). In the latter case DM particles are produced via slepton pair, $e^+e^- \to \tilde{\ell}^+\tilde{\ell}^- \to \ell^+\ell^-\chi_0\chi_0$. First of all, the signature of this process is quite different from the one in our problem (3.26), (3.27). Second, the energy of the observable lepton - which is a decay product of the slepton is measurable well

in each individual event, in contrast with our case, where a similar decay product, W, is seen as dijet or lepton plus neutrino with poorly measurable energy in each individual event. Therefore, the approach used in the analysis of slepton production (cf. [217, 218, 219]) cannot be applied directly to our problem.

3.2.2 Cross-section formulae for D-particles with spin, s_D

We express the discussed cross sections via

$$\sigma_0 \equiv \sigma(e^+e^- \to \gamma \to \mu^+\mu^-) = 4\pi\alpha^2/3s\,. \tag{3.18}$$

The total cross section of e^+e^- annihilation at ILC for $\sqrt{s} > 200$ GeV is $\sim 10\ \sigma_0$. The annual integrated luminosity $\mathcal{L}$ for the ILC project [214] gives the number of events of

$$\mathcal{L}\sigma_0 \sim 3 \cdot 10^5. \tag{3.19}$$

The process $e^+e^- \to D^+D^-$ represents a significant fraction of all e^+e^- annihilation events – see (3.22), (3.24), figure 3.1 and Table 3.2. With the luminosity (3.19), the annual number of events associated with D^+D^- production will be between $0.6 \cdot 10^5$ and $3 \cdot 10^5$, depending on $2M_+/\sqrt{s}$ and s_D, and about $1/3$ of them (in the mode with e or μ plus dijet) are suitable for our analysis.

Note before we proceed that the energies, γ-factors and velocities of D^+ are

$$E_+ = \frac{\sqrt{s}}{2}, \quad \gamma_+ = \frac{\sqrt{s}}{2M_+}, \quad \beta_+ = \sqrt{1 - 4M_+^2/s}. \tag{3.20}$$

The amplitude of the process $e^+e^- \to D^+D^-$ is given by the sum of the annihilation cross-section $\sigma_{\gamma\gamma}$, the Z annihilation cross-section σ_{ZZ} and an interference term $\sigma_{\gamma Z}$. This is given by equation 3.22, and may be factorised in terms of the QED only cross-section (equation 3.21).

$$\sigma_{\gamma\gamma} = \begin{cases} \sigma_0\beta_+\left[1 + \frac{2M_+^2}{s}\right] & \text{if } s_D = \frac{1}{2} \\ \sigma_0\frac{\beta_+^3}{4} & \text{if } s_D = 0 \end{cases} \tag{3.21}$$

$$\sigma = \sigma_{\gamma\gamma} + \sigma_{\gamma Z} + \sigma_{ZZ} = \sigma_{\gamma\gamma}\left[1 + \frac{\kappa_{\gamma Z}}{1 - \frac{M_Z^2}{s}} + \frac{\kappa_{ZZ}}{\left(1 - \frac{M_Z^2}{s}\right)^2}\right] \tag{3.22}$$

$$\begin{aligned} \kappa_{\gamma Z} &= \frac{\cos 2\theta_W(2\cos 2\theta_W - 1)}{4\cos^2\theta_W \sin^2\theta_W} \approx 0.089 \\ \kappa_{ZZ} &= \frac{\cos^2 2\theta_W + (\cos^2 2\theta_W + (\cos 2\theta_W - 1)^2))}{32\cos^4\theta_W \sin^4\theta_W} \approx 0.377 \end{aligned} \tag{3.23}$$

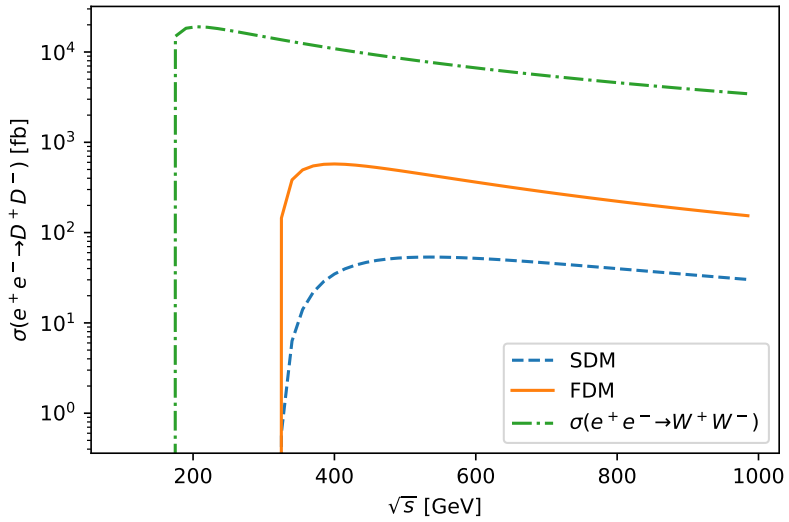

FIGURE 3.1: Comparing the cross section as a function of the center of mass energy, for fermion and scalar case. BP1 values are used. The green line corresponds to the dominant background process.

$\sqrt{s}$/GeV	300	500	500	500
M_+/GeV	120	120	160	200
$s_D = 0 : \sigma/fb$	81.0	87.7	58.9	28.0
$s_D = 1/2 : \sigma/fb$	1188.6	508.1	480.8	411.3

TABLE 3.2: Some values of $\sigma(e^+e^- \to D^+D^-)$

The benchmarks considered contain M_{D_2} at masses just above M_+, causing kinematic suppression of the decays $D^\pm \to D_2 W^\pm$. In general MSSM scenarios, there is a further contribution of the diagram with t-channel exchange of an additional D-odd particle (such as sleptons). For the minimal model discussed here, sleptons are decoupled causing no t-channel process. For example, if the mass of the selectron is more than 250 GeV (condition 2 in sect. 3 and [220]), the cross section for $s_D = 1/2$ can be reduced by a factor $\geqslant 0.6$, $\sigma_{MSSM} \geqslant 0.6\sigma(s_D = 1/2)$. Combining with numbers from figure 3.1 and Table 3.2 we obtain (for identical masses M_+ at a given beam energy $\frac{\sqrt{s}}{2}$):

$$\sigma(s_D = 1/2) > 4\sigma(s_D = 0). \tag{3.24}$$

• The experimental value of the $e^+e^- \to D^+D^-$ cross section is obtained by summing over all processes with signature (3.26), (3.27) (that is about 3/4 of the total cross section). By taking into account the known BR's for W decay the accuracy of this restoration of $\sigma(e^+e^- \to D^+D^-)$ can be improved.

For a known mass M_+, the cross section $\sigma_{min}(e^+e^- \to D^+D^-)$ is calculated with reasonable precision with equation (3.22). The strong inequality (3.24) allows

to determine the spin s_D from the obtained values of cross sections even with a handful of well-reconstructed events.

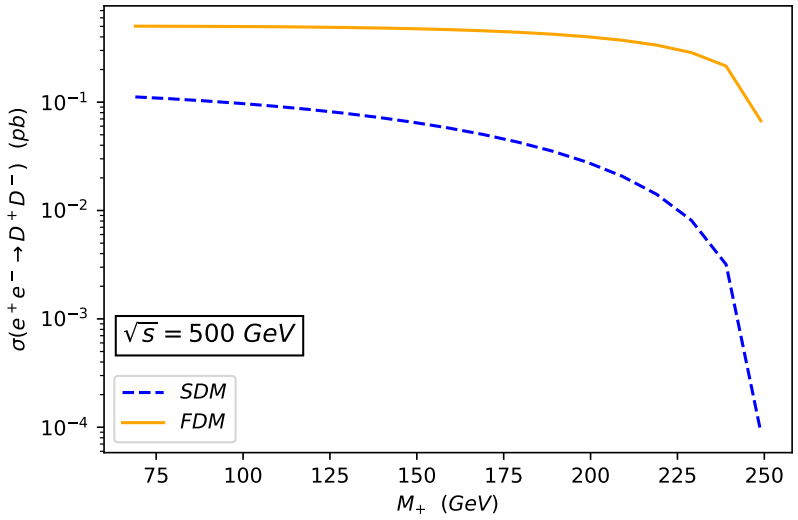

FIGURE 3.2: Comparing the cross section as a function of the mass of $D_\pm$, for fermion and scalar case. BP1 values are used, except for D^+ which is scanned over.

3.2.3 The signature

• **If $M_2 > M_+$ or D_2 is absent**, once produced, particles D^+ decay fast (with a unit probability) to $DW^\pm$,

$$e^+e^- \to D^+D^- \to DDW^+W^- . \tag{3.25}$$

The observable states are decay products of W with a large missing transverse energy $\not{E}_T$ carried away by the invisible D-particle, and the missing mass of particles escaping observation $M(\not{E}_T)$ is large. In contrast to the LHC, where a large flux of low $p_\perp$ particles demands an additional $p_\perp$ cut off, at e^+e^- LC the flux of low $p_\perp$ particles is small.

Therefore, the signatures of the process in the modes suitable for observation are

$$\boxed{\begin{array}{c} e^+e^- \to DD(W \to q\bar{q})(W \to q\bar{q}): \quad \text{Two dijets + } \textit{nothing}, \\ \text{with energy of each dijet } < \frac{\sqrt{s}}{2}, \text{ with large } \not{E}_T \text{ and large } M(\not{E}_T). \end{array}} \tag{3.26a}$$

$$\boxed{\begin{array}{c} e^+e^- \to DD(W \to \ell\nu)(W \to q\bar{q}): \quad \text{One dijet} + e \text{ or } \mu + \textit{nothing}, \\ \text{with energy of each dijet or lepton } < \frac{\sqrt{s}}{2}, \text{ with large } \not{E}_T \text{ and large } M(\not{E}_T). \end{array}} \tag{3.26b}$$

At $M_W^* > 5$ GeV, the branching ratios for different channels of W decay are roughly identical for on-shell W [220] and off-shell W. In particular, the fraction of events with signature (3.26a) is $0.676^2 \approx 0.45$. The fraction of events with signature (3.26b) is $2 \cdot 0.676 \cdot 2 \cdot (1 + 0.17) \cdot 0.108 \approx 0.33$ (here 0.17 is a fraction of μ or e from the decay of τ). At $M_W^* < 5$ GeV, $BR(e\nu)$ and $BR(\mu\nu)$ increase, while the dijet becomes a set of a few hadrons.

• **If $M_+ > M_2$**, when analysing the main process $e^+e^- \to D^+D^-$, *one more decay channel is added,* $D^+ \to D_2W^\pm \to DZW^\pm$. Its branching ratio $B = BR(D^+ \to D_2W^+)$ is typically less than 0.5. Particle D_2 decays fast to DZ, creating new cascades $e^+e^- \to D^+D^- \to DW^+D_2W^- \to DDW^+W^-Z$, $e^+e^- \to D^+D^- \to D_2W^+D_2W^- \to DDW^+W^-ZZ$. As a result, the signature of the processes $e^+e^- \to D^+D^-$ in the modes suitable for observation contains both (3.26) and processes with decay W's or Z's in the mentioned cascades:

$$\boxed{(4 \text{ dijets}, 0\ l^\pm) \div (1 \text{ dijet}, 5\ l^\pm) \text{ with large } \not{E}_T \text{ and large } M(\not{E}_T) + \textit{nothing}} \tag{3.27}$$

Note that the processes with invisible decay $Z \to \nu\bar{\nu}$ (we denote these states as Z_n, their $BR = 20\%$) have signature (3.26).

3.2.4 *W* energy distribution

Here we consider the energy distribution of W with an effective mass M_W^*. We have, in the rest frame of $D^\pm$, a two-particle decay $D^\pm \to DW^\pm$ with

$$E_W^D(M_W^*) = \frac{M_+^2 + M_W^{*2} - M_D^2}{2M_+}, \quad p_W^D(M_W^*) = \frac{\sqrt{(M_+^2 - M_W^{*2} - M_D^2)^2 - 4M_D^2 M_W^{*2}}}{2M_+} \tag{3.28}$$

.

Denoting θ as the W^+ escape angle in the D^+ rest frame with respect to the direction of D^+ motion in the laboratory frame, and using $c \equiv \cos\theta$, we find the energy of W^+ in the laboratory frame as

$$E_W = \gamma_D(E_W^D + c\beta_D p_W^D) \Rightarrow$$
$$\boxed{E_W^{(-)}(M_W^*) < E_W < E_W^{(+)}(M_W^*), \ \textit{where} \ E_W^{(\pm)}(M_W^*) = \gamma_D(E_W^D \pm \beta_D p_W^D)\,.} \tag{3.29}$$

In particular, **at $M_+ - M_D > M_W$** (on-shell case) we have $M_W^* = M_W$, and the kinematical edges of the W energy distribution are

$$E_W^{(\pm)}(M_W) = \gamma_D(E_W^D(M_W) \pm \beta_D p_W^D(M_W)) \\ = \frac{E}{2}\left[1 + \frac{M_W^2 - M_D^2}{M_+^2} \pm \frac{\sqrt{(M_+^2 - M_W^2 - M_D^2)^2 - 4M_D^2 M_W^2}}{M_+^2}\sqrt{1 - \frac{M_+^2}{E^2}}\right] \tag{3.30}$$

3.2.5 Single lepton energy distributions in process (3.26b)

3.2.5.1 Signal Evaluation Kinematics

We study the distribution of muons over its energy E_μ, by the differential cross-section $d\sigma^\mu(E_\mu|M_+, M_D)/dE_\mu$.

The fraction of such events for each separate lepton, e^+, e^-, μ^+ or μ^-, is about 0.08, while their sum is about 0.33 of the total cross section of the process. We will speak, for definiteness, $\ell = \mu^-$ and neglect the muon mass so that in the W rest frame and the laboratory system with W energy E_W respectively

$$E_\mu^W = |p|_\mu^W = M_W^*/2\,, \qquad \gamma_W = E_W/M_W^*,\ \ \beta_W = \sqrt{1 - \gamma_W^{-2}}. \tag{3.31}$$

Just as above, we denote θ_1 as the escape angle of μ relative to the direction of the W in the laboratory frame and use $c_1 = \cos\theta_1$.

The muon energy in the laboratory frame is

$$E_\mu = \gamma_W\,(1 + c_1\beta_W)\,(M_W^*/2) \equiv E_W\,(1 + c_1\beta_W)\,/2 \Rightarrow \\ E_\mu^{(+)}(M_W^*, E_W) \geqslant E_\mu \geqslant E_\mu^{(-)}(M_W^*, E_W), \\ \textit{where}\ \ E_\mu^{(\pm)}(M_W^*, E_W) = (E_W \pm \sqrt{E_W^2 - M_W^{*2}})/2\,. \tag{3.32}$$

In particular, at $M_+ - M_D > M_W$ (on shell case) we have $M_W^* = M_W$, and at given E_W

$$E_\mu^{(+)}(M_W, E_W) \geqslant E_\mu \geqslant E_\mu^{(-)}(M_W, E_W) \\ \textit{with}\ \ E_\mu^{(\pm)}(M_W, E_W) = (E_W \pm \sqrt{E_W^2 - M_W^2})/2. \tag{3.33}$$

It is easy to check that the muon energy energy interval is located entirely within the W energy interval. Therefore, all muon energies lie within the interval determined by the highest value of W energy, i.e. by equation (3.32) with $E_W = E_W^{(+)}$ from equation (3.30).

With a shift of E_W from these boundaries inwards, the density of states in the E_μ distribution grows monotonically due to contributions of smaller E_W values up

to $E_\mu^{(\pm)}$ values, corresponding to the lowest value of W energy $E_W^{(-)}$ from equation (3.30):

$$\varepsilon_k^\pm \equiv E_\mu^{(\pm)} = \frac{E_W^{(-)} \pm \sqrt{(E_W^{(-)})^2 - M_W^2}}{2}. \tag{3.34}$$

With these points the energy distributions of muons have kinks. Between these kinks, the E_μ-distribution is approximately flat.

The cascade $D^- \to DW^- \to D\tau^-\nu \to D\mu^-\nu\nu\nu$ modifies the spectra just discussed. The energy distribution of τ produced in the decay $W \to \tau\nu$ is the same as that for μ or e, discussed above (within the accuracy of $\sim M_\tau/M_W^*$). Once produced, τ decays to $\mu\nu\nu$ in 17 % of cases (the same for decay to $e\nu\nu$). These muons are added to those discussed above.

In the τ rest frame, the energy of muon is $E_\mu^\tau = y\,M_\tau/2$ with $y \leqslant 1$. The energy spectrum of muons is $dN/dy = 2(3-2y)y^2$ (see textbooks). The signal evaluation is presented as energy distributions of muons in the Lab frame. It is clear that this contribution is strongly shifted towards the soft end of the entire muon energy spectrum.

In a well known approach, one measures the edges in the energy distributions of dijets, representing W in the decay $D^\pm \to DW^\pm$ [215, 216]. However, the individual jet energies and consequently, effective masses of dijets cannot be measured with a high precision. The observed lower edge of the W energy distribution in the dijet mode are smeared by this uncertainty. One can only hope for a sufficiently accurate measurement of the upper edge of the W energy distribution, E^+ (3.30).

We suggest to extract the second quantity for description of masses from the lepton energy spectra. The lepton energy is measurable with a high accuracy. We found above that the singular points of the energy distribution of the leptons in the final state with signature (3.26a) are kinematically determined, and therefore can be used for a mass measurement.

M1) If a D_2 particle is absent or $M_2 > M_+$, the results (3.32)-(3.34) describe the energy distributions completely. The shape of the energy distribution of leptons (with one peak or two kinks) allows to determine which case is realized, $M_+ - M_D > M_W$ or $M_+ - M_D < M_W$.

At $M_+ - M_D > M_W$, the positions of the upper edge in the dijet energy distribution E_{on}^+ (3.30) and the lower kink in the muon energy distribution ε_k^- (3.34) give us two equations necessary for the determination of M_D and M_+. We reproduce

these equations for clarity

$$E^{\pm}_{on} = \frac{\sqrt{s}}{2M_+}\left(E^{rest} \pm \beta_+ |p|^{rest}_W\right), \quad \varepsilon^-_k = \frac{E^-_{on} - \sqrt{(E^-_{W,on})^2 - M^2_W}}{2},$$
$$\text{where } E^{rest} = \frac{M^2_+ + M^2_W - M^2_D}{2M_+}, \quad |p|^{rest}_W = \frac{\sqrt{(M^2_+ - M^{*2}_W - M^2_D)^2 - 4M^2_D M^{*2}_W}}{2M_+},$$
$$\beta_+ = \sqrt{1 - \frac{4M^2_+}{s}}. \tag{3.35}$$

By solving simultaneous equations these are used to find equations for masses M_+ and M_D independent of each other.

The position of the upper edge in the dijet energy distribution E^+_{on} should be extracted from all events with signature (3.26), (3.27), the position of the lower kink in the muon energy distribution ε^+_k can be extracted from events with signature (3.26b) only.

M2) The observation of the process $e^+e^- \to DD_2$ would suggest the inequality $\boldsymbol{M_2 < M_+}$ holds. In this case the position of the upper edge in the dijet energy distribution is the same as in the previous case. The position of the lower edge in the dijet energy distribution is either shifted or smeared, in this case the method of [215, 216] becomes completely inapplicable. Taking into account a new decay channel $D^- \to D_2 W^-$ with subsequent decays $D_2 \to DZ_n$, $W^- \to \mu^- \nu$ changes the position of the main singularities in the muon energy spectrum very weakly. Therefore the above mentioned procedure for finding M_+ and M_D may be used in this case as well. The opportunity to extract new singularities from the data for the case M1 is explored in section 3.3.3.

A more detailed analysis reveals two sources of distortion of the signal evaluation (we neglected them in our preliminary analysis).

1. The final width of W and $D^{\pm}$ (Z and D_2) leads to a blurring of the kinematic features derived above. This effect increases with the growth of $M_+ - M_D$.

2. The energy spectra under discussion will be smoothed due to QED initial state radiation (ISR), final state radiation (FSR) and beamstrahlung (BS).

3.2.5.2 Mass Determination

Here we will discuss the case where $W^{\pm}$ are produced onshell, i.e $\boldsymbol{M_+ - M_D > M_W}$.

We analyse distortion of the key features of the muon energy distribution for the process discussed, at parton level, as presented in figure 3.3 left and right for SDM and FDM respectively (at BP1). Here the blue line corresponds to the production of $D^{\pm}DW^{\mp}$ and the subsequent decay of the W boson, i.e W-width effects are

not included. The yellow line corresponds to a simulation of the full production cross-section, taking into account all widths. This effect smooths ϵ_k^+ considerably, but the dominant distortion effect comes from the effects of ISR and BS (RAD), as shown by the green line. In CalcHEP, ISR is modelled as in Jadach, Skrzypek, and Ward [221], and BS by that of P. Chen [222]. The key observation here is that the left hand kink, ϵ_k^-, remains visible.

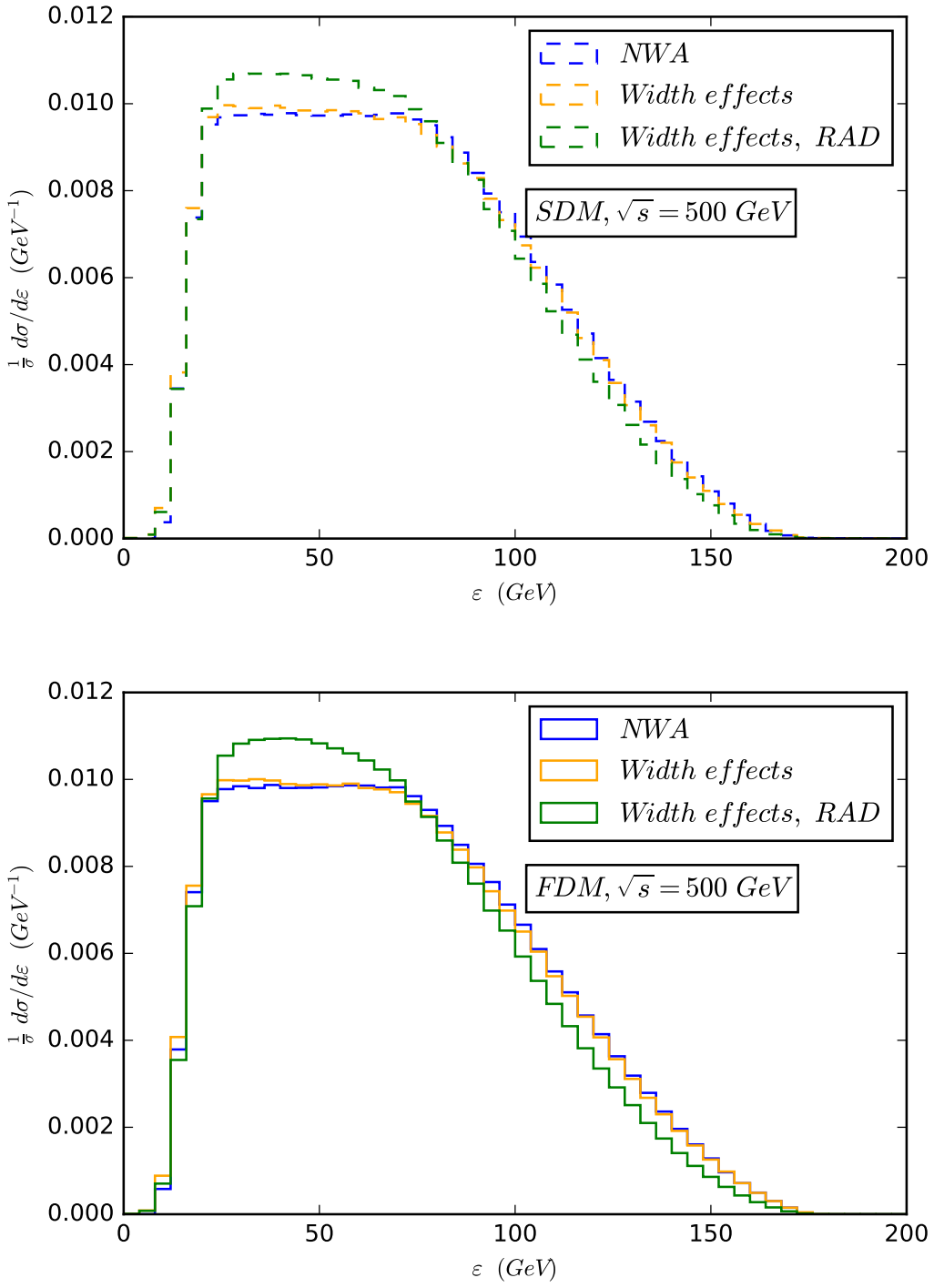

FIGURE 3.3: Muon energy distribution at BP1 for SDM (top) and FDM (bottom).

In figure 3.4, we compare the muon energy distributions for SDM and FDM, including all width and RAD effects. For the SDM case, the left plot shows the energy distribution of muons for the case of the matrix element independent of

θ_1. Since the positions of kinks are kinematically determined, it is not surprising that the calculations for distinct models (containing different angular dependence) show variations in shapes, but do not perturb the position of kinks. We see that for FDM, ϵ_k^+ is less well preserved than for SDM. Also, the higher energy tail demonstrates the small difference in behaviour, however has no impact on the endpoint, ϵ^+, required for the measurement of mass. This small difference between overall shapes suggests that the muon energy is not a good observable to differentiate between spins of DM, but conversely that it is a good observable for spin-independent measurements of mass.

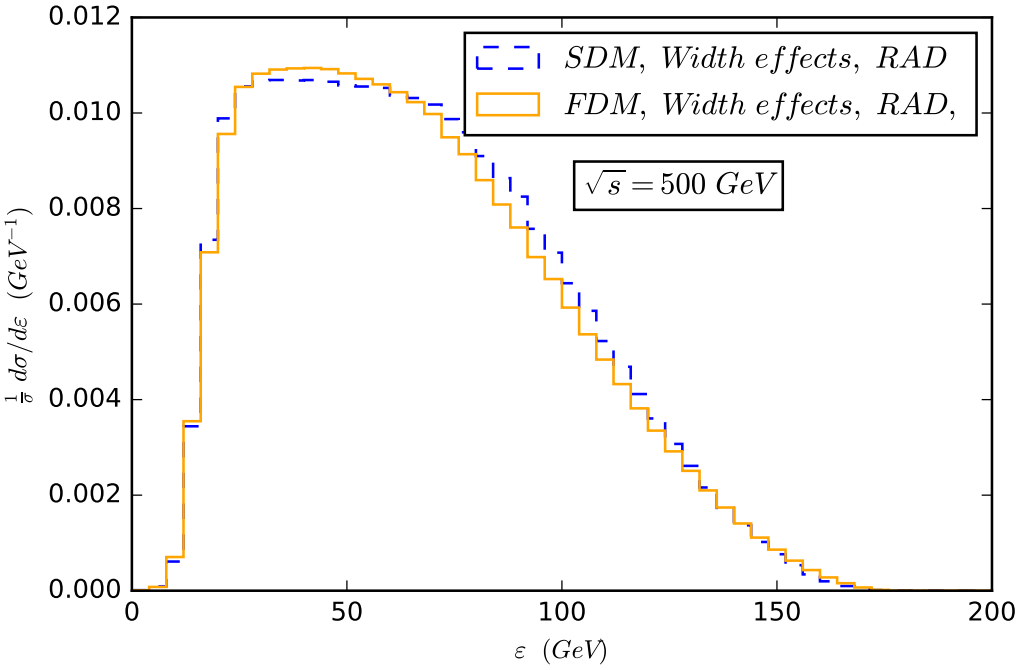

FIGURE 3.4: Comparing SDM and FDM Muon Energy Distributions using BP1 values, including width and radiation effects.

The right plot of figure3 shows the muon energy distribution for the off-shell W decay case. Its peak disagrees with the equation derived for this point, $\varepsilon_p = \sqrt{s}/2(1 + c_1\beta_+)(1 - M_D/M_+)/2$. Here c_1 is the cosine of the angle between the W boson in the lab frame and the muon that decays from it. In the $M_+ = 120$ GeV and $M_D = 60$ GeV case with $\sqrt{(s)} = 500$ GeV it is expected that $\varepsilon_p = 136.88$ GeV. As can be seen by figure1, the peak occurs at roughly 12 GeV, far from the expected value.

The problem lies with this c_1 term. At this peak, M_W^* is a maximum so that $M_W^* = M_+ - M_D$ and therefore $c_1 = 1$ for this maximum value. However, in CalcHEP c_1 is not constrained to make these plots.

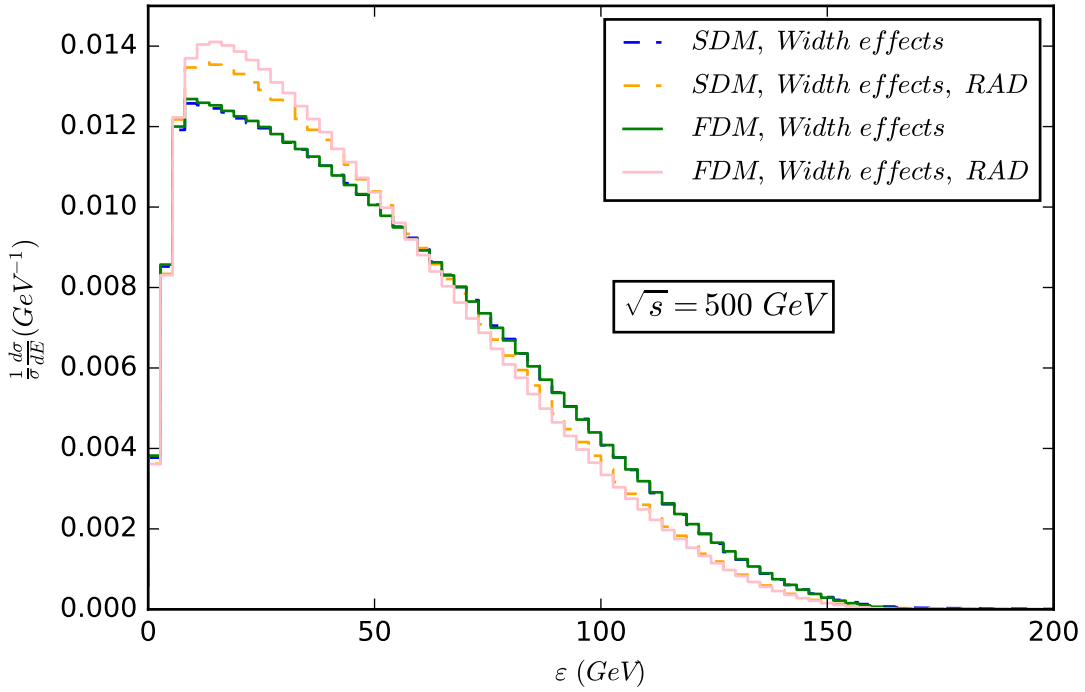

FIGURE 3.5: Muon energy distribution for $M_D = 60$GeV, $M_+ = 120$GeV, with both fermion and scalar dark matter models, showing the disagreement in peak placement.

We apply a cut to the parameter $P(e2, N2)$, the angle between the muon and the direction of the boosting of this particle set i.e the W boson these decay from. With this cut, a change in the distribution is observed. The peak is shifted along the x-axis, closer to the expected range.

Observation of events with signature (3.26), (3.27) will be a clear *signal* for DM particle candidates. The non-observation of such events will allow to find lower limits for masses M_+, as was shown in [181, 182, 183]. One can hope that these limits will be close to the beam energy $\frac{\sqrt{s}}{2}$.

At $M_+ < \frac{\sqrt{s}}{2}$, the cross section $e^+e^- \to D^+D^-$ is a large fraction of the total cross section of e^+e^- annihilation, and it makes this observation a very realistic task.

3.2.6 Spin determination

An effective way to determine the spin of DM is through the angle of the $W^\pm$ which may be determined from a dijet pair with invariant mass close to the W mass. This is most powerful when the mass gap between DM and its charged partner is sufficient to allow an on-shell W boson to propagate. This may be seen in figure 3.6, where BP1 and BP2 correspond to representative parameter points (see section 3.1.3) with on-shell and off-shell W boson production respectively.

The dominant background, BG1 (see section 3.3.1 for details) is from the SM di-W production process, which is dominated by the t-channel neutrino exchange diagram, resulting in $W^{\pm}$ bosons being produced mostly along the beamline. For BP1, $W^{\pm}$ bosons are mostly produced transverse to the beam direction for SDM whilst for FDM the $W^{\pm}$ are mostly produced along the beamline, however the distribution is much flatter than BG1, giving a good possibility to distinguish these signals from background and each other. For BP2 however, the t-channel diagram becomes more important, as the intermediate $D^{\pm}$ in s-channel signal diagram is pushed further off-shell.

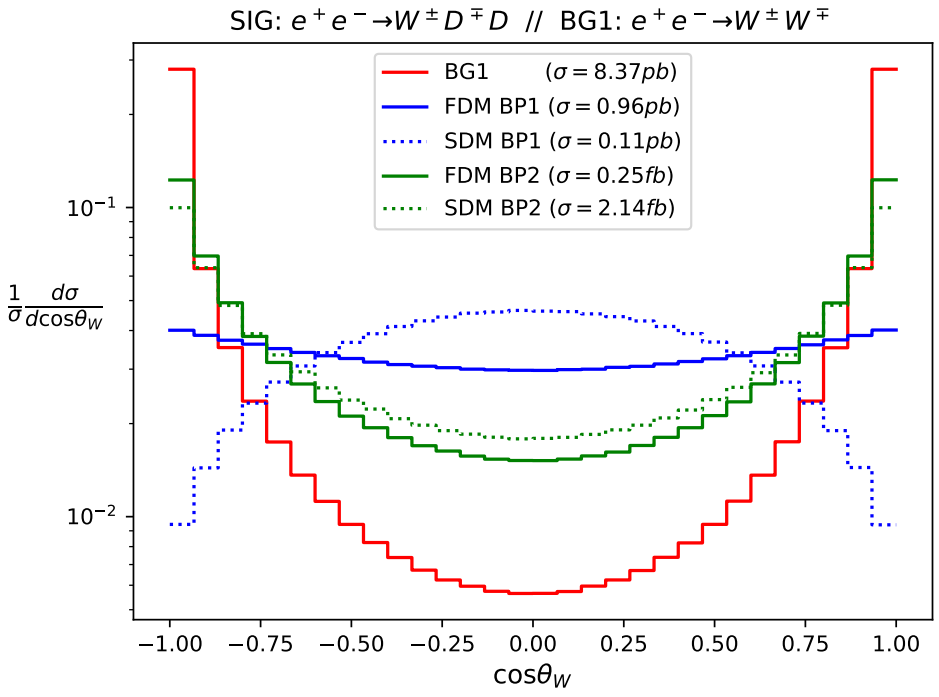

FIGURE 3.6: The angular distribution of $W^{\pm}$ with respect to beam direction in the lab frame.

3.3 Signal versus background analysis and determination of mass/spin

In this section, we discuss potential sources of background and simple strategies to reduce their presence in an analysis. For analyses designed to determine clear kinematic features such as those discussed in section 3.2.3, these "backgrounds" may also include non-SM processes. We then perform accurate detector level optimization of analyses for discovery, mass and spin determination.

3.3.1 Background to the process with signature (3.26)

We show here that the cross sections of possible background processes (with suitable simple cuts) are $\sim$ 10 – 100 times less than the cross section of the signal process and therefore they can be neglected at analysis. Note that some of our estimates can be corrected due to ISR and beamstrahlung.

BG1

The process $e^+e^- \to W^+W^-$ gives the same final state as those with signature (3.26). However, many of its features are not permitted by this signature, especially the lack of large missing mass. This fact allow to exclude the BG1 process from analysis with a good confidence applying suitable cuts.

Let us discuss e.g. the observable mode $\mu^- + jj + \not{E}_T$.

(a) For the process BG1, the energy of each dijet $E_{jj} = \frac{\sqrt{s}}{2}$.

Application of a cut in the dijet energy $E_{jj} < E^c$ with large enough $\frac{\sqrt{s}}{2} - E^c$ keeps all dijets from the signal process and leaves only a small fraction of events from BG1.

The dijet energy E_{jj} in BG1 can be less than E^c only if W^- (seen as $\ell^-\nu$) is strongly off shell with an effective mass much higher than M_W. The probability of such situation is estimated easily, it is $\delta_{W1a} \approx \Gamma_w M_W/(\pi\frac{\sqrt{s}}{2}(\frac{\sqrt{s}}{2} - E^c))$.

(b) For BG1 the missing mass $M(\not{E}_T) = 0$. Application of cut $M(\not{E}_T) > M^c$ with suitable M^c keeps all events of the signal process but diminishes the contribution of BG1 in the events with signature (3.26A) even further.

BG2

The same (in its content) final state as we consider for the signal process can be achieved via mechanism without at least one intermediate $D^\pm$ in s-channel, e.g.

$$e^+e^- \to (W^- \to \mu^-\bar{\nu})(W^+ \to D(D^+ \to DW^+ \to Dq\bar{q})).$$

To simplify the text, we will comment here about the case $M_{D_2} > M_+$ only.

The contribution of this mechanism to the total cross section is at least a factor α times less than that of the signal process. Indeed, in the signal process the value of the cross section is given by the second order (in electroweak coupling) process $e^+e^- \to D^+D^-$. It includes the intermediate decay $D^+ \to DW^+$ with probability 1, the corresponding cross section is $\sim \alpha/s$ (an additional α in the formal diagram is compensated by the small D^+ width Γ^+ in the denominator of propagator). In the process BG2 we have third order process with decays in final stage (if $M_+ - M_D < M_W$ that is even the fourth order process). The neutrino exchange term enhances this contribution only logarithmically. BG2 may be reduced by variation of longitudinal polarization of initial electron or additionally by the cut in transverse momentum of muon $p_{\mu\perp} > 40$ GeV, however in this study we discuss only for unpolarized initial states as kinematic cuts are sufficient.

The interference of this BG2 mechanism with the signal one is also very small. In particular, in the signal process final leptons ($\ell^-\nu$) and D, arise from an intermediate D with effective mass $M_+ \pm (\sim \Gamma^+)$, while in the process BG2 the analogous effective mass range does not contain the majority of the cross section.

Therefore, the contribution of mechanism BG2 can be neglected with accuracy better than 1%.

BG3

$e^+e^- \to DD_2 \to DD^+W^- \to DDW^+W^-$. This background is absent if $M_{D_2} < M_+$ or $M_{D_2} + M_D > \sqrt{s}$. If $\sigma(e^+e^- \to DD_2)$ is not small at given $\sqrt{s}$, this fact will be seen via an observation of the process $e^+e^- \to DDZ$ (B.2). The cross section $\sigma(BG3) < \sigma(e^+e^- \to DDZ)$, i.e. it is much less than $\sigma(e^+e^- \to D^+D^- \to DDW^+W^-)$ (roughly, by one order of magnitude). In this process all recorded particles move in one hemisphere in contrast to the signal process, where they move in two opposite hemispheres. Therefore, the contribution of this background process may be reduced additionally by application of suitable cuts.

BG4

In the SM processes with an observed state, satisfying criterion (3.26), large $\not{E}_T$ is carried away by additional neutrinos. The corresponding cross section is at least one electroweak coupling constant squared $g^2/4\pi$ or $g'^2/4\pi$ smaller than σ_0, with $g^2/4\pi \sim g'^2/4\pi \sim \alpha$. Therefore, $\sigma(BG4) \lesssim 0.01\sigma(e^+e^- \to D^+D^-)$.

3.3.2 Signal versus background analysis

A useful kinematic observable at the ILC is the missing mass of the system (equation 3.36), reconstructed from the visible particles. Without RAD effects, this would enable removal of all background processes at parton level.

$$M_{miss} = \left| (\sqrt{s}, 0, 0, 0) - \sum_{vis} P_{vis} \right| \tag{3.36}$$

Here we present results for calculation of signal and background at luminosity of $500 fb^{-1}$ (prediction for end of run 1). Events are simulated at parton level in CalcHEP before being passed to PYTHIA for hadronization and finally Delphes for fast detector simulation using the ILD detector card based on [134]. We set the R parameter in the antikt jet clustering algorithm to 0.8, which improves dijet reconstruction; the standard value of 0.5 reconstructs additional soft jets close to the jet cone radius, smearing the Breit-Wigner for the W-boson reconstructed from dijet.

BP1 for process with signature (3.26)

Signal processes are produced via the process $e^+e^- \to (D^+ \to Djj)(D^- \to D\mu\nu)$. The dominant background, BG1, is produced via full 2-4 process $e^+e^- \to W+W- \to j,j,\mu,\nu$. Both BG2 and BG3 are included, as well as interference between them, by $e^+e^- \to W^-DD^+$ with subsequent decays to D,D,j,j,μ,ν. The final SM background process, BG4, is produced via $e^+e^- \to W^+W^-Z$ with decays to j,j,μ,ν,ν,ν. We present the key distributions for kinematic cuts (figs 3.7 3.8 3.9) for BP1 although these are similar for BP2. The dijet energy distribution exhibits a tail at higher E_{jj}, as a result of the t-channel process mediated by an electron neutrino. These are detector level distributions, where we have applied an initial veto requiring at least 2 jets and a single muon. The red shaded regions show the proposed cut regions (as outlined in table 3.3).

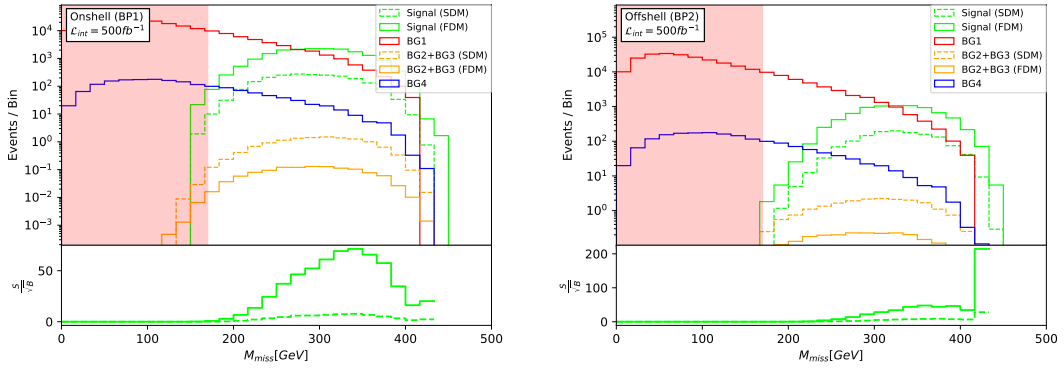

FIGURE 3.7: Missing mass at detector level

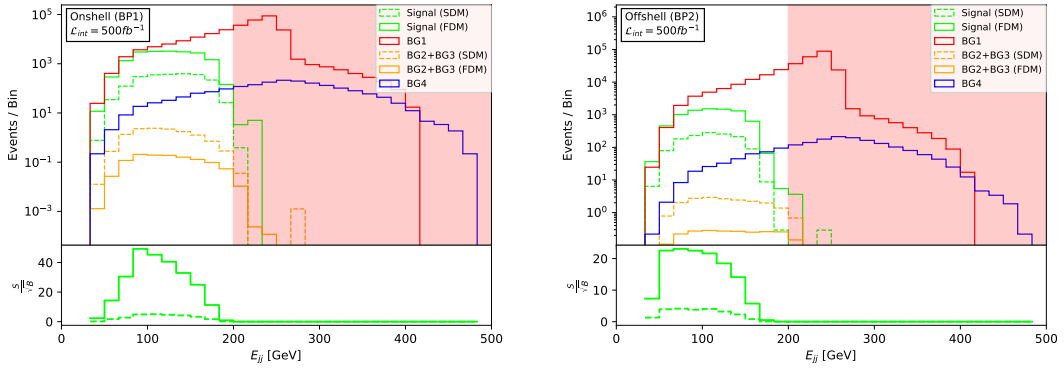

FIGURE 3.8: Energy of W boson reconstructed from dijet at detector level

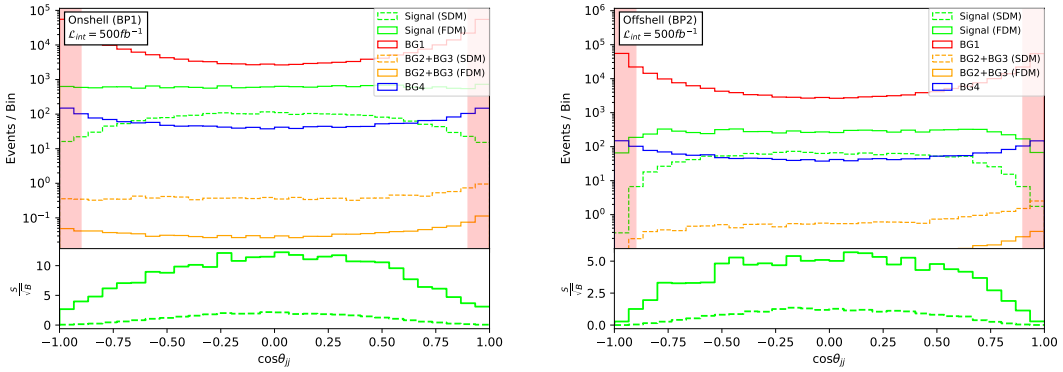

FIGURE 3.9: Scattering angle of W as reconstructed from dijet at detector level.

Based on these results, we propose the analysis cut-flow as described in Table 3.3.

BP1 cut flow

	SDM				**FDM**			
	S	B	S/B	α	S	B	S/B	α
No cuts	2098	332588	0.006	3.63	17962	334254	0.054	30.27
$M_{miss} > 170$	2095	83143	0.025	7.18	17922	84810	0.211	55.92
$E_{jj} < 200$	2094	67130	0.031	7.96	17917	68796	0.260	60.84
$\lvert\cos\theta_{jj}\rvert < 0.9$	2046	29526	0.069	11.52	15993	31038	0.515	73.75
$\lvert\cos\theta_{\mu}\rvert < 0.9$	1947	24306	0.081	12.02	14893	25766	0.578	73.86

BP2 cut flow

	SDM				**FDM**			
	S	B	S/B	α	S	B	S/B	α
No cuts	1370	284290	0.005	2.56	8138	284273	0.029	15.05
$M_{miss} > 170$	1370	39323	0.0349	6.79	8136	39307	0.207	37.35
$E_{jj} < 200$	1369	36177	0.0379	7.06	8123	36161	0.225	38.60
$\lvert\cos\theta_{jj}\rvert < 0.9$	1360	18647	0.0730	9.62	7815	18634	0.419	48.06
$\lvert\cos\theta_{\mu}\rvert < 0.9$	1326	14398	0.0922	10.58	7420	14386	0.516	50.25

TABLE 3.3: Cutflow for BP1 (top) and BP2 (bottom) showing efficiency and significance, $\alpha = \frac{S}{\sqrt{S+B}}$. Cuts are applied sequentially from top to bottom.

3.3.3 Mass determination

3.3.3.1 Kinematic fitting

We may fit the approximate shape of the muon energy distribution using a piecewise function. The functional form has power law dependence for the tail regions, and a constant for the plateau region between the two kinks (eq 3.37).

$$f(\epsilon) = \begin{cases} b\left(\frac{\epsilon}{\epsilon_k^-}\right)^a & \text{if } \epsilon \leq \epsilon_k^- \\ b & \text{if } \epsilon_k^- < \epsilon < \epsilon_k^+ \\ b\left(1 - \frac{\epsilon - \epsilon_k^+}{\epsilon^+ - \epsilon_k^+}\right)^c & \text{if } \epsilon_k^+ \leq \epsilon < \epsilon^+ \\ 0 & \text{if } \epsilon^+ \leq \epsilon \end{cases} \tag{3.37}$$

Analysis of the shape of the muon energy using this piecewise function is conducted using the expected number of events, produced via monte carlo for each model at BP1. Here we generate the pseudo-experimental data set by neglecting theory errors. This data set corresponds to the expected number of events in each bin from a large MC sample (often called the *Asimov data set*), allowing us to predict the expected mass resolutions. The discrepancy between this piecewise function and the detector level distributions for each model results in a bias on the estimator, to capture this we include a methodological error (conservatively set to be 10% of signal for each bin). The signal plus background is calculated for realistic statistics, corresponding to cross-section times luminosity for each process. The cuts outlined in table 3.3 are applied, excluding the angular cuts; these angular cuts smear ϵ_k^- considerably, whilst other cuts give approximately uniform modulation of the signal distribution.

The profile χ^2 is calculated by minimising over nuisance parameters a, b, c, analogous to fitting experimental the signal with fixed $\epsilon_k^-, \epsilon_k^+, \epsilon^+$ (which may be determined from $M_D, M_+, \sqrt{s}$). Here, the mean collision energy after RAD was used (calculated to be 477.78 GeV from the RAD model used). The minimum of this profiled χ^2 corresponds to the global minimum for the fit, when M_D, M_+ are also allowed to vary. From the 1σ contour, we may extract the errors on the masses. Although this shape fitting procedure is less sensitive than template fitting, it has the key advantage of being model independent. To obtain comparable precision for SDM, we would require approximately 40 times more luminosity.

		$500 fb^{-1}$	$20 ab^{-1}$
FDM	M_D	$58.4^{+5.7}_{-6.0}$	$57.6^{+1.9}_{-2.2}$
	M_+	$158.1^{+4.0}_{-3.7}$	$157.4^{+2.7}_{-2.4}$
SDM	M_D	$66.0^{+19.2}_{-64.3}$	$64.3^{+3.2}_{-6.1}$
	M_+	$161.3^{+14.7}_{-52.8}$	$161.0^{+3.3}_{-3.9}$

TABLE 3.4: Mass resolutions for BP1 kinematic fitting procedure.

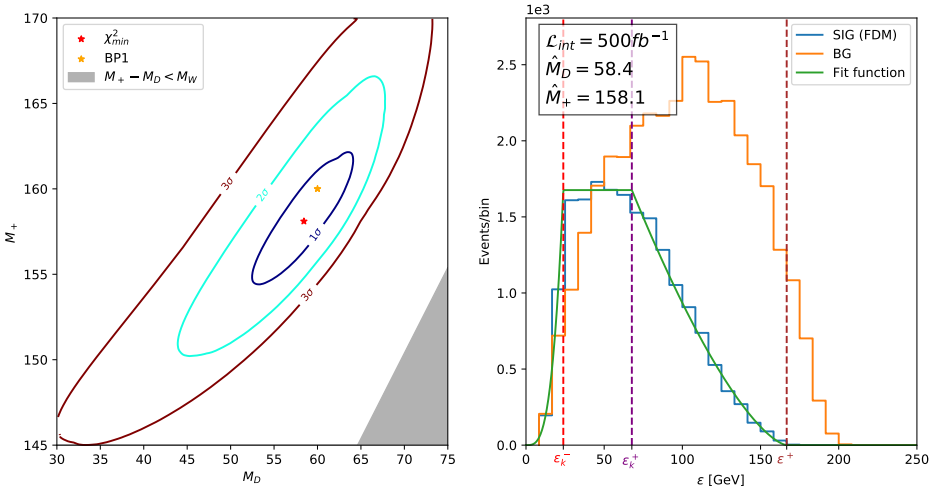

FIGURE 3.10: Profile χ^2 value for kinematic fitting of BP1 (left) and muon energy distribution with best fit (right), for FDM.

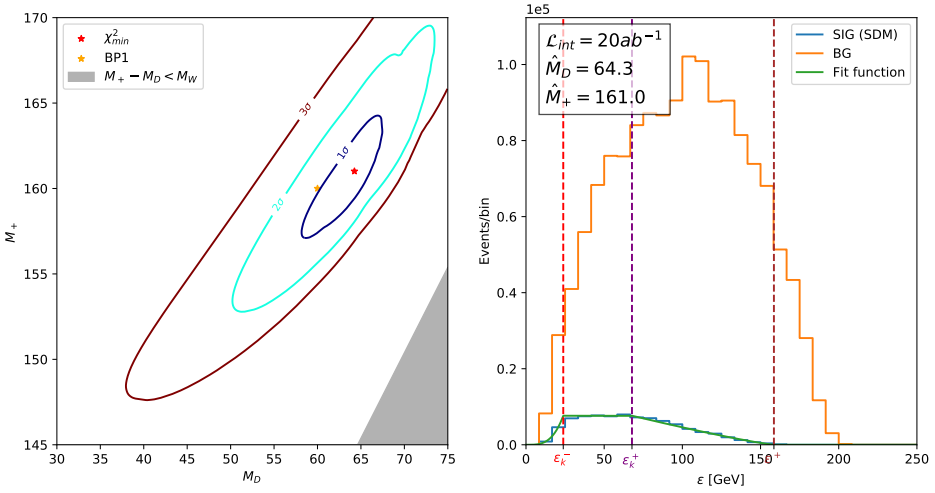

FIGURE 3.11: Profile χ^2 value for kinematic fitting of BP1 (left) and muon energy distribution with best fit (right), for SDM.

3.3.3.2 Template fitting

For off-shell W bosons in the semi-leptonic decay channel (BP2), there are no longer clear kinematic features and so Monte Carlo template fitting was employed. Here, a grid of event level Monte Carlo distributions in muon energy were produced in a 13x13 grid for $M_D = 168.0 \rightarrow 170.0$and $M_+ = 118.0 \rightarrow 122.0$. Then, using a 2D linear interpolation in M_D,M_+, we may calculate the χ^2 contour presented in figs 3.12, 3.13 . Although this strategy yields better accuracy, information about the overall normalisation of the distributions was used, making this

approach more model dependent. We may also now use angular cuts, improving the signal significance and signal-to-background ratio.

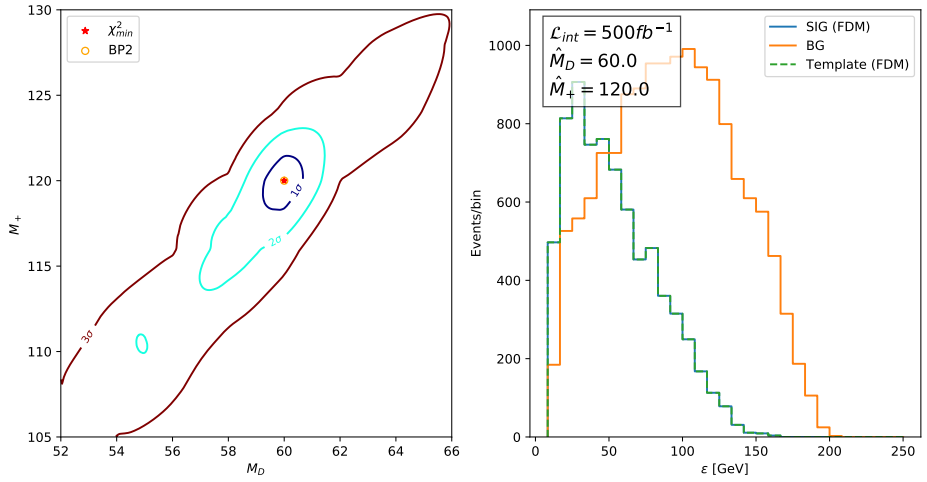

FIGURE 3.12: Profile χ^2 value for template fitting of BP2 (left) and muon energy distribution with best fit (right), for FDM.

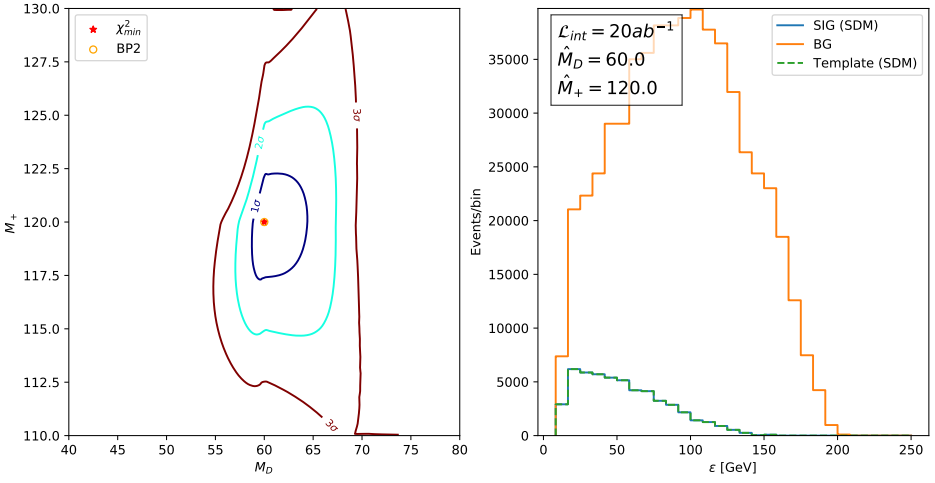

FIGURE 3.13: Profile χ^2 value for template fitting of BP2 (left) and muon energy distribution with best fit (right), for SDM.

		$500fb^{-1}$	$20ab^{-1}$
FDM	M_D	$60.0^{+0.7}_{-0.8}$	$60.0^{+0.1}_{-0.1}$
	M_+	$120.0^{+1.5}_{-1.7}$	$120.0^{+0.2}_{-0.3}$
SDM	M_D	$60.0^{+24.1}_{-19.7}$	$60.0^{+4.4}_{-1.3}$
	M_+	$120.0^{+22.3}_{-45.9}$	$120.0^{+2.3}_{-2.7}$

TABLE 3.5: Mass resolutions for BP2 shape fitting procedure.

3.3.4 Spin discrimination

The angular distribution of W bosons reconstructed from dijets appears to show different behaviour for scalar and fermionic DM candidates. Here we perform a binned composite likelihood analysis to estimate discriminating power of these distributions, assuming that a signal of one model is present. Here we assume that the mass of the DM is precisely known, however a more complete treatment would involve a simultaneous fit of mass and spin. Events are generated with the model assigned to "Assumed nature" in table 3.6, before statistical comparison with the alternative model is conducted. We perform the analysis for two cases; using only the shape (signal strength becomes a nuisance parameter μ, which may vary to maximise the likelihood) and also using the signal strength predicted by the specific model realisations (here $\mu = 1$). In table 3.6 we present the luminosity required to exclude a given hypothesis at the expected 95% confidence level. Distributions used here are after the M_{miss} and E_{jj} cuts of table 3.3 only.

$$\frac{d\sigma}{d\cos\theta} \propto \begin{cases} 1-\cos^2\theta, & \text{if SDM} \\ (1+\frac{s}{4M_+^2})-(1-\frac{s}{4M_+^2})\cos^2\theta, & \text{if FDM} \end{cases} \tag{3.38}$$

The D^+ angular distribution is given by equation 3.38. As M_+ increases to half centre of mass, the angular behaviour for FDM flattens making it more difficult to discriminate.

	$\mathcal{L}_{int}$ to differentiate at 95% CL / fb^{-1}			
	Shape only		Shape and cross-section	
Assumed nature	SDM	FDM	SDM	FDM
BP1	974.9	30.08	1.9	3.4
BP2	2320.2	117.9	9.6	13.2

TABLE 3.6: Integrated luminosity required to discriminate between spin of DM within these models using binned composite likelihoods.

3.4 Conclusions

We consider models in which stability of dark matter particles D is ensured by conservation of new quantum number referred to as D-parity. Besides these models contain charged particles $D^\pm$ with the same D-parity. (Examples – Inert Doublet Model with scalar D-particles and MSSM with D-particle of spin 1/2 and D-parity equal R-parity). In these models we have studied the energy distribution of single lepton in the process like $e^+e^- \to D^+D^- \to DDW^\pm(\to qq)W^\mp(\to \ell\nu)$, having high enough cross section. Simple analysis allows us to establish that this

distribution has singular points, kinks, peaks and end points, which are driven by kinematics only, and therefore are model-independent. Based on this analysis, we propose to use the mentioned distribution at future linear e^+e^- collider ILC, CLIC, etc. for the precise measurement of masses of dark matter particles and charged particles $D^{\pm}$.

This method is in several aspects superior to the standard approaches discussed elsewhere.

1) It uses leptons which are copious and can be accurately measured in contrast with jets which individual energy can be measured only with lower precision.

2) These singularities are robust and survive even when superimposed on top of any smooth background.

In addition, even a rough measurement of cross sections with a very clean signature allows to determine spin of DM particles based on the results of mentioned kinematical measurements.

Chapter 4

Any Room Left for Technicolor? Dilepton Searches at the LHC and Beyond

Now we move the focus away from dark matter and towards a collider probe for technicolor. Technicolor models of electroweak symmetry breaking [52, 53, 54] solve the hierarchy problem by naturally generating a strong coupling regime in the TeV energy range and a resulting composite higgs. They predict a large bound state spectrum. LHC data has been used to study dilepton constraints on the parameter space of technicolor vector and axial vector resonances in [223, 224], recently updated in [225]. To date that analysis have been presented in a large phenomenological parameter space. Our goal here is to study where UV complete models are likely to lie in that parameter space, whether the constraints are stringent enough to exclude the paradigm, and to motivate further analysis or colliders that might do so.

Strongly coupled models have been pressured by the precision electroweak data [226] (which warns against extended electroweak sectors) and the discovery of a light higgs [36, 35]. However, given our paucity of tools for computing in strongly coupled environments, there has been a hope that within the space of strongly coupled gauge theories are some that might still be tuned to the data. Walking theories [227], that lie close to the edge of the conformal window in gauge theories with varying N_c and N_f, represent a sensible argument that such fine tuned models may exist with both small higgs mass [228, 229, 230, 231, 232] and electroweak precision data S parameter [58].

A clear prediction of these models though is their large bound state spectrum which must emerge close to the electroweak scale. Light pseudo-Goldstone modes could, but need not, exist and when they do are hard to pin down because their

mass is determined by breaking of the chiral symmetries by the potentially unknown origin of flavour physics (which could be strong). We will therefore concentrate on the vector(ρ) and pseudo-vector(A) mesons of such theories which are probably more robust in their mass predictions.

As a test case, we will present our theoretical predictions for SU(N_c) technicolor theories with N_f flavours in the fundamental representation. There is a choice as to how many of these N_f flavours form SU(2)$_L$ doublets. The S parameter [233] suggests more than one doublet is unlikely. Further if more than one doublet contributes to determining the electroweak scale through F_Π (the pion decay constant [234]) then the entire scale of the technicolor theory moves down potentially making these states more accessible. If there is a single doublet then there will be just a single triplet of spin one particles (each of the ρ and A) that are most easily experimentally accessible (since they mix with the W and Z and can be produced singly in electroweak processes). Placing constraints on the single doublet theory therefore offers techicolor the maximal chance of escape and we will concentrate on this (since such models will be the last ones standing). We will though also present results for the spectrum of theories with multiple electroweak doublets.

We wish to predict the masses and decay constants of the ρ and A states in the space of strongly coupled models. Lattice techniques have begun the job [235, 236] but they are computationally hard when the dynamics is spread over a wide range of scales and it will take many years of hard work to understand the full N_c, N_f parameter space. To make progress more quickly we will describe the dynamics using holography [237, 238, 239]. Holography provides a rigorous method of computation in a selection of strongly coupled gauge theories close to $N = 4$ supersymmetric gauge theory including theories with quarks [240, 241, 242, 243]. In the quenched (probe) limit the key ingredient to determine the spectrum is the running anomalous dimension of the quark bilinear ($\bar{q}q$), γ [244, 245]. Embracing that observation we can construct holographic models of generic gauge theories [246, 247]. The predictions for the QCD ($N_c = N_f = 3$) spectrum lie surprisingly close to observation at the 10% level and one can hope as one moves away to theories with e.g. walking behaviour that the models will continue to make sensible predictions of the spectrum. For the purist the approach we use lays down a ball park estimate and challenges them to estimate the parameter space of the models more accurately.

For generic N_c, N_f the spectrum will look QCD-like with a heavy σ (higgs) and a large value for the S parameter. The "last hope" for technicolor (which one might hope to exclude) is that the (unknown) IR running is sufficiently fine tuned that it can generate a light higgs and low S. The holographic models allow the σ to become light if the running around the chiral symmetry breaking scale is near conformal [246]. Most likely, if any, only a single choice of N_c and N_f will generate suitable walking and hence a suitably light composite higgs. Since we

cannot guess that theory we will instead tune the IR running of every choice of theory (ie N_f, N_c) such that a 125 GeV state is generated. There is also a 5d gauge coupling in the holographic model that allows the ρ and A masses to be tuned together to achieve low values of S (this is the only way to achieve small S in the simple holographic model presented) - again we do this for all theories. Of course this means that the spectrum in most (if not all) cases will be wrong but our philosophy is to show where the theories might lie if treated most favourably to set the benchmark for total exclusion.

To compare the predictions to data we will use the constraints placed on the phenomenological model of techni–ρ and A proposed in [59, 248]. The philosophy, based on the ideas of hidden local symmetry [249, 250, 251], is to describe the vector mesons as the massive gauge bosons of a broken gauged $\mathrm{SU}(N_f)_L \otimes \mathrm{SU}(N_f)_R$ symmetry. The two main signals relevant for phenomenology are Drell-Yan production and Vector Boson Fusion [223, 224]. In each case a single ρ or A is produced through mixing with the electroweak gauge bosons via the combined mass matrix determined from the action. Constraints on this model (for the case of a single electroweak doublet), from Drell-Yan processes, have recently been updated in [225] to the March 2018 LHC results on CMS dilepton resonance search [252]. The holographic model makes predictions for the parameters of the phenomenological model so the constraints can be directly applied.

The results of the analysis in brief are that the technicolor theories that emerge are rather odd - they enter the strong coupling at a scale of 700 TeV or above before settling on an IR fixed point that trigger symmetry breaking at the 1 TeV or so range. We find the IR theory constructed in the way described is largely independent of the UV theory. The result is that the bound states of the theory know, through the strong interactions, of rather high scales and their holographic wave functions stretch to large UV scales. The result is that the ρ and A masses increase to $M_\rho \simeq 4$ TeV. Such theories, with the specific couplings we have found, are beyond the reach of the current LHC dilepton searches. However, they do motivate new signatures to explore and future colliders with higher energies which could probe these scales. In a sense such theories display the issues that any extension of the standard model that addresses the hierarchy problem must now encounter - to make the higgs light there must be tuning at one part in 100 or so and new states must be pushed to high scale.

In the next two sections we will review our holographic model used to estimate the parameter space for technicolor models and the phenomenological analysis of [225] before bringing the two together to show the exclusion in section 3. The act of forcing a small S parameter in the holographic model corresponds to enforcing ρ-A degeneracy and this places the models in the parameter space of the phenomenological model where a measure of that degeneracy, a, is close to zero (that the holographic predictions match the model's parameter space is tested

by this fact). Unfortunately this is the toughest edge of the parameter space to probe experimentally. The reader who wishes to cut to the chase should inspect Figure 4.2 where the bounds on the models in the coupling versus A mass parameter space are shown with the holography predictions for the parameter space of technicolor overlayed.

4.1 Holographic Model

Our holographic model is the Dynamic AdS/QCD model which is described in detail in [246, 247]. The action is

$$\begin{aligned} S &= -\int d^4x\, du, \mathrm{Tr}\, u^3 \left[\tfrac{1}{r^2}|DX|^2 \right. \\ &\left. + \tfrac{\Delta m^2(r)}{u^2}|X|^2 + \tfrac{1}{2\kappa^2}(F_V^2 + F_A^2)\right], \end{aligned} \tag{4.1}$$

Here u is the holographic coordinate dual to energy scale, and X is a field dual to the quark condensate $\bar{q}q$. The solution of its equation of motion, which can be found numerically, describes the vacuum of the theory. We pick the on mass shell condition $|X|(u = X_0) = X_0$ with $|X|'(X_0) = 0$ and require $|X| = 0$ in the UV so all techniquarks are massless. Fluctuations of X describe the σ and π fields.

The vector and axial vector fields describe the operators $\bar{q}\gamma^\mu q$ and $\bar{q}\gamma^\mu\gamma_5 q$ and their fluctuations give the ρ and A spectrum and couplings.

The theory lives in a geometry

$$ds^2 = r^2 dx_{3+1}^2 + \frac{1}{r^2}du^2, \qquad r^2 = u^2 + |TrX|^2 \tag{4.2}$$

$|TrX|$ is included in the definition of r in the metric which provides a "back-reaction" on the metric in the spirit of probe brane models [243] and communicates the mass gap to the mesonic spectrum.

Δm^2 is a renormalization group scale/radially dependent mass term which can be fixed, for example, from the two loop running of the gauge coupling in the theory of interest as described in [246, 247] - this ansatz includes IR fixed points for the running for appropriate choices of N_c, N_f.

The spectrum of the theory is found by looking at linearized fluctuations of the fields about the vacuum where fields generically take the form $f(u)e^{ip.x}, p^2 = -M^2$. A Sturm-Louville equation results for $f(u)$ leading to a discrete spectrum. By substituting the wave functions back into the action and integrating over u the decay constants can also be determined. The normalizations of the fluctuations are determined by matching to the gauge theory expectations for the vector-vector, axial-axial and scalar-scalar correlators in the UV of the theory. This full

procedure is described in detail in [246, 247]. Note that in the holographic literature [246, 247] the dimension 2 coupling between the vector meson and it's associated source is normally written as F_V^2 whilst in the Weinberg sum rule literature [226] it is written as $m_V F_V$. We will adopt the latter definition here to fit the other literature on technicolor.

Our models will focus first on a single electroweak doublet of techni-quarks but we will assume the existence of technicolor singlet quarks to change the UV running of the coupling. In the computations of f_π and $F_{V/A}$ for the electroweak physics only the electroweak doublet contributes - so factors of N_f and N_c in these quantities reflect the values in a one doublet model. As discussed in the introduction we will further tune the IR running of γ in all our theories to generate a 125 GeV σ meson. To achieve this we set a value of α_{TC} where we deviate from the UV running. Below that scale we allow N_f to become a free parameter and pick a N_f^{IR} (which we stress is not the true value of N_f in the theory - in practice it is very similar for all cases and lies at 11.43) to let us tune the σ mass to the observed higgs mass value. This matching scale becomes a discontinuity in the

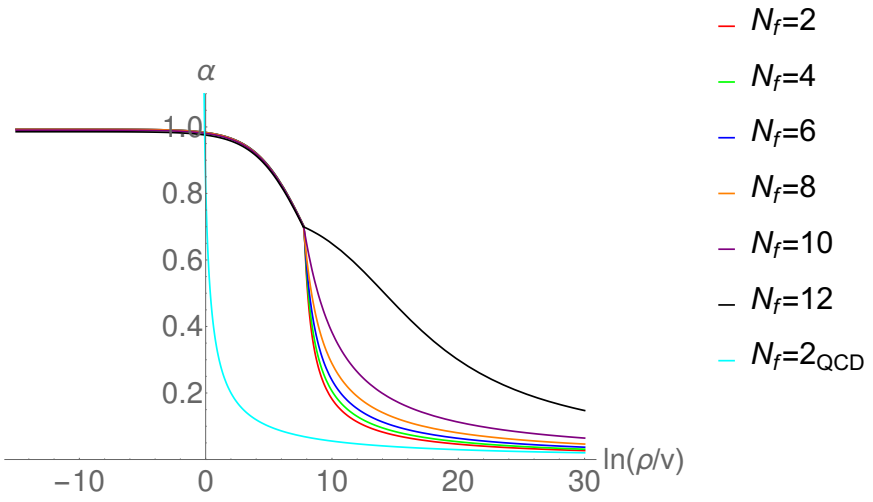

FIGURE 4.1: The running of α_{TC} against RG scale imposed on the holographic model with $N_c = 3$. The curve furthest to the left is for a technicolor model that is a scaled up version of QCD with the usual two loop result for the running. The next curve over is that same theory forced to have a IR fixed point to produce a light higgs (clearly we know for this theory that this assumption is wrong!). Moving further to the right we see the running as further singlet techi-quarks are added, again with N_f^{IR} chosen to give a light higgs. The IR of all such theories is shared and uniquely determined by needing the observed higgs mass.

running of α_{TC}, γ or the AdS scalar mass. In practice we deal with this by performing all computations in sections and matching the value of fields and their derivatives at the boundary point. To provide an estimate of the errors on the spectrum we allow the matching point in α_{TC} to vary from 0.3 to 0.7. In Figure 4.1 we show an example of the running in the theories we impose - clearly they all

share essentially the same IR which is fixed by the higgs mass value. We will discuss the implications further in the final section.

In the same spirit we will tune the coupling κ in the model to produce ρ–A degeneracy to ensure the electroweak S parameter

$$S = 4\pi \left[\frac{F_V^2}{M_V^2} - \frac{F_A^2}{M_A^2} \right] , \tag{4.3}$$

is sufficiently small (we pick $S = 0.1$ as a benchmark point), even though this will not actually be the case for most N_c, N_f theories. We are leaning over backwards to keep technicolor alive of course, but to understand a total exclusion on the parameter space this is sensible. Equally the models display the large tunings needed for viability. Note tuning κ to zero makes the Lagrangian terms for the ρ and A the same so that the A mass drops to that of the ρ. However, since the suppressed, first term in the action is the one which links the symmetry breaking X to the A, to maintain f_π^2 (which is the leading value in the AA correlator) one must raise the overall scale. This is the main source of the rise in the masses relative to a QCD-scaled up theory.

The parameter count in the holographic model is: for a particular theory with N_c, N_f the UV running of α (and hence the anomalous dimension γ) is fixed by the perturbative two loop result. The overall scale is set by requiring $F_\Pi = 246$ GeV. We then modify the IR running - we change it at scales below some matching value of $\alpha_{TC}^{\text{match}}$ (which we vary from 0.3 to 0.7 to provide the range of predictions, displayed as the horizontal width of the prediction curves in Figure 4.2) by adjusting the effective value of N_f in the IR and adjusting it to fix the σ meson mass to the observed higgs mass. The model then predicts M_ρ, F_ρ, M_A, F_A as a function of the 5d gauge coupling, κ. We tune κ to give $S = 0.1$. The remaining three predictions we will express as

$$M_A, \quad \tilde{g} = \frac{\sqrt{2} M_V}{F_V}, \quad \omega = \frac{1}{2} \left(\frac{F_\pi^2 + F_A^2}{F_V^2} - 1 \right) . \tag{4.4}$$

In fact for all our models $\omega < 0.05$ which is at a level where the experimental constraints are unchanged in the high energy reach regime so we suppress that parameter in our plots.

4.2 Phenomenological Model

The phenomenological model of the spin one states made from the electroweak doublet is [59, 248]

$$\begin{aligned}
\mathcal{L}_{\text{boson}} &= -\frac{1}{2}\text{Tr}\left[\widetilde{W}_{\mu\nu}\widetilde{W}^{\mu\nu}\right] - \frac{1}{4}\widetilde{B}_{\mu\nu}\widetilde{B}^{\mu\nu} \\
&- \frac{1}{2}\text{Tr}\left[F_{\text{L}\mu\nu}F_{\text{L}}^{\mu\nu} + F_{\text{R}\mu\nu}F_{\text{R}}^{\mu\nu}\right] \\
&+ m^2\ \text{Tr}\left[C_{\text{L}\mu}^2 + C_{\text{R}\mu}^2\right] + \frac{1}{2}\text{Tr}\left[D_\mu M D^\mu M^\dagger\right] \\
&- \tilde{g}^2\, r_2\ \text{Tr}\left[C_{\text{L}\mu} M C_{\text{R}}^\mu M^\dagger\right] \\
&- \frac{i\,\tilde{g}\,r_3}{4}\text{Tr}\left[C_{\text{L}\mu}\left(MD^\mu M^\dagger - D^\mu M M^\dagger\right)\right. \\
&+ \left. C_{\text{R}\mu}\left(M^\dagger D^\mu M - D^\mu M^\dagger M\right)\right] \\
&+ \frac{\tilde{g}^2 s}{4}\text{Tr}\left[C_{\text{L}\mu}^2 + C_{\text{R}\mu}^2\right]\text{Tr}\left[MM^\dagger\right] \\
&+ \frac{\mu^2}{2}\text{Tr}\left[MM^\dagger\right] - \frac{\lambda}{4}\text{Tr}\left[MM^\dagger\right]^2
\end{aligned} \tag{4.5}$$

where $\widetilde{W}_{\mu\nu}$ and $\widetilde{B}_{\mu\nu}$ are the ordinary electroweak field strength tensors, $F_{\text{L/R}\mu\nu}$ are the field strength tensors associated to the vector meson fields $A_{\text{L/R}}$ [1], and the $C_{\text{L}\mu}$ and $C_{\text{R}\mu}$ fields are $C_{\text{L}\mu} \equiv A_{\text{L}\mu} - \frac{g}{\tilde{g}}\widetilde{W_\mu}$ and
$C_{\text{R}\mu} \equiv A_{\text{R}\mu} - \frac{g'}{\tilde{g}}\widetilde{B_\mu}$

The matrix M takes the form

$$M = \frac{1}{\sqrt{2}}\left[v + H + 2\,i\,\pi^a\,\tau^a\right]\,, \qquad a = 1,2,3 \tag{4.6}$$

Here π^a are the Goldstone bosons produced in the chiral symmetry breaking, $v = \mu/\sqrt{\lambda}$ is the corresponding VEV, and H is the composite higgs. We assume the higgs has Standard Model yukawa couplings to the fermions. The covariant derivative is

$$D_\mu M = \partial_\mu M - i\,g\,\widetilde{W}_\mu^a\,\tau^a M + i\,g'\,M\,\widetilde{B}_\mu\,\tau^3\,. \tag{4.7}$$

When M acquires its VEV, the Lagrangian of equation (4.5) contains mixing matrices for the spin one fields. The mass eigenstates are the ordinary SM bosons, and two triplets of heavy mesons:ρ and A.

Including all the interactions with the electroweak gauge and higgs fields of dimension 4 needs six parameters: the mass, m and coupling $\tilde{g}$ of the new gauge

[1] In Ref. [59, 248], where the chiral symmetry is SU(4) there is an additional term whose coefficient is labelled r_1. With an SU(N)×SU(N) chiral symmetry this term is just identical to the s term.

fields, the higgs VEV v, and three couplings r_2, r_3 and s. The model then predicts

$$M_V^2 = m^2 + \frac{\tilde{g}^2\,(s - r_2)\,v^2}{4}, \quad M_A^2 = m^2 + \frac{\tilde{g}^2\,(s + r_2)\,v^2}{4} \tag{4.8}$$

and

$$F_V = \frac{\sqrt{2}M_V}{\tilde{g}}\,, F_A = \frac{\sqrt{2}M_A}{\tilde{g}}\chi\,, F_\pi^2 = (1 + 2\omega)\,F_V^2 - F_A^2\,, \tag{4.9}$$

where

$$\omega \equiv \frac{v^2\tilde{g}^2}{4M_V^2}(1 + r_2 - r_3)\,, \qquad \chi \equiv 1 - \frac{v^2\,\tilde{g}^2\,r_3}{4M_A^2}\,. \tag{4.10}$$

Without loss of generality we chose $s = 0$ here, noting that: a) the Z'/Z'' production rates, as well as the partial decay width of Z to fermions (di-jets and di-leptons) are independent of s (at the per-mil level); b) the branchings of Z' to dileptons increases by 10% at most for s reaching 10 in absolute value because of the $Z' \to ZH$ partial width decreases; c) we do not involve here higgs boson phenomenology and use only the dilepton channel to probe the WTC space.

Of the five remaining variables we set F_Π =246 GeV, and S =0.1. This leaves three degrees of freedom $M_A, \tilde{g}, \omega$ which can be experimentally constrained.

We have implemented the model in CalcHEP [253] using LanHEP [254] to derive the Feynman rules [223, 225]. The implementation of the model is publicly available at HEPMDB database [18] under hepmdb:1012.0102 ID. In this implementation we have extended the previous implementation [223](hepmdb:1012.0102) by nonzero s and ω parameters to be interpreted in the context of the holographic description.

The two main signals relevant for phenomenology were shown to be Drell-Yan production and Vector Boson Fusion. In each case a single ρ or A is produced through mixing with the electroweak gauge bosons via the combined mass matrix determined from the action. The Drell-Yan analysis has recently been updated to the latest 13 TeV LHC data in [225].

Phenomenologically the three parameters are treated as completely free parameters. The parameter count is the same as that of the holographic model which makes absolute predictions for these numbers as a function of N_c, N_f. We can therefore immediately superimpose the holographic predictions on the constraints from [225].

We have explored the dependence of the experimental constraints on the parameter ω. For $|\omega| < 0.3$ the impact on the exclusion regime is small and any changes occur at $M_A \simeq 1.5$ TeV. The high mass reach area is least affected. Given the holographic models place $\omega < 0.05$ in all cases we will simply suppress this parameter which is not playing a significant role in constraining the models.

A further useful parameter to monitor (although it is not independent) is a from

$$a 4\pi^2 F_\pi^4 = F_\rho^2 M_\rho^2 - F_A^2 M_A^2 \tag{4.11}$$

which provides a monitor of the second Weinberg sum rule or equally the degeneracy of the $\rho - A$ pair. Since the holographic model ensures a small S parameter precisely by such degeneracy it is not surprising the models lie near the $a = 0$ curve in the $\tilde{g} - M_A$ plane. Unfortunately this is the extreme of the parameter space analyzed in the phenomenological model previously which is hardest to probe experimentally. It is instructive to know it might be favoured in real models.

4.3 Results

Our first goal is to place the recent experimental limits on WTC [225] in the context of predictions for real models. In this paper we use LHC limits on dilepton resonance searches only and reinterpret them for WTC parameter space. The choice of dilepton signature is very well motivated since this is probably the most clean signature for search of the vector resonances. However, as we will see below, it becomes less efficient in the region of large values of $\tilde{g}$ where couplings of resonances to SM fermions are suppressed.

In Figure 4.2 we present the up-to-date LHC reach for the phenomenological WTC model, so the reader can see the current LHC potential to probe the model parameter space. We use here the CMS DY limits on Z' production at 13 TeV ($36 fb^{-1}$) from the dilepton (combined dielectron and dimuon) final state [252] for the reinterpretation to limits on the WTC parameter space. The CMS limit is expressed as a ratio, $R_\sigma = \sigma(pp \to Z' \to \ell^+\ell^-)/\sigma(pp \to Z \to \ell^+\ell^-)$, of Z' signal cross section in the dilepton final state to the cross section of a Z boson to the dilepton final state. CMS calculate this Z boson cross section to NNLO in the control region of $60 \leq m_{\ell^+\ell^-} 120$ GeV. CMS present the limit as R_σ to remove the dependency on the theoretical prediction of $\sigma(pp \to Z \to \ell^+\ell^-)$ and correlated experimental uncertainties. Using this limit we have found 95% CL limits on the WTC $\tilde{g} - M_A$ parameter space for the ρ and A separately and then overlay them to find overall combination. We have used CalcHEP to evaluate the signal at tree-level and modified the ZWPROD program [255] to evaluate mass-dependent QCD NNLO K-factor. The current LHC observed limit is indicated by the combined shaded area in Figure 4.2. One can clearly see that the LHC is currently not sensitive to the parameter space of WTC models predicted by holography, even those models with a large number of techni-doublets where $\tilde{g} \simeq 2.5$ and $M_A \simeq 4$ TeV.

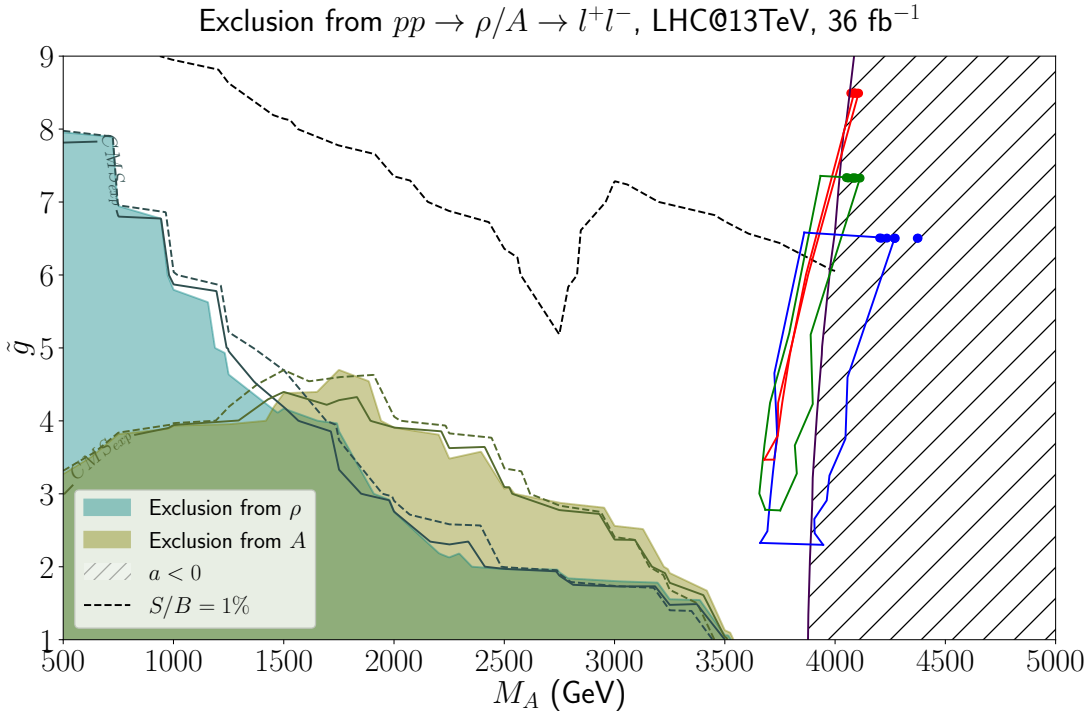

FIGURE 4.2: Shaded areas present 95% CL exclusion on the $M_A - \tilde{g}$ plane from the CMS observed limit on dilepton resonance searches at the LHC@13TeV with 36 fb^{-1}. Solid and dashed lines along the borders of the shaded area represent an expected CMS limit and our limit using binned likelihood method respectively. The predictions of our holographic model (tuned at each N_c, N_f to give S=0.1 and the correct higgs mass) are overlaid. The red colour indicates $N_c = 3$, green — $N_c = 4$ and blue — $N_c = 5$. The top edge of the box in each case is the one electroweak doublet theory result with the width representing an estimate of the theoretical error (we match the IR running at different values as described in the text). The points correspond to the motion of the right hand point on that line as the number of singlets is changed to vary the UV running - the effect is small because the theories share much the same IR running to generate m_h. Moving down in the box corresponds to increasing the number of electroweak techni-doublets from one to $2N_c$ where the theories are assumed to enter the conformal window. Parameter a, from the phenomenological model, is related to $\rho - A$ degeneracy and the holographic points lie near the line $a = 0$ as a result of tuning to a small S parameter.

Besides finding the observed limit as a reinterpretation of the CMS results we have closely reproduced an expected CMS limit (the solid lines along the borders of the shaded area in Figure 4.2 to be compared with the respective dashed lines from our approach) from the dilepton search in order to validate our approach and extend its use to projections for future collider energies and luminosities.

We have evaluated our expected limits using a binned likelihood method. We assume resonance widths are negligible compared to the gaussian-smearing effects of finite detector resolution. The signal hypothesis pdf is defined by a Gaussian of width equal to the detector resolution (1.2% of resonance mass), and a signal-strength modifier, μ, which is the expected number of events at the experiment.

Background is estimated by generating very high statistics for invariant dilepton mass distributions. Where there are few background events (e.g. $m_{\ell^+\ell^-} \geq$ 2 TeV at 13 TeV), we use the CL_s method alongside a toy Monté Carlo in order to construct the distribution of a single test-statistic for background only and signal+background hypotheses.

In Figure 4.2 we also present a dashed black line lying in the large $\tilde{g}$ region and indicating a 1% level of signal-to-background ratio (from the most optimistic expected systematic uncertainty) as an indication of the absolute limit of the dilepton signature potential to probe the WTC paradigm. This contour line is not expected to change with the increase of the collider energy since the irreducible dilepton background and the signal will scale the same way with the energy increase.

These results display a reach of 3.5 TeV in mass and couplings $\tilde{g} \sim 8$, which at first glance appears very constraining. However, let us first orient ourselves in theory space. QCD is a gauge theory that we are fully confident of the spectrum - we can therefore consider a techicolour model with an SU(3) gauge group and $N_f = 2$ light quarks (up to the influence of the strange quark) by scaling up QCD. We scale $f_\pi = 93$ MeV to $F_\Pi = 246$ GeV and find $M_\rho = 2.05$ TeV, $M_A = 3.25$ TeV, $S = 0.3$ and $\tilde{g} = 7$. This theory is roundly excluded simply by S and the absence of a light higgs candidate but provides some reference values to place on the exclusion plot Figure 4.2. It is not excluded purely in terms of the ρ, A bounds.

The minimal QCD scale up is already ruled out but we entertain here the possibility that a related theory with additional techniquark electroweak singlets can change the running so that the constraints on S and the higgs mass can be accommodated. In terms of the runnings of α_{TC} in Figure 4.1 for the $N_c = 3$, $N_f = 2$ case we would need to move the running from the left most profile (the two loop running for the theory) to the rather bizarre running shown to the right. The one loop coupling scale has moved close to 700 TeV then (here by "magic" since we know this does not happen in QCD!) the IR is modified to create a very conformal IR fixed point that allows a light higgs. We also vary our parameter κ to ensure $S = 0.1$. As an example of the effects of these changes consider the $N_c = 3, N_f = 2$ theory with the matching to the new IR running performed when $\alpha = 0.7$ - we find $M_A = 4.11$ TeV, $M_\rho = 3.63$ TeV, $F_A = 1.54$ TeV, and $F_\rho = 1.48$ TeV ($\omega = 0.047$ and is small as previously discussed - there is very little impact on the excluded regions from variation of this small size so we suppress discussion of it). This spectrum is shown in the $\tilde{g} - M_A$ plane in Figure 4.2 together with the current LHC constraints - the mutated SU(3) point corresponds to the top red point. In this mutation of QCD with exotic running the holographic model has predicted that the vector meson masses grow even further from exclusion by the LHC constraints. It seems reasonable that in a theory with strong coupling out to such a large scale the masses of the theory should be dragged to higher scales also.

We now perform this same analysis for varying N_c and N_f theories - it is possible that for one of these theories the IR running we impose is less fanciful. The spectrum comes from the predictions of our holographic model tuned at each N_c, N_f to give S=0.1 and the correct higgs mass. The red colour is for $N_c = 3$, green $N_c = 4$ and blue $N_c = 5$. The top edge of the box in each case corresponds to the one electroweak doublet theory result with the width representing an estimate of the theoretical error (we match the IR running at different values as described above in Section II).

It is simple to also include the effects of additional electroweak singlets on top of a single doublet since they only affect the running of the UV coupling. The points in Figure 4.2 correspond to the motion of the right hand point on the top line (the one doublet result) for each colour (value of N_c) as the number of electroweak singlets is also changed to vary the UV running - the effect is small because the theories share much the same IR running to generate m_h.

In Figure 4.2 we have also extended the spirit of this analysis to theories with additional techniquark electroweak doublets that change the UV running in a known fashion (making the coupling run more slowly) and then adjusting the IR and κ to match $S = 0.1$ and the higgs mass. The extra doublets tend to increase F_Π by $\sqrt{N_f}$ which reduces the overall mass scale. However, the need to reduce S (which grows as N_f) leads to a tuning of κ that increases the mass scale. The net result we find is that the mass scale of the mesons is largely unchanged. The decay constants F_A though do scale as $\sqrt{N_f}$ so $\tilde{g}$ falls with the addition of further doublets. The results are again shown in Figure 4.2 - here one should move down in the coloured box associated with each N_c. Moving down the box corresponds to increasing the number of electroweak techni-doublets from one to $2N_c$ where the theories are assumed to enter the conformal window. Note here the collider data is not directly applicable since it was generated for a single doublet theory but the masses of the mesons do appear beyond LHC also at this time.

It is notable that the holographic models all lie on or near the line where a, from the phenomenological model, is zero. The reason is that a parametrizes $\rho - A$ degeneracy and the points lie near the line $a = 0$ as a result of forcing a small S parameter. In the holographic model where κ is the only available parameter to tune this appears the unique solution. This makes it clear that in the phenomenological model much of the parameter space achieves S=0.1 by a complicated tuning of the two vector masses and their decay constants - it is not clear if these tunings are achievable in a UV complete model.

The broad conclusion of all of this analysis is that WTC models (if they exist) probably still lie well beyond the LHC's reach and are not yet fully excluded. At this point one has to again query how believable the running functions we have adopted are. Certainly the two loop runnings do include strongly coupled

IR fixed points yet we should be sceptical of the fixed point values computed in this (gauge dependent) way. The spirit of the analysis, guessing an IR fixed point behaviour, is therefore not unreasonable but our runnings are hugely fine tuned (at one part in 100 in N_f^{IR} which takes the value 11.43) to give the observed higgs mass. One might very reasonably conclude the chance of the real running falling on these tuned guesses is very low. On the other hand if such a tuned theory is the answer nature has chosen then one would encounter a light higgs and be able to deduce this tuning in the runnings! Here we do not wish to advocate this latter view particularly but our results do show the bizarre nature of a technicolor theory that survives the current constraints and that more work is needed experimentally to exclude them completely.

4.4 Beyond LHC

We have demonstrated that the LHC dilepton searches to date has not been able to exclude the WTC paradigm. A total exclusion would need not only a higher collider energy but also new signatures to probe 4-5 TeV resonances especially in the large $\tilde{g}$ region with very low dilepton rates. We illustrate this point in Figure 4.3 where we present projections for dilepton searches at 27(15 ab^{-1}) and 100 TeV (3 ab^{-1}) pp collider. One can see a dramatic improvement of the sensitivity (in comparison to LHC@13TeV and LHC@14TeV[2]) to the WTC parameter space at these future colliders, especially at 100 TeV where there is sensitivity to $\tilde{g} \simeq 4$ for M_A around 4 TeV with a dilepton search. At the same time one can see that these searches would cover models only with large number of techni-doublets, while models coupling with $\tilde{g} \simeq 8$ are still far from reach even at a 100 TeV collider if only the dilepton DY signature is used. An important observation of the two plots in Figure 4.3 is that using this channel, the sensitivity of a 100TeV is similar to a 27TeV collider with moderately increased luminosity, and as such there is little gain in going to higher energies.

One can see that dilepton signature becomes less efficient in probing the WTC parameter space for large values of $\tilde{g}$ where the couplings of the ρ/A to fermions are suppressed. Therefore exploration of higher values of $\tilde{g}$ motivates study of additional di-boson signatures either from DY production or from the additional vector boson fusion (VBF) production channel. One should note that VBF production of ρ/A followed by respective diboson(VV) or boson-higgs(VH) decay looks particularly promising in the very large $\tilde{g} \simeq 8-9$ region since neither production nor decay of new heavy resonances are suppressed by $1/\tilde{g}$. Moreover, the increase of collider energy can further enhance the significance of the VBF channel. An exploration of these additional VV/VH signatures and VBF production

[2]LHC@14 TeV with 3 ab^{-1} would be able to reach $\tilde{g} \simeq 4$ for M_A around 4 TeV as demonstrated in [225].

channel, which could potentially cover the whole WTC parameter space, will be the subject of a follow-up paper.

4.5 Conclusions

The technicolor paradigm has long been appealing but it has been under fire for years from precision electroweak data and the discovery of a light higgs. Here we have asked the question of whether it can be finally put to bed by LHC data for searches for techni-ρ and A states. To declare a theory dead one must take the most conservative approach so we have entertained the idea that tuning the IR running of the theory may generate a sufficiently light higgs (since we do not know which theory might have such IR running we have imposed it on a range of theories with different N_c, N_f in the hope to capture the true theory if it exists). Holography provides a very simple analysis that predicts the techni-ρ and A spectrum and couplings based on the input running of γ, the anomalous dimension of $\bar{q}q$, and therefore provides a good first estimate of the mass spectrum of these theories.

It is worth stressing that our analysis relies on our specific holographic model (although we have attempted to estimate theoretical error bars by varying the energy scale at which the IR walking coupling deviates from the UV running, which we present in Figures 2,3) and one might like to have a wider set of models to compare. Although there are many holographic models of QCD we know of only this model and the model of [256] which include a running anomalous dimension. The latter model does not predict light higgs particles in walking theories [257] because of the way the IR decoupling of the quarks is implemented. The model used here [247] totally decouples mesonic physics from scales below the IR quark mass (through the boundary conditions given below (1)) as one finds in top down probe brane models. See [258] for a more in depth analysis of this point – it will probably take future lattice simulations to untangle this issue. We use this model, which does generate a light higgs when the IR running is slow, in the spirit of giving technicolour a final chance. In the future we hope to test how generic the model's predictions are by looking at different origins of the dynamics such as in technicolour models where an Nambu-Jona-Lasinio term assists the symmetry breaking dynamics.

In our holographic model, we have found that tuning S to a small value naturally places these models on the $a = 0$ line of the phenomenological model that has been used previously for analysis. Our main result shows that these models still lie beyond the reach of the LHC via Drell-Yan dilepton resonance searches. We have also shown that the DY signal alone will not exclude the most minimal models even at a 100 TeV (3 ab^{-1}) pp collider which motivates future work on

bringing additional signatures and production channels at higher energy colliders that will exclude the paradigm.

The WTC models that survive here are fairly baroque, entering strong coupling at the 700 TeV or so scale and then running very slowly in the IR with the result that the resonances' masses are pushed up in scale. They also possess a large change to $\gamma = 2$ near the fixed point so display the walking mechanism that pushes away the flavour scale. The biggest lesson perhaps to learn from this analysis is the difficulties that a light higgs leave for all Beyond the Standard Model theories which now must possess IR fine tuning and and push new physics to high scales. On the other hand these models provide some motivation to build higher energy colliders and explore new signatures to fully probe the model parameter space.

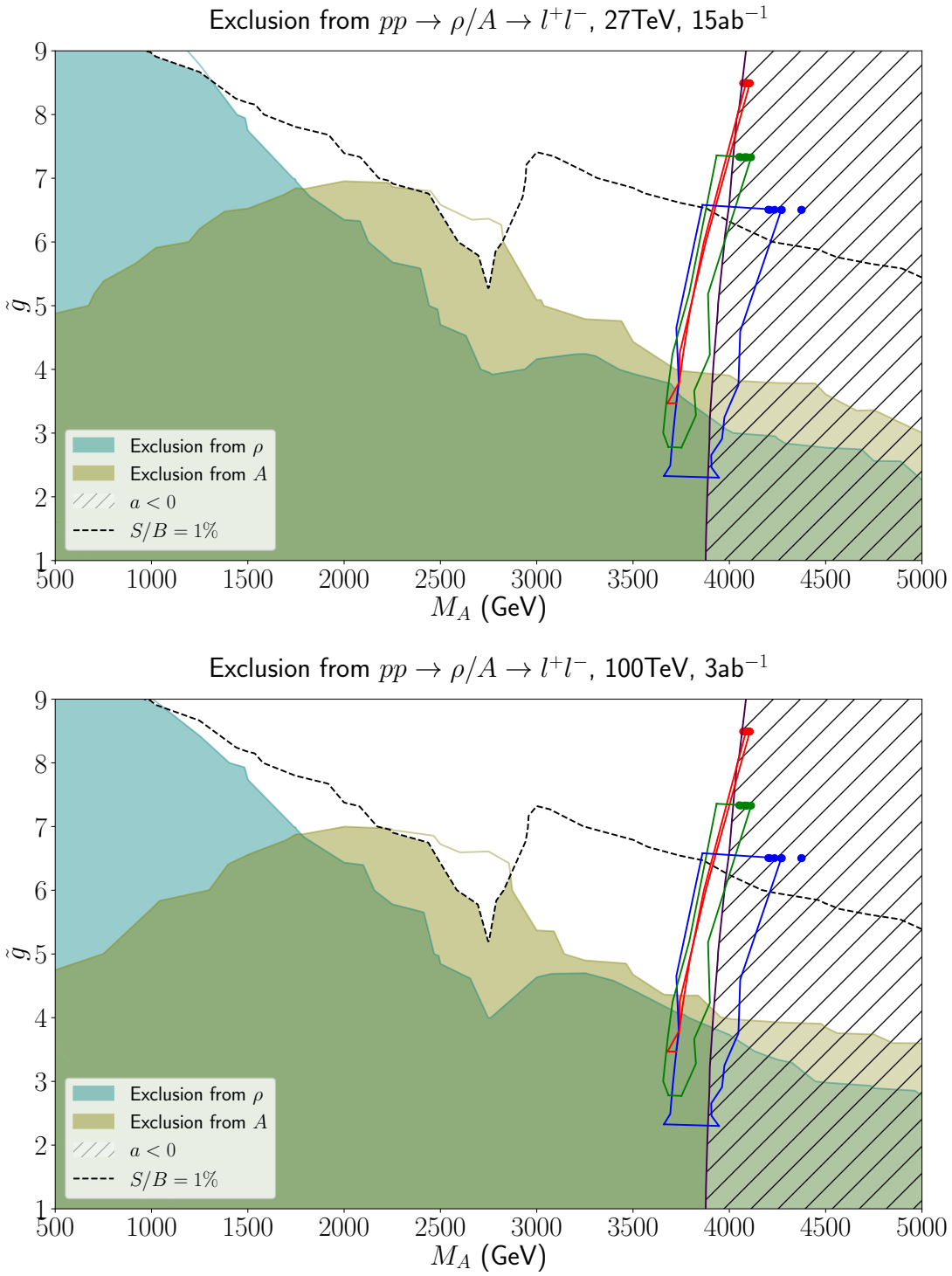

FIGURE 4.3: Shaded areas present 95% CL projected exclusion on the $M_A - \tilde{g}$ plane for 27(15 ab^{-1}) (top) and 100 TeV (3 ab^{-1})(bottom) pp collider from dilepton DY resonance searches. The notations are the same as in Figure 4.2.

Chapter 5

Tools

5.1 HEPMDB

HEPMDB [18] is a public, online database of particle physics models, defined by feynman rules stored in LanHEP output [10] of UFO[259] model formats. It also includes a user-friendly javascript interface to run simulations using CalcHEP [13] and MadGraph [260] asynchronously on the IRIDIS4 High Performance Computing cluster.

Ongoing support and development for the platform has seen us migrate from IRIDIS3 to IRIDIS4. The ongoing aims for HEPMDB are to:

(a) collect HEP models for various multipurpose Matrix Element (ME) generators like CalcHEP [261], CompHEP [262, 263], FeynArts [264, 265], MadGraph/MadEvent [266, 14, 267, 259], AMEGIC ++/COMIX within SHERPA [268, 269]. and WHIZARD [270]. Under "HEP models" we denote the set of particles, Feynman rules and parameters written in the format specific for a given package;

(b) collect models' sources which can be used on the HEPMDB to generate HEP models for various ME generators using FeynRules [11] or LanHEP [271] which automate the process of generating Feynman Rules, particle spectra, etc.. Under the "model source" we denote the model (lagrangian etc.) written in the form of input for FeynRules or LanHEP. For the moment, FeynRules interfaces to CompHEP, CalcHEP, FeynArts, GoSam [272], MadGraph/MadEvent, SHERPA and WHIZARD [273] are available. Currently LanHEP works with CalcHEP, CompHEP, FeynArts and GoSam. Also, the latest LanHEP version 3.15 has an option under testing of outputting the model in UFO format [259] which provides a way to interface it with MadGraph/MadEvent;

(c) allow users to upload their models onto a server in order to perform evaluation of HEP processes and event generation for their own models using the

full power of the High Performance Computing (HPC) cluster standing behind the HEPMDB itself. HPC cluster at Southampton University, IRIDIS3 is the state-of-the-art fastest university owned HPC resource in the UK which has 1008 8-core compute nodes (Intel Nehalem 2.26 GHz), at least 24GB of memory per node connected with fast infiniband network for parallel communication. This is one of the very powerful features of the HEPMDB: it provides a web interface to various ME generators which can then also be run directly on the HPC cluster. This way, users can preform calculations for any model from HEPMDB (including their own models which they can upload) avoiding problems related to installing the actual software, which can sometimes be quite cumbersome;

(d) cross check and validate models for different ME generators. We should note that similar functionality is also provided by the FeynRules web validation framework which is also presented in these proceedings. However, the FeynRules web validation is mainly geared towards comparing FeynRules models and can use its knowledge of the model format to provide a throughout and highly automatized test procedure for those, while HEPMDB works in a more generic way and will provide access to more model formats at the price of slightly less automatization. Also, one should stress that uploads and evaluations at HEPMDB are available to *all users*. This is an important new feature of HEPMDB as compared to FeynRules website.

(e) collect predictions and specific features of various models in the form of (sub)database of signatures and perform comparison of various model predictions with experimental data. There are a lot of different aspects related to this problem details of which are outside the scope of the current short contribution. We would like to mention though, that this task includes a comprehensive development of a database of signatures as well as development of the format of presentation of these signatures. This format will be consistent with the format which will be used by the experimentalists for the presentation of the LHC data, discussed at the workshop in the context of the "Les Houches Recommendations for the Presentation of LHC Results" activity.

(f) trace the history of the model modifications (in case modifications take place), and makes available all the versions of the model. Through this application, we stress the importance of reproducibility of the results coming from HEPMDB or from a particular model downloaded from HEPMDB.

5.2 PhenoData

PhenoData is an online database that allows the user to store digitized data from plots or tables used in a given paper, for which there is no public data available.

There was a demand for such a service in the phenomenology community, stemming from the lack of availability of data associated with plots or tables on some papers. This resulted in multiple people digitising the same plots. Although the initial intended usage is within the HEP phenomenology community, PhenoData may have further application to other fields.

The interface was designed to be quick and easy to use; JavaScript (and the JavaScript library jQuery) were used alongside php to accomplish this. Fast development was enabled by use of Bootstrap; a HTML, CSS, and JS framework for building responsive, mobile-first projects on the web. The user system is shared with HEPMDB [18].

A registered user may create an entry for a given paper, consisting of a title and various reference formats; including DOI, arXiv, preprint. Any user may then attach individual records for each plot or table contained within the paper. In order to store data in this structure, the document-orientated database MongoDB was used. These attached items consist of a label and data file to be uploaded. In addition, the user may upload an image in any standard format, although .pdf is preferrable. If a .pdf is uploaded then there will be automatic conversion to .png, and both formats will be stored. For plots, this data file is then parsed and an interactive plot is displayed (using plotly) side-by-side with the uploaded image for comparison. TeX style formatting is supported for all titles and labels.

All data can be viewed or downloaded without registration. A registered user (of HEPMDB) may also edit their own uploads. Each uploader is contactable via an email form, or alternatively you may leave a comment on the paper record which is publically viewable.

MongoDB is an open-source document-oriented database program licensed under Free Software Foundation's GNU AGPL v3. It stores data in flexible, JSON-like documents, meaning fields can vary from document to document and data structure can be changed over time. The scalability and flexibility of MongoDB enables unrestricted development of PhenoData.

The ability to upload and download large amounts of data was a concern of initial users. To enable a streamlined interaction with the database for such users, a RESTful API was developed using Lumen, a widely used MVC framework. Through a common format as described in the API help pages, and an auth-key generated for each user, a simple batch script may be used to upload many items concurrently.

Chapter 6

Conclusions

In chapter 2 we have suggested and pursued the concept of a sytematic classification of MCDM models. We have shown that fermion DM contained within a non-chiral electroweak multiplet is still compatible with observation, although many scenarios may be excluded. If DM is Dirac, then $Y = 0$ is required by DD experiments. If DM is PseudoDirac then despite the cancellation in the NLO DD cross-section (cross-section decreases with Y), the NLO corrections to masses would drive the neutral particle to not be lightest for $M_D < 50GeV$ when $Y > 1/2$. This causes such scenarios to be ruled out by invisible Z decays, leaving only $Y = 0, 1/2$ as suitable candidates. The next generation of DD experiments have the sensitivity to discover, but not completely exclude such models.

By analysing the phenomenology of the representative model containing a Dirac fermion singlet and pseudoscalar mediator in detail at NLO, we demonstrate that non-trivial dark sectors can arise in corners of parameter space of such simple models. In particular, parameter points excluded by a naive treatment of simplified models with mediators can lead to the exclusion of parameter points which could still be realised by nature. Future work to complete the picture of MCDM models with two additional multiplets, will involve the treatment of scalar and vector DM.

In chapter 3, model independent methods are demonstrated to extract the masses for DM and a charged partner (assuming such particles are observed) using kinematical features of the energy distributions of charged leptons at e^+e^- colliders with $\sqrt{s} = 250GeV$. These methods are tested for two simple but realistic models (which generate the correct relic abundance and avoid DD bounds), and shown to be able to deduce these masses to a precision of $\sim 5 - 20\%$ at an integrated luminosity of $500fb^{-1}$.

Furthermore, there appears to be the capacity to discriminate between the spin of DM in these models, by measuring the angular distribution of $W^{\pm}$ bosons via

their reconstruction from jets or charged leptons. If the model-predicted cross-section values are used, discrimination between such models at 95% CL is possible at luminosites less than $13.2 fb^{-1}$, whilst using shape information only would require $\lesssim 2ab^{-1}$.

In Chapter 4, we demonstrate that our holographic model of WTC cannot be excluded by the DY signal alone even for projections of a 100 TeV pp collider at 3 ab^{-1}).

Decoding the underlying theory of nature requires a broad and varied approach to balance the challenges of surveying and interpreting experimental searches whilst revering the predictive power of more complete models. In order to realise the power of the "bottom-up" approach, the required technical infrastructure is in development by several groups [19, 21, 15, 18, 24], however the challenge is ongoing to systematise prototyping of toy-models and the combined statistical inference over the many disjoint experiments.

Appendix A

A.1 Radiative mass corrections (no additional mediators)

For a non-chiral fermion, the self-energy from a single diagram with some boson V in the loop is given by

$$\begin{aligned} i\Sigma(p) &= g^2 \int \frac{d^4k}{(2\pi)^4} \frac{\gamma^\mu (p+k+M_D)\gamma^\nu(-g_{\mu,\nu})}{[(p+k)^2 - M_D^2][k^2 - m_V^2]} \\ &= \frac{i}{(4\pi)^2}\left[C_0 + C_D^A A(M_D^2) + C_V^A A(m_V^2) + C_B B(M_D^2, m_V^2)\right] \end{aligned}$$

where p is the external momenta and k the loop momenta. The coefficients are found to be

$$\begin{aligned} C_0 &= (2g^2 + \delta_M)M_D + (-g^2 + \delta_Z)p \\ C_D^A &= -\frac{g^2}{p^2}p \\ C_V^A &= \frac{g^2}{p^2}p \\ C_B &= g^2\left[2p - 4M_D - \frac{p}{p^2}(p^2 + m_V^2 - M_D^2)\right] \\ &= \frac{g^2}{p^2}(p^2 + M_D^2 - m_V^2)p - 4g^2 M_D \end{aligned}$$

Here, **A** and **B** are the 1 and 2 point Passarino-Veltman integrals, as defined in [274]. The divergent parts of which are absorbed using the $\bar{M}S$ counterterms

$$\delta_Z = -\frac{g^2}{\hat{\epsilon}}, \quad \delta_M = \frac{4g^2}{\hat{\epsilon}}, \quad \frac{1}{\hat{\epsilon}} \equiv \frac{2}{4-D} - \gamma_E + \log 4\pi \tag{A.1}$$

We may then define a function of r, where $r \equiv \frac{m_V}{M_D}$,

$$f(r) = \frac{16\pi^2}{M_D g^2}\Sigma(p = M_D)$$
$$= \frac{r}{2}\left[2r^3\log(r) - 2r + \sqrt{r^2-4}\left(r^2+2\right)\log\left(A\right)\right] - 4$$

where $A = \left(r^2 - 2 - r\sqrt{r^2-4}\right)/2$. Combining contributions from all diagrams, we find the total self-energy,

$$\Sigma^{(tot)}(n,Q,Y) = \frac{M_D g^2}{16\pi^2}Q^2 f_\gamma + \frac{(Qc_w^2 - Y)^2}{c_w^2}f_Z + \left[C_{W^+}(n,Q,Y)^2 + C_{W^-}(n,Q,Y)^2\right]f_W \tag{A.2}$$

Here, $f_X \equiv f\left(\frac{m_V}{M_D}\right)$, Q is the electric charge and Y is the hypercharge (using convention of $Q = T_3 + Y$). The coupling to $W^\pm$ may be expressed as $C_{W^\pm} = \frac{1}{2\sqrt{2}}\sqrt{n^2 - (2Q - 2Y \pm 1)^2}$ where n is dimension of the multiplet. This leads to an expression for the difference between the pole masses of two members of a given multiplet

$$M_Q - M_{Q'} = (-\Sigma_Q^{(tot)}(M_D)) - (-\Sigma_{Q'}^{(tot)}(M_D)) \tag{A.3}$$
$$= \frac{M_D g^2}{16\pi^2}(Q - Q')\left[(Q + Q' - 2Y)(f_W - f_Z) + (Q + Q')(f_Z - f_\gamma)s_w^2\right] \tag{A.4}$$

$$f(r) = \frac{r}{2}\left[2r^3\log(r) - 2r + \sqrt{r^2-4}\left(r^2+2\right)\log\left(A\right)\right] - 4 \tag{A.5}$$

where $A = \left(r^2 - 2 - r\sqrt{r^2-4}\right)/2$

A more numerically stable expression also exists for f(r),

$$f(r) = \frac{r}{2}\left[2r^3\log(r) - 2r - \sqrt{r^2-4}\left(r^2+2\right)\log\left(B\right)\right] - 4 \tag{A.6}$$

where $B = \left(r^2 - 2 + r\sqrt{r^2-4}\right)/2$

$$\lim_{r\to 0} f(r) = -4 + 2\pi r - 3r^2 + \frac{3\pi r^3}{4} + \mathcal{O}\left(r^4\right)$$
$$\lim_{r\to\infty} f(r) = 6\log r - \frac{5}{2} + \frac{1}{r^2}\left(8\log r - \frac{8}{3}\right) + \mathcal{O}\left(r^{-4}\right)$$

A.2 Direct detection calculation

For simplicity, we compute in zero momentum transfer limit from the start, here ξ is just the four couplings (with vector, axial couplings removed - note $a_V, a_A = \frac{1}{2}$ for W exchange diagrams). For the case of Dirac DM, couplings to quark types may be different in general, as such diagrams A and B (untwisted and twisted topologies) must be calculated independently.

$$iM_A = \xi_A \int_l \frac{J_D^{\mu\nu} J_{q,A}^{\rho\sigma} g_{\mu\rho} g_{\nu\sigma}}{\mathcal{D}_A}$$
$$iM_B = \xi_B \int_l \frac{J_D^{\mu\nu} J_{q,B}^{\rho\sigma} g_{\mu\sigma} g_{\nu\rho}}{\mathcal{D}_B}$$

where

$$J_D^{\mu\nu} = \bar{u}(\mathrm{p})\gamma^\mu(p + l + m_{D^+})\gamma^\nu u(\mathrm{p}) \tag{A.7}$$

$$J_{q,A}^{\rho\sigma} = \bar{u}(q)\gamma^\rho \left(a_V - a_A\gamma_5\right)(q - l + m_Q)\gamma^\sigma \left(a_V - a_A\gamma_5\right) u(q) \tag{A.8}$$

$$J_{q,B}^{\rho\sigma} = \bar{u}(q)\gamma^\rho \left(a_V - a_A\gamma_5\right)(q + l + m_Q)\gamma^\sigma \left(a_V - a_A\gamma_5\right) u(q) \tag{A.9}$$

$$\mathcal{D}_A = ((p + l)^2 - m_{D^+}^2)(l^2 - m_V^2)^2((q - l)^2 - m_Q^2) \tag{A.10}$$

$$\mathcal{D}_B = ((p + l)^2 - m_{D^+}^2)(l^2 - m_V^2)^2((q + l)^2 - m_Q^2) \tag{A.11}$$

$$\int_l \equiv \int \frac{d^D l}{(2\pi)^D} \tag{A.12}$$

Removing spin-dependent terms, we end up with the structures given in numerators n_A and n_B

$$\begin{aligned} n_A &= J_D^{\mu\nu} J_{q,A}^{\rho\sigma} g_{\mu\rho} g_{\nu\sigma} \\ &= -4m_{D^+} m_Q (a_A^2 - a_V^2) < 1 >< 1 > \\ &+ 2(a_A^2 + a_V^2)\left[(p + l).(q - l) < \gamma^\mu >< \gamma_\mu > + < q - l >< p + l >\right] \\ &- 2m_{D^+}(a_A^2 + a_V^2) < 1 >< q - l > + 2m_Q(a_A^2 - a_V^2) < p + l >< 1 > \end{aligned}$$

$$
\begin{aligned}
\eta_B &= J_D^{\mu\nu} J_{q,B}^{\rho\sigma} g_{\mu\sigma} g_{\nu\rho} \\
&= -4 m_{D^+} m_Q (a_A^2 - a_V^2) < 1 >< 1 > \\
&+ 2(a_A^2 + a_V^2) \left[(p+l).(q+l) < \gamma^\mu >< \gamma_\mu > + < q+l >< p+l > \right] \\
&- 2 m_{D^+} (a_A^2 + a_V^2) < 1 >< q+l > + 2 m_Q (a_A^2 - a_V^2) < p+l >< 1 >
\end{aligned}
$$

The full result may be expressed in terms of weighted Passarino-Veltman functions (using the conventions of PackageX [275]).

$$
\begin{aligned}
\frac{i\mathcal{M}_{\mathcal{A}}}{\xi_A}(4\pi)^2 = A_1 < q >< 1 > + A_2 < q >< p > + A_3 < 1 >< 1 > \\
+ A_4 < 1 >< p > + A_5 < \gamma^\mu >< \gamma_\mu >
\end{aligned}
$$

$$
\begin{aligned}
\frac{i\mathcal{M}_{\mathcal{B}}}{\xi_B}(4\pi)^2 = B_1 < q >< 1 > + B_2 < q >< p > + B_3 < 1 >< 1 > \\
+ B_4 < 1 >< p > + B_5 < \gamma^\mu >< \gamma_\mu >
\end{aligned}
$$

All A_i C functions have argument $\left(m_D^2, m_D^2 + m_q^2 + 2p.q, m_q^2; m_V, m_{D^\pm}, m_Q\right)$.

$$
\begin{aligned}
A_1 &= -2\left(m_q \left(a_A^2 + a_V^2\right) \mathbf{C}_{22}^{\{2,1,1\}} + \left(a_A^2 (m_q + m_Q) + a_V^2 (m_q - m_Q)\right) \mathbf{C}_2^{\{2,1,1\}}\right) \\
A_2 &= 2\left(a_A^2 + a_V^2\right)\left(\mathbf{C}_{12}^{\{2,1,1\}} + \mathbf{C}_0^{\{2,1,1\}} + \mathbf{C}_2^{\{2,1,1\}} + \mathbf{C}_1^{\{2,1,1\}}\right) \\
A_3 &= -2\Big(- m_D \left(m_q \left(a_A^2 + a_V^2\right) \mathbf{C}_{12}^{\{2,1,1\}} + m_Q \left(a_A^2 - a_V^2\right) \mathbf{C}_1^{\{2,1,1\}}\right) \\
&\quad + \left(a_A^2 (m_{D^\pm}(m_q + 2m_Q) - m_D m_Q)\right. \\
&\quad \left. + a_V^2 (m_D m_Q + m_{D^\pm}(m_q - 2m_Q))\right) \mathbf{C}_0^{\{2,1,1\}} + m_{D^\pm} m_q \left(a_A^2 + a_V^2\right) \mathbf{C}_2^{\{2,1,1\}}\Big) \\
A_4 &= -2\left(a_A^2 + a_V^2\right)\left(m_D \mathbf{C}_{11}^{\{2,1,1\}} + (m_D - m_{D^\pm}) \mathbf{C}_1^{\{2,1,1\}}\right) \\
A_5 &= -\left(a_A^2 + a_V^2\right)\left(\mathbf{B}_0^{\{2,1\}}\left(m_D^2; m_V, m_{D^\pm}\right) + \mathbf{B}_0^{\{2,1\}}\left(m_q^2; m_V, m_Q\right) + m_{D^\pm}^2 \mathbf{C}_0^{\{2,1,1\}} + m_Q^2 \mathbf{C}_0^{\{2,1,1\}}\right. \\
&\quad \left. + 2\mathbf{C}_{00}^{\{2,1,1\}} + m_D^2\left(-\mathbf{C}_0^{\{2,1,1\}}\right) - m_q^2 \mathbf{C}_0^{\{2,1,1\}} - 2p.q \mathbf{C}_0^{\{2,1,1\}}\right)
\end{aligned}
$$

All B_i C functions have argument $\left(m_D^2, m_D^2 + m_q^2 - 2p.q, m_q^2; m_V, m_{D^\pm}, m_Q\right)$.

$$
\begin{aligned}
B_1 &= 2\left(m_q\left(a_A^2+a_V^2\right)\mathbf{C}_{22}^{\{2,1,1\}}+\left(a_A^2(m_q+m_Q)+a_V^2(m_q-m_Q)\right)\mathbf{C}_2^{\{2,1,1\}}\right)\\
B_2 &= 2\left(a_A^2+a_V^2\right)\left(\mathbf{C}_{12}^{\{2,1,1\}}+\mathbf{C}_0^{\{2,1,1\}}+\mathbf{C}_2^{\{2,1,1\}}+\mathbf{C}_1^{\{2,1,1\}}\right)\\
B_3 &= -2\Big(-m_D\left(m_q\left(a_A^2+a_V^2\right)\mathbf{C}_{12}^{\{2,1,1\}}+m_Q\left(a_A^2-a_V^2\right)\mathbf{C}_1^{\{2,1,1\}}\right)\\
&\quad+\left(a_A^2(m_{D^\pm}(m_q+2m_Q)-m_Dm_Q)\right.\\
&\quad\left.+a_V^2(m_Dm_Q+m_{D^\pm}(m_q-2m_Q))\right)\mathbf{C}_0^{\{2,1,1\}}+m_{D^\pm}m_q\left(a_A^2+a_V^2\right)\mathbf{C}_2^{\{2,1,1\}}\Big)\\
B_4 &= 2\left(a_A^2+a_V^2\right)\left(m_D\mathbf{C}_{11}^{\{2,1,1\}}+(m_D-m_{D^\pm})\mathbf{C}_1^{\{2,1,1\}}\right)\\
B_5 &= \left(a_A^2+a_V^2\right)\left(\mathbf{B}_0^{\{2,1\}}\left(m_D^2;m_V,m_{D^\pm}\right)+\mathbf{B}_0^{\{2,1\}}\left(m_q^2;m_V,m_Q\right)+m_{D^\pm}^2\mathbf{C}_0^{\{2,1,1\}}+m_Q^2\mathbf{C}_0^{\{2,1,1\}}\right.\\
&\quad\left.+2\mathbf{C}_{00}^{\{2,1,1\}}+m_D^2\left(-\mathbf{C}_0^{\{2,1,1\}}\right)-m_q^2\mathbf{C}_0^{\{2,1,1\}}+2p.q\mathbf{C}_0^{\{2,1,1\}}\right)
\end{aligned}
$$

For the surviving cases where either DM is majorana or $Y=0$, diagrams A and B may be combined. Here we take expansion of the combined integral around small quark momentas, analogous to Hisano [97]. Using irreducible decomposition of the following quark operator, where in last line the antisymmetric piece is dropped as it does not contribute to the nuclear matrix element [119].

$$
\begin{aligned}
\bar{q}i\partial^\mu\gamma^\nu q &= \bar{q}\left[\frac{i\partial^\mu\gamma^\nu+i\partial^\nu\gamma^\mu}{2}-\frac{1}{4}g^{\mu\nu}i\partial\right]q+\bar{q}\left[\frac{i\partial^\mu\gamma^\nu-i\partial^\nu\gamma^\mu}{2}\right]q+\frac{1}{4}g^{\mu\nu}\bar{q}i\partial q\\
&= \mathcal{O}_{\mu\nu}^q+\frac{1}{4}g^{\mu\nu}m_q\bar{q}q
\end{aligned}
$$

$$
\begin{aligned}
\frac{i\mathcal{M}}{\xi}(4\pi)^2 &= A<1><1>+B<p^\mu p^\nu>[\mathcal{O}_{\mu\nu}+\frac{1}{4}g_{\mu\nu}m_q<1>]\\
&\quad+(C+D)<\gamma^\mu p^\nu>[\mathcal{O}_{\mu\nu}+\frac{1}{4}g_{\mu\nu}m_q<1>]\\
&\equiv \Pi_A<1><1>+\Pi_B<p^\mu p^\nu>[\mathcal{O}_{\mu\nu}]\\
&\quad+\Pi_C<\gamma^\mu p^\nu>[\mathcal{O}_{\mu\nu}]
\end{aligned}
$$

using $x\equiv m_V^2/m_D^2$ and $b_x\equiv\sqrt{1-x/4}$ and taking the limit that the internal DM partner mass goes to m_D, we recover the result of [97].

$$\lim_{y\to 0}\Pi_A = \frac{4m_q}{m_V^3}(a_V^2 - a_A^2)g_S(x)$$
$$\lim_{y\to 0}\Pi_B = \frac{8}{m_D^2 m_V^3}(a_A^2 + a_V^2)g_{T2}(x)$$
$$\lim_{y\to 0}\Pi_C = \frac{8}{m_D m_V^3}(a_A^2 + a_V^2)g_{T1}(x)$$

The contribution from the triangle diagram, again with couplings extracted as ξ is given by

$$\frac{i\mathcal{M}}{\xi}(4\pi)^2 = \Delta < 1 >< 1 > \tag{A.13}$$

Where in the limit of no mass split between DM and partners, $\Delta = \frac{2m_q}{m_V}g_H(x)$.

$$g_H(x) = -\frac{2}{b_x}(2 + 2x - x^2)\arctan\frac{2b_x}{\sqrt{x}} + 2\sqrt{x}(2 - x\log x)$$
$$g_S(x) = \frac{1}{4b_x}(x^2 - 2x + 4)\arctan\frac{2b_x}{\sqrt{x}} + \frac{1}{4}\sqrt{x}(2 - x\log x)$$
$$g_{T2}(x) = \frac{1}{4b_x}x(x^2 - 4x + 2)\arctan\frac{2b_x}{\sqrt{x}} - \frac{1}{4}\sqrt{x}\,(1 - 2x - x(2 - x)\log x]$$
$$g_{T1}(x) = \frac{1}{3}b_x(2 + x^2)\arctan\frac{2b_x}{\sqrt{x}} + \frac{1}{12}\sqrt{x}(1 - 2x - x(2 - x)\log x)]$$

These expressions are in agreement with and mirror the conventions of [97]. However, when m_{D^+} is different to m_D then sizable modifications to these results may occur.

The two-loop result for coupling of DM to gluons via loops of heavy quarks was also derived in [97], and we make use of this result in this work. The relevant loop factor is given by:

$$f_G = f_G^{(a)} + f_G^{(b)} + f_G^{(c)}$$

$$f_G^{(a)} = \frac{\alpha_s\alpha_2^2}{4\pi}\left[\frac{n^2 - (4Y^2 + 1)}{8m_W^3}g_W(w, y) + \frac{Y^2}{4m_Z^3 cos^4\theta_W}g_z(z, y)\right] \tag{A.14}$$

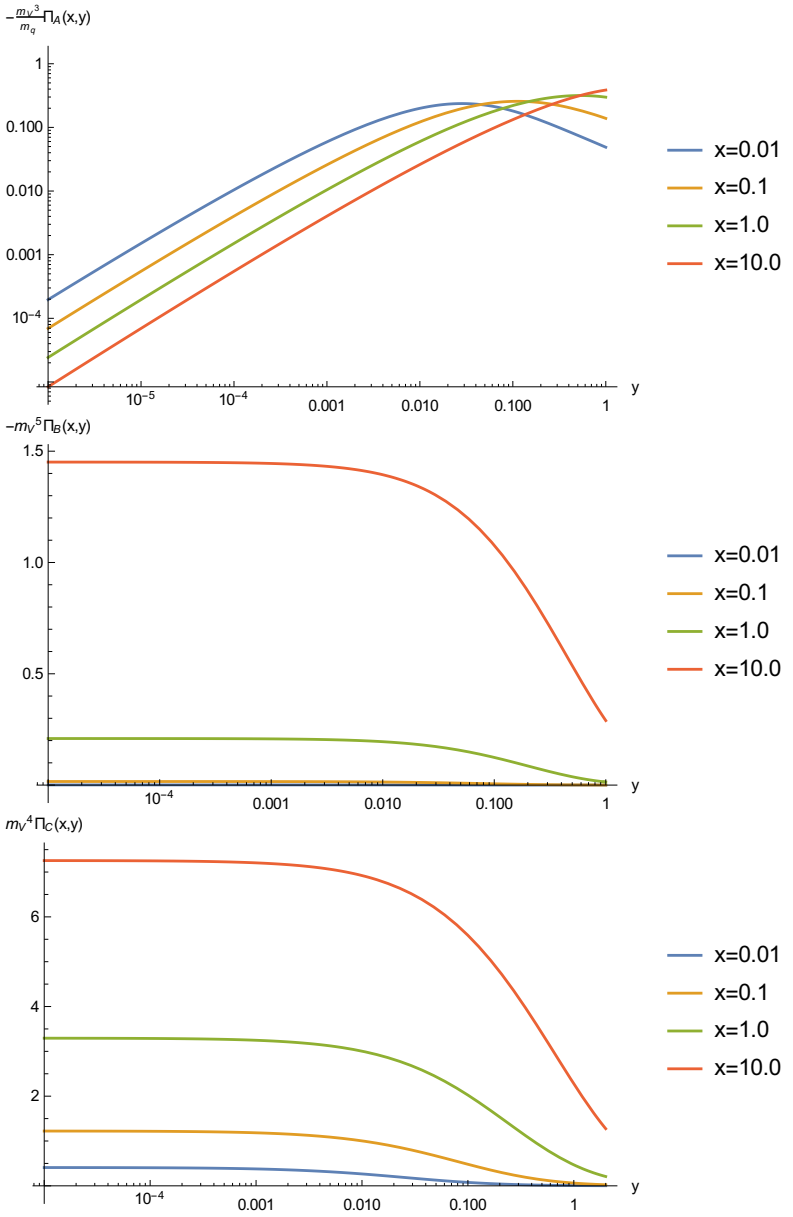

FIGURE A.1: Loop functions scaling behaviour with $y = m_{D^*}/m_D$, where m_{D^*} represents internal DM partner mass (for $a_A = a_V = 1/2$)

$$f_G^{(b)} + f_G^{(c)} = -\frac{\alpha_s}{12\pi}\frac{\alpha_2^2}{4m_h^2}\sum_{Q=c,b,t} c_Q \left[\frac{n^2-(4Y^2+1)}{8m_W} g_H(w) + \frac{Y^2}{4m_Z cos^4\theta_W} g_H(z)\right] \tag{A.15}$$

Where $w \equiv m_W^2/m_D^2$, $z \equiv m_Z^2/m_D^2$, $y \equiv m_t^2/m_D^2$ (m_t is the top quark mass).

$$g_W(w,y) = 2g_{B1}(w) + g_{B3}(w,y) \tag{A.16}$$

with

$$g_{\mathrm{B3}}(x,y) = g_{\mathrm{B3}}^{(1)}(x,y) + c_b g_{\mathrm{B3}}^{(2)}(x,y). \tag{A.17}$$

$$\begin{aligned}
g_{\mathrm{B3}}^{(1)}(x,y) &= \frac{-x^{3/2}}{12(y-x)} + \frac{-x^{3/2}y^2}{24(y-x)^2}\log y - \frac{x^{5/2}(x-2y)}{24(y-x)^2}\log x \\
&\quad - \frac{x^{3/2}\sqrt{y}(y+2)\sqrt{4-y}}{12(y-x)^2}\tan^{-1}\left(\frac{\sqrt{4-y}}{\sqrt{y}}\right) \\
&\quad + \frac{x(x^3-2(y+1)x^2+4(y+1)x+4y)}{12(y-x)^2\sqrt{4-x}}\tan^{-1}\left(\frac{\sqrt{4-x}}{\sqrt{x}}\right), \\
g_{\mathrm{B3}}^{(2)}(x,y) &= \frac{-x^{3/2}y}{12(y-x)^2} + \frac{-x^{5/2}y^2}{24(y-x)^3}\log y + \frac{x^{5/2}y^2}{24(y-x)^3}\log x \\
&\quad + \frac{x^{3/2}\sqrt{y}(-6y+xy^2-2xy-2x)}{12(y-x)^3\sqrt{4-y}}\tan^{-1}\left(\frac{\sqrt{4-y}}{\sqrt{y}}\right) \\
&\quad + \frac{-xy(x^2y-2xy-6x-2y)}{12(y-x)^3\sqrt{4-x}}\tan^{-1}\left(\frac{\sqrt{4-x}}{\sqrt{x}}\right),
\end{aligned} \tag{A.18}$$

$$g_{\mathrm{Z}}(z,y) = \left[\sum_{q=u,d,s,c,b}\left\{(a_q^V)^2+(a_q^A)^2\right\} - 2\sum_{Q=c,b} c_Q\left\{(a_q^V)^2-(a_q^A)^2\right\}\right]\times 4 g_{\mathrm{B1}}(z) + g_t(z,y)\,. \tag{A.19}$$

$$g_{\mathrm{B1}}(x) = -\frac{1}{24}\sqrt{x}(x\log(x)-2) + \frac{(x^2-2x+4)\tan^{-1}(\frac{2b_x}{\sqrt{x}})}{24 b_x}\,, \tag{A.20}$$

$$g_t(z,y) = g_t^{\text{no-log}}(z,y) + g_t^{\log}(z,y). \tag{A.21}$$

$$g_t^{\text{no-log}}(z,y) = (a_t^V)^2\, G_{t1}(z,y) + (a_t^A)^2\, G_{t2}(z,y), \tag{A.22}$$

$$
\begin{aligned}
G_{t1}(z,y) = & -\frac{\sqrt{z}(12y^2 - zy + z^2)}{3(4y-z)^2} \\
& + \frac{z^{3/2}(48y^3 - 20zy^2 + 12z^2y - z^3)}{6(4y-z)^3}\,\log z + \frac{2z^{3/2}y^2(4y-7z)}{3(4y-z)^3}\,\log(4y) \\
& - \frac{z^{3/2}\sqrt{y}(16y^3 - 4(2+7z)y^2 + 14(2+z)y + 5z)}{3(4y-z)^3\sqrt{1-y}}\,\tan^{-1}\left(\frac{\sqrt{1-y}}{\sqrt{y}}\right) \\
& - \tan^{-1}\left(\frac{\sqrt{4-z}}{\sqrt{z}}\right) \\
& \times \frac{48(z^2-2z+4)y^3 - 4z(5z^2-10z+44)y^2 + 12z^3(z-2)y - z^3(z^2-2z+4)}{3(4y-z)^3\sqrt{4-z}},
\end{aligned}
$$

$$
\begin{aligned}
G_{t2}(z,y) = & \frac{\sqrt{z}(2y-z)}{(4y-z)} - \frac{z^{3/2}(8y^2 - 8zy + z^2)}{2(4y-z)^2}\,\log z - \frac{4z^{3/2}y^2}{(4y-z)^2}\,\log(4y) \\
& + \frac{4z^{3/2}\sqrt{y}(2y^2 - y - 1)}{(4y-z)^2\sqrt{1-y}}\,\tan^{-1}\left(\frac{\sqrt{1-y}}{\sqrt{y}}\right) \\
& - \frac{8z(z^2-2z+1)y - (z^2-2z+4)(8y^2+z^2)}{(4y-z)^2\sqrt{4-z}}\,\tan^{-1}\left(\frac{\sqrt{4-z}}{\sqrt{z}}\right).
\end{aligned}
\tag{A.23}
$$

$$
g_t^{\log}(z,y) = 4z^{3/2}y^2\left(A_1\, y\,[I_1 + I_2] + A_2\,[I_3 + I_4]\right), \tag{A.24}
$$

with

$$
\begin{aligned}
A_1 &= -2(a_t^V)^2 + 4(a_t^A)^2, \\
A_2 &= -(a_t^V)^2 + (a_t^A)^2,
\end{aligned}
\tag{A.25}
$$

following numerical integral were calculated using gsl library.

$$
\begin{aligned}
I_1 &= \int_0^\infty \mathrm{d}t\, \frac{(\sqrt{t+4} - \sqrt{t})\left(\log\left[\sqrt{t+4y} + \sqrt{t}\right] - \log\left[\sqrt{t+4y} - \sqrt{t}\right]\right)}{[t+z]^2\,[t+4y]^{5/2}\,t}, \\
I_2 &= \int_0^\infty \mathrm{d}t\, \frac{1}{2} \times \frac{(t+2-\sqrt{t}\sqrt{t+4})\left(\log\left[\sqrt{t+4y} + \sqrt{t}\right] - \log\left[\sqrt{t+4y} - \sqrt{t}\right]\right)}{[t+z]^2\,[t+4y]^{5/2}\,t^{1/2}}, \\
I_3 &= \int_0^\infty \mathrm{d}t\, \frac{(\sqrt{t+4} - \sqrt{t})\left(\log\left[\sqrt{t+4y} + \sqrt{t}\right] - \log\left[\sqrt{t+4y} - \sqrt{t}\right]\right)}{[t+z]^2\,[t+4y]^{5/2}}, \\
I_4 &= \int_0^\infty \mathrm{d}t\, \frac{1}{2} \times \frac{\sqrt{t}(t+2-\sqrt{t}\sqrt{t+4})\left(\log\left[\sqrt{t+4y} + \sqrt{t}\right] - \log\left[\sqrt{t+4y} - \sqrt{t}\right]\right)}{[t+z]^2\,[t+4y]^{5/2}}.
\end{aligned}
$$

A.3 h-ψ-ψ in pseudoscalar model

A.3.1 Direct detection

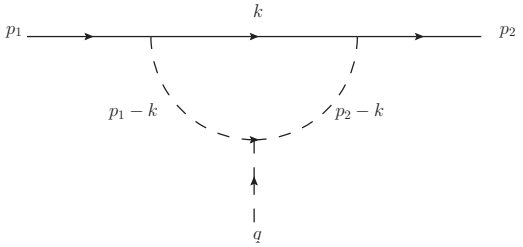

FIGURE A.2: Feynman diagrams for DM DD

Here $p_1(p_2)$ is the incoming(outgoing) momentum of fermion ψ and q is the incoming momentum of h (SM higgs boson).

$$\bar{u}(p_2)i\delta Yu(p_1) = \frac{-i\lambda_{aH}}{2}(iY_\psi)^2 v\mu^{2\epsilon}\int\frac{d^dk}{(2\pi)^d}\frac{\bar{u}(p_2)\gamma^5(-i)i(k+m_\psi)(-i)\gamma^5u(p_1)}{(k^2-m_\psi^2)((p_1-k)^2-m_a^2)((p_2-k)^2-m_a^2)}$$

$$\begin{aligned}\Upsilon(s) \equiv \left(\frac{ie^{-\gamma_E\epsilon}}{(4\pi)^{d/2}}\right)^{-1}\mu^{2\epsilon}\int\frac{d^dk}{(2\pi)^d}\frac{(k+m_\psi)}{(k^2-m_\psi^2)((p_1-k)^2-m_a^2)((p_2-k)^2-m_a^2)}\\ = m_D\big[C_0(m_D^2,s,m_D^2,m_D,m_a,m_a)+\\ C_1(m_D^2,s,m_D^2,m_D,m_a,m_a)+C_2(m_D^2,s,m_D^2,m_D,m_a,m_a)\big]\end{aligned}$$

Where C_i correspond to the 3-point Passarino-Veltman integrals [276, 127]. Here, $s = -q^2$.

In the limit where $q^2 \to 0$ as is relevant for DM direct detection, and substituting onshell conditions (i.e $p_1^2 = m_\psi^2, p_2^2 = m_\psi^2$, $p_1.p_2 = -q^2/2 + m_\psi^2$), we find the following expression

$$\delta Y = \frac{-\lambda_{aH}Y_\psi^2}{32\pi^2}\frac{v}{m_\psi}\Delta\left(\frac{m_a^2}{m_\psi^2}\right)$$

$$\begin{aligned}\Delta(\beta) &\equiv m_\psi\Upsilon(s=0)\\ &= \frac{(\beta-4)(\beta-1)\log(\beta) - 2\left(\beta+(\beta-3)\sqrt{(\beta-4)\beta}\log\left(\frac{\beta+\sqrt{(\beta-4)\beta}}{2\sqrt{\beta}}\right)-4\right)}{2(\beta-4)}\end{aligned}$$

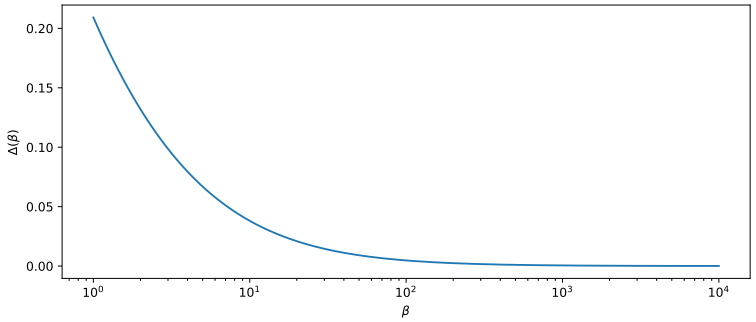

FIGURE A.3: Dimensionless loop function Δ as a function of β.

A.3.2 Relic

For the relic we should consider $\bar{D}D \to h$ process.

$$\bar{v}(p_2)\delta Y u(p_1) = i\frac{\lambda_{aH}}{2} v Y_\psi^2 \int \frac{d^d k}{(2\pi)^d} \frac{\bar{v}(p_2)\gamma^5(k+m_\psi)\gamma^5 u(p_1)}{(k^2-m_\psi^2)((p_1-k)^2-m_a^2)((p_2-k)^2-m_a^2)} \tag{A.26}$$

$$= -\frac{\lambda_{aH} v Y_\psi^2}{32\pi^2} \bar{u}(p_2) v(p_1) \mathrm{Y}(s) \tag{A.27}$$

The relevant quantity, required in order to find the relic density via the Boltzmann equation is given by

$$\mathrm{Y}_{Relic} \equiv \mathrm{Y}(s = 4m_\psi^2(1+1/(2x)) \tag{A.28}$$

Where $x \equiv m_\psi/T$. It is worth noting that around freeze-out (at $x \approx 20$), this loop function is insensitive to x.

A.3.3 Higgs invisible

$$\bar{u}(p_2)\delta Y v(p_1) = i\frac{\lambda_{aH}}{2} v Y_\psi^2 \int \frac{d^d k}{(2\pi)^d} \frac{\bar{u}(p_2)\gamma^5(k+m_\psi)\gamma^5 v(p_1)}{(k^2-m_\psi^2)((p_1-k)^2-m_a^2)((p_2-k)^2-m_a^2)} \tag{A.29}$$

$$= -\frac{\lambda_{aH} v Y_\psi^2}{32\pi^2} \bar{v}(p_2) u(p_1) \mathrm{Y}(s) \tag{A.30}$$

Where now, we assume Higgs is on-shell and so $s = m_H^2$.

$$\mathrm{Y}_{H\to\psi\psi} \equiv \mathrm{Y}(s = m_H^2) \tag{A.31}$$

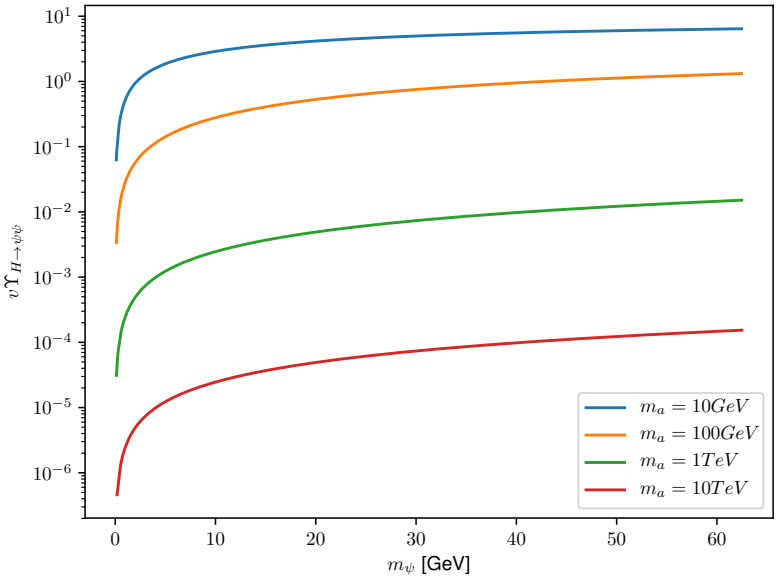

FIGURE A.4: Higgs vev (246GeV) multiplied by loop function, $\Upsilon_{H\to\psi\psi}$, for Higgs invisible decays to pair of ψ, evaluated at various mass points.

Appendix B

B.1 Process $e^+e^- \to Z \to DD^A \to DDZ$

One more process leading to production of D-odd particles at ILC is also observable at $M_A + M_D < \sqrt{s}$ (in particular, at $\frac{\sqrt{s}}{2} > M_+ > M_A$):

$$e^+e^- \to Z \to DD^A \to DDZ. \tag{B.1}$$

This process has a clear signature in the modes suitable for observation

The e^+e^- or $\mu^+\mu^-$ pair with large $\not{E}_T$ and large $M(\not{E}_T)$ + *nothing*. The effective mass of this dilepton is $\leqslant M_Z$, its energy is typically less than $\frac{\sqrt{s}}{2}$. (B.2a)

A quark dijet with large $\not{E}_T$ and large $M(\not{E}_T)$ + *nothing*. The effective mass of this dijet is $\leqslant M_Z$, its energy is typically less than $\frac{\sqrt{s}}{2}$. (B.2b)

At $M_A < M_+$ the BR for channel with signature (B.2a) is 0.06, for the channel with signature (B.2b) – 0.7. We skip channel $Z \to \tau^+\tau^-$ with BR=0.03, 20% of decays of Z are invisible ($Z \to \nu\bar{\nu}$).

At $M_A > M_+$ BR's for processes with signature (B.2) become less, since new decay channels $D^A \to D^{\mp}W^{\pm} \to DW^+W^-$ are added with signature

$e^+e^- \to DD^A \to DDW^+W^-$: Two quark dijets or dijet + single lepton or two leptons in one hemisphere with large $\not{E}_T$ and large $M(\not{E}_T)$ + *nothing*. The effective mass of this system is $\leqslant M_Z$, its energy is typically less than $\frac{\sqrt{s}}{2}$. (B.3)

The cross section of the process $e^+e^- \to DD^A$ is model dependent. In the IDM it is determined unambiguously, in MSSM result depends on mixing angles and on the nature of fermions D and D^A (Dirac or Majorana). In all considered cases at $\sqrt{s} > 200$ GeV this cross section is smaller than $0.1\sigma_0$. Since the BR for events with signature (B.2a) is 0.06, at the luminosity (3.19) annual number of events with this signature is smaller than $2 \cdot 10^3$. This number looks insufficient for kinematical

analysis with high enough precision, (but limitations for masses can be obtained (cf. [181, 182, 183] for LEP)).

Nevertheless we describe, for completeness, the energy distributions of Z in this process. The obtained equations are similar to (3.20), (3.28)–(3.30) for new kinematics.

The γ-factor and velocity of D^A in c.m.s. for e^+e^- are

$$\gamma_A = \frac{s + M_A^2 - M_D^2}{2\sqrt{s}M_A}, \quad \beta_A = \frac{\sqrt{(s^2 - M_A^2 - M_D^2)^2 - 4M_D^2 M_A^2}}{s + M_A^2 - M_D^2}. \tag{B.4}$$

For production of Z with an effective mass M^* ($M^* = M_Z$ at $M_A - M_D > M_Z$ and $M^* \leqslant M_A - M_D$ at $M_A - M_D < M_Z$) in the rest frame of D^A

$$E_Z^{rest} = \frac{M_A^2 + M^{*2} - M_D^2}{2M_A}, \qquad p_Z^{rest} = \frac{\sqrt{(M_A^2 - M^{*2} - M_D^2)^2 - 4M_D^2 M^{*2}}}{2M_A}. \tag{B.5}$$

At $M_A - M_D > M_Z$ the Z-boson energy E_Z lies within the interval with edges

$$E_{Z,on}^- = \gamma_A(E_Z^{rest} - \beta_A |p|_Z^{rest}), \quad E_{Z,on}^+ = \gamma_A(E_Z^{rest} + \beta_A |p|_Z^{rest}). \tag{B.6}$$

At $M_A - M_D < M_Z$ similar equations are valid for each value of M^*. Absolute upper and lower edges of the energy distribution of Z are reached at $M^* = 0$:

$$E_{Z,off}^{\pm} = \gamma_A(1 \pm \beta_a)(M_A^2 - M_D^2)/(2M_A)\,. \tag{B.7}$$

The peak in the energy distribution of dilepton appears at $M^* = M_A - M_D$:

$$E_{Z,p} = \gamma_A(M_A - M_D)\,. \tag{B.8}$$

Masses M_D and M_A. At first sight, measurement of kinematical edges of the dilepton spectrum (B.6) (at $M_A - M_D > M_Z$) gives two equations for M_D and M_A, allowing for determination of these masses. At $M_A - M_D < M_Z$, the same procedure can be performed separately for each value of the effective mass of dilepton [277]. In the latter case, the absolute edges of the dilepton energy spectrum (B.7) and the position of the peak in this spectrum (B.8) could be also used for measuring M_D and M_A.

In any case, the upper edge in the dijet energy spectrum E_Z^+ (B.6), (B.7) (signature (B.2)) gives one equation, necessary to find M_A and M_D. In principle, necessary additional information gives position of lower edge in the dilepton energy spectrum E_Z^-. However, as it was noted above, the anticipated number of events with signature (B.2a) looks insufficient for obtaining precise results. Together with good results for M_D and M_+, one can hope to find an accurate value of M_A.

B.2 Derivations

B.2.1 $\varepsilon^{\pm}$ derivations

Starting with:

$$\varepsilon = \gamma_{WL}(1 + c_1\beta_{WL})(\tfrac{M^*}{2})$$

plugging in the γ_{WL} and β_{WL} terms for the off-shell case:

$$\gamma_{WL} = \tfrac{E^{\pm}_{off}}{M^*}, \beta_{WL} = \sqrt{1 - (\tfrac{M^*}{E^{\pm}_{off}})^2}$$

gives the off-shell ε variable:

$$\varepsilon_{off} = \tfrac{E^{\pm}_{off}}{M^*}(1 + c_1\sqrt{1 - (\tfrac{M^*}{E^{\pm}_{off}})^2})(\tfrac{M^*}{2}).$$

Simplifying this down gives:

$$\begin{aligned}
\varepsilon_{off} &= \tfrac{E^{\pm}_{off}}{2}(1 + c_1\sqrt{1 - (\tfrac{M^*}{E^{\pm}_{off}})^2}) \\
\varepsilon_{off} &= \tfrac{E^{\pm}_{off}}{2}(1 + c_1\sqrt{\tfrac{1}{E^{\pm 2}_{off}}(E^{\pm 2}_{off} - M^{*2})}) \\
\varepsilon_{off} &= \tfrac{E^{\pm}_{off}}{2} + c_1\tfrac{E^{\pm}_{off}}{2}\sqrt{\tfrac{1}{E^{\pm 2}_{off}}(E^{\pm 2}_{off} - M^{*2})}) \\
\varepsilon_{off} &= \tfrac{E^{\pm}_{off}}{2} + c_1\tfrac{1}{2}\sqrt{(E^{\pm 2}_{off} - 0)}) \\
\varepsilon_{off} &= \tfrac{E^{\pm}_{off}}{2} + c_1\tfrac{E^{\pm}_{off}}{2}.
\end{aligned}$$

Now c_1 is set to ± 1 for the corresponding maximum or minimum in muon enegy distribution:

$$\varepsilon^{\pm} = \tfrac{E^{\pm}_{off}}{2} \pm \tfrac{E^{\pm}_{off}}{2}.$$

This gives a maximum muon energy of:

$$\varepsilon^{+} = \tfrac{E^{+}_{off}}{2} + \tfrac{E^{+}_{off}}{2} = E^{+}_{off}$$

and minimum muon energy of:

$$\varepsilon^{-} = \tfrac{E^{-}_{off}}{2} - \tfrac{E^{-}_{off}}{2} = 0.$$

B.2.2 ε_p derivation

$$\text{Starting with: } \varepsilon = \gamma_{WL}(1 + c_1\beta_{WL})(M_W/2).$$

Replace M_W with M^* for the off-shell case:

$$\varepsilon = \gamma_{WL}(1 + c_1\beta_{WL})(M^*/2)$$

and substitute the γ_{WL} and β_{WL} variables for the off-shell peak in $M*$ case:

$$\gamma_{WL} = E_p/M^* = \sqrt{s}/2(1 - M_D/M_+)/M^*$$
$$\beta_{WL} = \sqrt{1 - M^{*2}/E_{WL}^2} = \sqrt{1 - \frac{M^{*2}}{s/4(1-M_D/M_+)^2}}$$

gives an ε for the off-shell case at M^*=$M_+ - M_D$ (peak).

$$\varepsilon = \frac{\sqrt{s}/2(1-M_D/M_+)}{M^*}(1 + c_1\sqrt{1 - \frac{M^{*2}}{s/4(1-M_D/M_+)^2}})(M^*/2).$$

Replace M^* by $M_+ - M_D$ for max M^*:

$$\varepsilon_p = \sqrt{s}/2\frac{(1-M_D/M_+)}{M_+-M_D}(1 + c_1\sqrt{1 - \frac{M_+^2-M_D^2}{s/4(1-\frac{M_D}{M_+})^2}})(\frac{M_+-M_D}{2}).$$

Simplifying this down:

$$\varepsilon_p = \frac{\sqrt{s}/2(1-\frac{M_D}{M_+})}{M_+-M_D}(1 + c_1\sqrt{1 - (\frac{M_+-M_D}{s/4(1-\frac{M_D}{M_+})})^2})(\frac{M_+-M_D}{2})$$
$$\varepsilon_p = \frac{\sqrt{s}/2(1-\frac{M_D}{M_+})}{M_+(1-\frac{M_D}{M_+})}(1 + c_1\sqrt{1 - (\frac{M_+(1-\frac{M_D}{M_+})}{\sqrt{s}/2(1-\frac{M_D}{M_+})})^2})(M_+(\frac{1-\frac{M_D}{M_+}}{2}))$$
$$\varepsilon_p = \sqrt{s}/2(1 + c_1\sqrt{1 - (\frac{M_+}{\sqrt{s}/2})^2})(\frac{1-M_D/M_+}{2})$$
$$\varepsilon_p = \sqrt{s}/2(1 + c_1\beta_+)(1 - M_D/M_+)/2.$$

Now c_1 is set to $+1$ corresponding to the maximum in M^*:

$$\varepsilon_p = \sqrt{s}/2(1 + \beta_+)(1 - M_D/M_+)/2.$$

B.2.3 Simultaneous equations procedure for finding M_+ and M_D

Equations (4.1) give two simultaneous equations:

$$\frac{4\varepsilon^{+2} + M_W^2}{4\varepsilon^+} = \frac{\sqrt{s}/2}{M_+}\left(\frac{M_+^2 + M_W^2 - M_D^2}{2M_+} + \sqrt{1 - \frac{M_+^2}{s/4}}\frac{\sqrt{M_+^4 + M_W^4 + M_D^4 - 2M_+^2M_W^2 - 2M_+^2M_D^2 - 2M_W^2M_D^2}}{2M_+}\right)$$

$$\frac{4\varepsilon_k^{-2} + M_W^2}{4\varepsilon_k^-} = \frac{\sqrt{s}/2}{M_+}\left(\frac{M_+^2 + M_W^2 - M_D^2}{2M_+}0 - \sqrt{1 - \frac{M_+^2}{s/4}}\frac{\sqrt{M_+^4 + M_W^4 + M_D^4 - 2M_+^2M_W^2 - 2M_+^2M_D^2 - 2M_W^2M_D^2}}{2M_+}\right)$$

Solving the simultaneous equations produces the equation of M_D in terms of M_+:

$$M_D^2 = M_W^2 - M_+^2\left[\frac{1}{\sqrt{s}/2}\left(\frac{4\varepsilon^{+2} + M_W^2}{4\varepsilon^+} + \frac{4\varepsilon_k^{-2} + M_W^2}{4\varepsilon_k^-}\right) - 1\right]$$

and substituting this onto (1) results in the polynomial of M_+:

$$-M_+^4(\alpha+\beta)^2 + 4M_+^2 s/4(\alpha\beta + M_W^2) - 4M_W^2 s^2/16 = 0$$

where:

$$\alpha = \frac{4\varepsilon^{+2} + M_W^2}{4\varepsilon^+}, \beta = \frac{4\varepsilon_k^{-2} + M_W^2}{4\varepsilon_k^-}.$$

This gives 4 roots for M_+:

$$M_+ = \pm\sqrt{2}\sqrt{\frac{-\sqrt{s^2/16(\alpha^2 - M_W^2)(\beta^2 - M_W^2)} + \alpha\beta s/4 + s/4M_W^2}{(\alpha+\beta)^2}}$$

$$M_+ = \pm\sqrt{2}\sqrt{\frac{\sqrt{s^2/16(\alpha^2 - M_W^2)(\beta^2 - M_W^2)} + \alpha\beta s/4 + s/4M_W^2}{(\alpha+\beta)^2}}.$$

Two of these roots will be positive and the top equation will correspond to the physical mass of $D^\pm$.

By rearranging the equation of M_D in terms of M_+ to give M_+ in terms of M_D and substituting this into the M_+ polynomial, the polynomial for M_D has the form:

$$-\left(\frac{M_W^2-M_D^2}{\alpha+\beta-\sqrt{s}/2}\right)^2(\alpha+\beta)^2+4\frac{M_W^2-M_D^2}{\alpha+\beta-\sqrt{s}/2}\sqrt{s}/2(\alpha\beta+M_W^2)-4M_W^2s/4=0$$

which gives two real and two complex roots for M_D. Out of the two real roots, one is positive and gives the physical mass for D.

B.3 Multivariate cuts

Here, we present multivariate cuts which could further boost the potential for the ILC to observe a signal at these benchmark points.

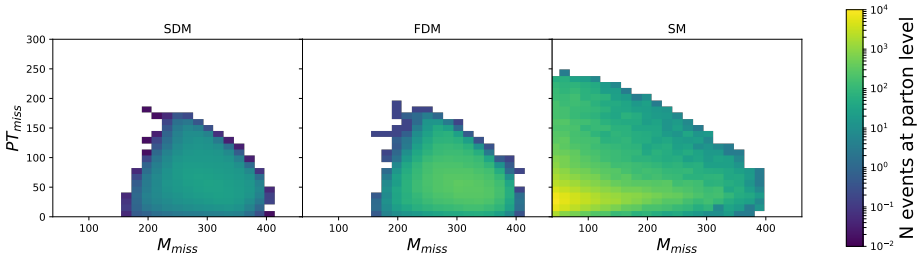

FIGURE B.1: Dalitz plot in PTmiss Mmiss plane, shows potential of multivariate cut at BP1.

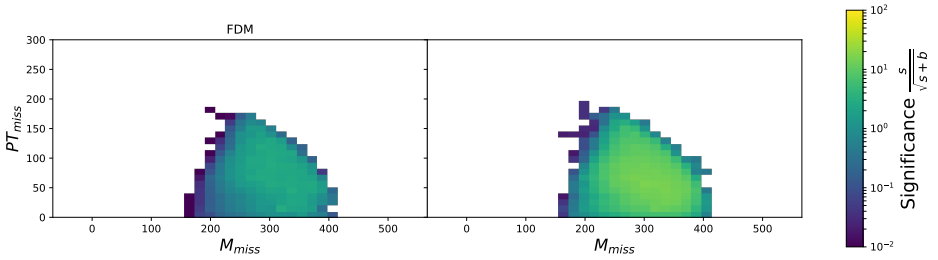

FIGURE B.2: Dalitz plot in PTmiss Mmiss plane, shows potential of multivariate cut at BP1.

References

[1] S. Giagu, *WIMP Dark Matter Searches With the ATLAS Detector at the LHC*, *Front. in Phys.* **7** (2019) 75.

[2] V. C. Rubin, N. Thonnard and W. K. Ford, Jr., *Rotational properties of 21 SC galaxies with a large range of luminosities and radii, from NGC 4605 /R = 4kpc/ to UGC 2885 /R = 122 kpc/*, *Astrophys. J.* **238** (1980) 471.

[3] L. J. Hall, K. Jedamzik, J. March-Russell and S. M. West, *Freeze-In Production of FIMP Dark Matter*, *JHEP* **03** (2010) 080 [0911.1120].

[4] J. Cooley, *Overview of non-liquid noble direct detection dark matter experiments*, *Physics of the Dark Universe* **4** (Sep, 2014) 92–97.

[5] T. R. Slatyer, *Indirect Detection of Dark Matter*, in *Theoretical Advanced Study Institute in Elementary Particle Physics: Anticipating the Next Discoveries in Particle Physics*, 10, 2017. 1710.05137.

[6] **LUX-ZEPLIN** Collaboration, D. Akerib *et. al.*, *Projected WIMP sensitivity of the LUX-ZEPLIN dark matter experiment*, *Phys. Rev. D* **101** (2020), no. 5 052002 [1802.06039].

[7] A. Belyaev, A. Coupe, N. Evans, D. Locke and M. Scott, *Any Room Left for Technicolor? Dilepton Searches at the LHC and Beyond*, *Phys. Rev. D* **99** (2019), no. 9 095006 [1812.09052].

[8] A. Belyaev, G. Cacciapaglia and D. Locke, *Minimal consistent dark matter models for collider an direct detection characterisation: fermion dark matter*, *Publication upcoming*.

[9] F. A. G. I. H. T. L. D. Belyaev, A. and A. Pukhov, *Decoding dark matter at future e^+e^- colliders*, *Publication upcoming*.

[10] A. Semenov, *LanHEP - a package for automatic generation of Feynman rules from the Lagrangian. Updated version 3.1*, 1005.1909.

[11] N. D. Christensen and C. Duhr, *FeynRules - Feynman rules made easy*, *Comput. Phys. Commun.* **180** (2009) 1614–1641 [0806.4194].

[12] F. Staub, *SARAH*, *arXiv:0806.0538* **[hep-ph]** (2008) [0806.0538].

[13] A. Belyaev, C. N. D. and A. Pukhov, *CalcHEP 3.4 for collider physics within and beyond the Standard Model*, *Comput. Phys. Commun.* **184** (2013) 1729 [1207.6082].

[14] J. Alwall, M. Herquet, F. Maltoni, O. Mattelaer and T. Stelzer, *MadGraph 5 : Going Beyond*, *JHEP* **06** (2011) 128 [1106.0522].

[15] G. Belanger, F. Boudjema, A. Pukhov and A. Semenov, *micrOMEGAs: A Tool for dark matter studies*, *Nuovo Cim.* **C033N2** (2010) 111–116 [1005.4133].

[16] T. Sjöstrand, S. Ask, J. R. Christiansen, R. Corke, N. Desai, P. Ilten, S. Mrenna, S. Prestel, C. O. Rasmussen and P. Z. Skands, *An Introduction to PYTHIA 8.2*, *Comput. Phys. Commun.* **191** (2015) 159–177 [1410.3012].

[17] **DELPHES 3** Collaboration, J. de Favereau *et. al.*, *DELPHES 3, A modular framework for fast simulation of a generic collider experiment*, *JHEP* **1402** (2014) 057 [1307.6346].

[18] M. Bondarenko, A. Belyaev, L. Basso, E. Boos, V. Bunichev *et. al.*, *High Energy Physics Model Database : Towards decoding of the underlying theory (within Les Houches 2011: Physics at TeV Colliders New Physics Working Group Report)*, 1203.1488.

[19] **GAMBIT** Collaboration, P. Athron *et. al.*, *GAMBIT: The Global and Modular Beyond-the-Standard-Model Inference Tool*, *Eur. Phys. J. C* **77** (2017), no. 11 784 [1705.07908]. [Addendum: Eur.Phys.J.C 78, 98 (2018)].

[20] M. Papucci, K. Sakurai, A. Weiler and L. Zeune, *Fastlim: a fast LHC limit calculator*, *Eur. Phys. J. C* **74** (2014), no. 11 3163 [1402.0492].

[21] S. Kraml, S. Kulkarni, U. Laa, A. Lessa, W. Magerl, D. Proschofsky-Spindler and W. Waltenberger, *SModelS: a tool for interpreting simplified-model results from the LHC and its application to supersymmetry*, *Eur. Phys. J. C* **74** (2014) 2868 [1312.4175].

[22] **LHC Reinterpretation Forum** Collaboration, W. Abdallah *et. al.*, *Reinterpretation of LHC Results for New Physics: Status and Recommendations after Run 2*, *SciPost Phys.* **9** (2020), no. 2 022 [2003.07868].

[23] A. Belyaev, J. Blandford and D. Locke, "Phenodata database." https://hepmdb.soton.ac.uk/phenodata, Jan. 2017.

[24] E. Maguire, L. Heinrich and G. Watt, *HEPData: a repository for high energy physics data*, *J. Phys. Conf. Ser.* **898** (2017), no. 10 102006 [1704.05473].

[25] L. Edelhäuser, J. Heisig, M. Krämer, L. Oymanns and J. Sonneveld, *Constraining supersymmetry at the LHC with simplified models for squark production*, *JHEP* **12** (2014) 022 [1410.0965].

[26] L. Edelhäuser, M. Krämer and J. Sonneveld, *Simplified models for same-spin new physics scenarios*, *JHEP* **04** (2015) 146 [1501.03942].

[27] C. Arina, M. E. C. Catalan, S. Kraml, S. Kulkarni and U. Laa, *Constraints on sneutrino dark matter from LHC Run 1*, *JHEP* **05** (2015) 142 [1503.02960].

[28] S. Kraml, U. Laa, L. Panizzi and H. Prager, *Scalar versus fermionic top partner interpretations of $t\bar{t} + E_T^{\rm miss}$ searches at the LHC*, *JHEP* **11** (2016) 107 [1607.02050].

[29] J. Alwall, P. Schuster and N. Toro, *Simplified Models for a First Characterization of New Physics at the LHC*, *Phys. Rev. D* **79** (2009) 075020 [0810.3921].

[30] C. G. Lester and D. J. Summers, *Measuring masses of semiinvisibly decaying particles pair produced at hadron colliders*, *Phys. Lett.* **B463** (1999) 99–103 [hep-ph/9906349].

[31] M. Burns, K. Kong, K. T. Matchev and M. Park, *Using Subsystem MT2 for Complete Mass Determinations in Decay Chains with Missing Energy at Hadron Colliders*, *JHEP* **03** (2009) 143 [0810.5576].

[32] H.-C. Cheng and Z. Han, *Minimal Kinematic Constraints and m(T2)*, *JHEP* **12** (2008) 063 [0810.5178].

[33] N. D. Christensen, T. Han, Z. Qian, J. Sayre, J. Song and Stefanus, *Determining the Dark Matter Particle Mass through Antler Topology Processes at Lepton Colliders*, *Phys. Rev.* **D90** (2014) 114029 [1404.6258].

[34] N. D. Christensen and D. Salmon, *New method for the spin determination of dark matter*, *Phys. Rev.* **D90** (2014), no. 1 014025 [1311.6465].

[35] **ATLAS** Collaboration, G. Aad *et. al.*, *Observation of a new particle in the search for the Standard Model Higgs boson with the ATLAS detector at the LHC*, *Phys. Lett. B* **716** (2012) 1–29 [1207.7214].

[36] **CMS** Collaboration, S. Chatrchyan *et. al.*, *Observation of a New Boson at a Mass of 125 GeV with the CMS Experiment at the LHC*, *Phys. Lett. B* **716** (2012) 30–61 [1207.7235].

[37] G. F. Giudice, *Naturally Speaking: The Naturalness Criterion and Physics at the LHC*, 0801.2562.

[38] M. Bauer and T. Plehn, *Yet another introduction to dark matter*, 2018.

[39] E. W. Kolb and M. S. Turner, *The early universe*. Frontiers in physics. Westview Press, Boulder, CO, 1990.

[40] J. M. Cline, *TASI Lectures on Early Universe Cosmology: Inflation, Baryogenesis and Dark Matter*, *PoS* **TASI2018** (2019) 001 [1807.08749].

[41] **MACHO** Collaboration, C. Alcock *et. al.*, *The MACHO project: microlensing detection efficiency*, *Astrophys. J. Suppl.* **136** (2001) 439–462 [astro-ph/0003392].

[42] **EROS2** Collaboration, T. Lasserre, *Galactic dark matter search with EROS2*, *Prog. Part. Nucl. Phys.* **48** (2002) 289–290. [,289(2002)].

[43] R. H. Cyburt, B. D. Fields, K. A. Olive and T.-H. Yeh, *Big Bang Nucleosynthesis: 2015*, *Rev. Mod. Phys.* **88** (2016) 015004 [1505.01076].

[44] G. F. Smoot, *COBE observations and results*, *AIP Conf. Proc.* **476** (1999), no. 1 1–10 [astro-ph/9902027].

[45] **WMAP** Collaboration, G. Hinshaw *et. al.*, *Nine-Year Wilkinson Microwave Anisotropy Probe (WMAP) Observations: Cosmological Parameter Results*, *Astrophys. J. Suppl.* **208** (2013) 19 [1212.5226].

[46] **Planck** Collaboration, R. Adam *et. al.*, *Planck 2015 results. I. Overview of products and scientific results*, *Astron. Astrophys.* **594** (2016) A1 [1502.01582].

[47] D. J. E. Marsh, *Axions and ALPs: a very short introduction*, in *13th Patras Workshop on Axions, WIMPs and WISPs*, 12, 2017. 1712.03018.

[48] G. Gelmini and P. Gondolo, *DM Production Mechanisms*, 1009.3690.

[49] **XENON** Collaboration, E. Aprile *et. al.*, *The XENON1T Dark Matter Experiment*, *Eur. Phys. J.* **C77** (2017), no. 12 881 [1708.07051].

[50] **LZ** Collaboration, D. S. Akerib *et. al.*, *The LUX-ZEPLIN (LZ) Experiment*, *Nucl. Instrum. Meth. A* **953** (2020) 163047 [1910.09124].

[51] F. Kahlhoefer, *Review of LHC Dark Matter Searches*, *Int. J. Mod. Phys. A* **32** (2017), no. 13 1730006 [1702.02430].

[52] S. Weinberg, *Implications of Dynamical Symmetry Breaking*, *Phys. Rev. D* **13** (1976) 974–996. [Addendum: Phys.Rev.D 19, 1277–1280 (1979)].

[53] L. Susskind, *Dynamics of Spontaneous Symmetry Breaking in the Weinberg-Salam Theory*, *Phys. Rev. D* **20** (1979) 2619–2625.

[54] E. Farhi and L. Susskind, *Technicolor*, *Phys. Rept.* **74** (1981) 277.

[55] S. Dimopoulos and J. R. Ellis, *Challenges for Extended Technicolor Theories*, *Nucl. Phys. B* **182** (1982) 505–528.

[56] S. Dimopoulos and L. Susskind, *Mass Without Scalars*, *Nucl. Phys. B* **155** (1979) 237–252.

[57] R. S. Chivukula, *Lectures on technicolor and compositeness*, in *Theoretical Advanced Study Institute in Elementary Particle Physics (TASI 2000): Flavor Physics for the Millennium*, 6, 2000. hep-ph/0011264.

[58] R. Sundrum and S. D. H. Hsu, *Walking technicolor and electroweak radiative corrections*, *Nucl. Phys. B* **391** (1993) 127–146 [hep-ph/9206225].

[59] R. Foadi, M. T. Frandsen, T. A. Ryttov and F. Sannino, *Minimal Walking Technicolor: Set Up for Collider Physics*, *Phys. Rev. D* **76** (2007) 055005 [0706.1696].

[60] R. Foadi, M. T. Frandsen and F. Sannino, *125 GeV Higgs boson from a not so light technicolor scalar*, *Phys. Rev. D* **87** (2013), no. 9 095001 [1211.1083].

[61] D. Locke, "PhenoAnalysis." https://github.com/D-Locke/PhenoAnalysis, 2018.

[62] J. Goodman, M. Ibe, A. Rajaraman, W. Shepherd, T. M. Tait *et. al.*, *Constraints on Dark Matter from Colliders*, *Phys.Rev.* **D82** (2010) 116010 [1008.1783].

[63] **ATLAS** Collaboration, G. Aad *et. al.*, *Search for dark matter candidates and large extra dimensions in events with a photon and missing transverse momentum in pp collision data at $\sqrt{s} = 7$ TeV with the ATLAS detector*, *Phys.Rev.Lett.* **110** (2013), no. 1 011802 [1209.4625].

[64] **ATLAS** Collaboration, G. Aad *et. al.*, *Search for dark matter in events with a hadronically decaying W or Z boson and missing transverse momentum in pp collisions at $\sqrt{s} = 8$ TeV with the ATLAS detector*, *Phys.Rev.Lett.* **112** (2014), no. 4 041802 [1309.4017].

[65] **ATLAS** Collaboration, G. Aad *et. al.*, *Search for dark matter in events with a Z boson and missing transverse momentum in pp collisions at $\sqrt{s}$=8 TeV with the ATLAS detector*, *Phys.Rev.* **D90** (2014), no. 1 012004 [1404.0051].

[66] **ATLAS** Collaboration, G. Aad *et. al.*, *Search for new particles in events with one lepton and missing transverse momentum in pp collisions at $\sqrt{s}$ = 8 TeV with the ATLAS detector*, *JHEP* **1409** (2014) 037 [1407.7494].

[67] **CMS** Collaboration, V. Khachatryan *et. al.*, *Search for physics beyond the standard model in final states with a lepton and missing transverse energy in proton-proton collisions at $\sqrt{s}$ = 8 TeV*, *Phys.Rev.* **D91** (2015), no. 9 092005 [1408.2745].

[68] **CMS** Collaboration, V. Khachatryan *et. al.*, *Search for the production of dark matter in association with top-quark pairs in the single-lepton final state in proton-proton collisions at sqrt(s) = 8 TeV*, 1504.03198.

[69] O. Buchmueller, M. J. Dolan and C. McCabe, *Beyond Effective Field Theory for Dark Matter Searches at the LHC*, *JHEP* **1401** (2014) 025 [1308.6799].

[70] C. Cheung and D. Sanford, *Simplified Models of Mixed Dark Matter*, *JCAP* **1402** (2014) 011 [1311.5896].

[71] B. Dutta, Y. Gao and T. Kamon, *Probing Light Nonthermal Dark Matter at the LHC*, *Phys.Rev.* **D89** (2014), no. 9 096009 [1401.1825].

[72] G. Busoni, A. De Simone, J. Gramling, E. Morgante and A. Riotto, *On the Validity of the Effective Field Theory for Dark Matter Searches at the LHC, Part II: Complete Analysis for the s-channel*, *JCAP* **1406** (2014) 060 [1402.1275].

[73] M. Papucci, A. Vichi and K. M. Zurek, *Monojet versus the rest of the world I: t-channel models*, *JHEP* **1411** (2014) 024 [1402.2285].

[74] Y. Bai and J. Berger, *Lepton Portal Dark Matter*, *JHEP* **1408** (2014) 153 [1402.6696].

[75] A. Berlin, T. Lin and L.-T. Wang, *Mono-Higgs Detection of Dark Matter at the LHC*, *JHEP* **1406** (2014) 078 [1402.7074].

[76] K. Hamaguchi, S. P. Liew, T. Moroi and Y. Yamamoto, *Isospin-Violating Dark Matter with Colored Mediators*, *JHEP* **1405** (2014) 086 [1403.0324].

[77] G. Busoni, A. De Simone, T. Jacques, E. Morgante and A. Riotto, *On the Validity of the Effective Field Theory for Dark Matter Searches at the LHC Part III: Analysis for the t-channel*, *JCAP* **1409** (2014) 022 [1405.3101].

[78] C. Balázs and T. Li, *Simplified Dark Matter Models Confront the Gamma Ray Excess*, *Phys.Rev.* **D90** (2014), no. 5 055026 [1407.0174].

[79] O. Buchmueller, M. J. Dolan, S. A. Malik and C. McCabe, *Characterising dark matter searches at colliders and direct detection experiments: Vector mediators*, *JHEP* **1501** (2015) 037 [1407.8257].

[80] J. Abdallah, A. Ashkenazi, A. Boveia, G. Busoni, A. De Simone *et. al.*, *Simplified Models for Dark Matter and Missing Energy Searches at the LHC*, 1409.2893.

[81] P. Harris, V. V. Khoze, M. Spannowsky and C. Williams, *Constraining Dark Sectors at Colliders: Beyond the Effective Theory Approach*, *Phys.Rev.* **D91** (2015), no. 5 055009 [1411.0535].

[82] D. Racco, A. Wulzer and F. Zwirner, *Robust collider limits on heavy-mediator Dark Matter*, *JHEP* **1505** (2015) 009 [1502.04701].

[83] T. Jacques and K. Nordstrom, *Mapping monojet constraints onto Simplified Dark Matter Models*, 1502.05721.

[84] **CMS** Collaboration, V. Khachatryan *et. al.*, *Search for dark matter, extra dimensions, and unparticles in monojet events in proton-proton collisions at* $\sqrt{s}$ *= 8 TeV*, 1408.3583.

[85] **ATLAS** Collaboration, G. Aad *et. al.*, *Search for dark matter in events with heavy quarks and missing transverse momentum in pp collisions with the ATLAS detector*, *Eur.Phys.J.* **C75** (2015), no. 2 92 [1410.4031].

[86] **CMS** Collaboration, V. Khachatryan *et. al.*, *Search for new phenomena in monophoton final states in proton-proton collisions at* $\sqrt{s}$ *= 8 TeV*, 1410.8812.

[87] **ATLAS** Collaboration, G. Aad *et. al.*, *Search for new phenomena in events with a photon and missing transverse momentum in pp collisions at* $\sqrt{s} = 8$ *TeV with the ATLAS detector*, *Phys.Rev.* **D91** (2015), no. 1 012008 [1411.1559].

[88] **ATLAS** Collaboration, G. Aad *et. al.*, *Search for new phenomena in final states with an energetic jet and large missing transverse momentum in pp collisions at* $\sqrt{s} = 8$ *TeV with the ATLAS detector*, 1502.01518.

[89] N. G. Deshpande and E. Ma, *Pattern of Symmetry Breaking with Two Higgs Doublets*, *Phys.Rev.* **D18** (1978) 2574.

[90] M. Cirelli, N. Fornengo and A. Strumia, *Minimal dark matter*, *Nucl. Phys. B* **753** (2006) 178–194 [hep-ph/0512090].

[91] T. Hambye, F.-S. Ling, L. Lopez Honorez and J. Rocher, *Scalar Multiplet Dark Matter*, *JHEP* **0907** (2009) 090 [0903.4010].

[92] R. Ding and Y. Liao, *Spin 3/2 Particle as a Dark Matter Candidate: an Effective Field Theory Approach*, *JHEP* **04** (2012) 054 [1201.0506].

[93] M. O. Khojali, A. Goyal, M. Kumar and A. S. Cornell, *Minimal Spin-3/2 Dark Matter in a simple s-channel model*, *Eur. Phys. J.* **C77** (2017), no. 1 25 [1608.08958].

[94] M. O. Khojali, A. Goyal, M. Kumar and A. S. Cornell, *Spin-3/2 Dark Matter in a simple t-channel model*, *Eur. Phys. J.* **C78** (2018), no. 11 920 [1705.05149].

[95] M. Asorey and D. García-Álvarez, *Higher spin dark matter*, *AIP Conf. Proc.* **1241** (2010), no. 1 1192–1197.

[96] S. Weinberg, *Baryon and Lepton Nonconserving Processes*, *Phys. Rev. Lett.* **43** (1979) 1566–1570.

[97] J. Hisano, K. Ishiwata, N. Nagata and T. Takesako, *Direct Detection of Electroweak-Interacting Dark Matter*, *JHEP* **07** (2011) 005 [1104.0228].

[98] R. Essig, *Direct Detection of Non-Chiral Dark Matter*, *Phys. Rev. D* **78** (2008) 015004 [0710.1668].

[99] A. DiFranzo, K. I. Nagao, A. Rajaraman and T. M. P. Tait, *Simplified Models for Dark Matter Interacting with Quarks*, *JHEP* **11** (2013) 014 [1308.2679]. [Erratum: JHEP01,162(2014)].

[100] M. R. Buckley, D. Feld and D. Goncalves, *Scalar Simplified Models for Dark Matter*, *Phys. Rev. D* **91** (2015) 015017 [1410.6497].

[101] S. Baek, P. Ko, M. Park, W.-I. Park and C. Yu, *Beyond the Dark matter effective field theory and a simplified model approach at colliders*, *Phys. Lett.* **B756** (2016) 289–294 [1506.06556].

[102] M. Bauer, U. Haisch and F. Kahlhoefer, *Simplified dark matter models with two Higgs doublets: I. Pseudoscalar mediators*, *JHEP* **05** (2017) 138 [1701.07427].

[103] J. March-Russell, S. M. West, D. Cumberbatch and D. Hooper, *Heavy Dark Matter Through the Higgs Portal*, *JHEP* **07** (2008) 058 [0801.3440].

[104] L. Lopez-Honorez, T. Schwetz and J. Zupan, *Higgs portal, fermionic dark matter, and a Standard Model like Higgs at 125 GeV*, *Phys. Lett.* **B716** (2012) 179–185 [1203.2064].

[105] G. Arcadi, A. Djouadi and M. Raidal, *Dark Matter through the Higgs portal*, *Phys. Rept.* **842** (2020) 1–180 [1903.03616].

[106] M. Magg and C. Wetterich, *Neutrino Mass Problem and Gauge Hierarchy*, *Phys. Lett.* **94B** (1980) 61–64.

[107] T. P. Cheng and L.-F. Li, *Neutrino Masses, Mixings and Oscillations in SU(2) x U(1) Models of Electroweak Interactions*, *Phys. Rev.* **D22** (1980) 2860.

[108] G. Lazarides, Q. Shafi and C. Wetterich, *Proton Lifetime and Fermion Masses in an SO(10) Model*, *Nucl. Phys.* **B181** (1981) 287–300.

[109] C.-H. Chen and T. Nomura, *Inert Dark Matter in Type-II Seesaw*, *JHEP* **09** (2014) 120 [1404.2996].

[110] A. Biswas and A. Shaw, *Explaining Dark Matter and Neutrino Mass in the light of TYPE-II Seesaw Model*, *JCAP* **1802** (2018), no. 02 029 [1709.01099]. [Erratum: JCAP1907,E01(2019)].

[111] P.-H. Gu, *Double type II seesaw mechanism accompanied by Dirac fermionic dark matter*, *Phys. Rev.* **D101** (2020), no. 1 015006 [1907.10019].

[112] R. A. Lineros and M. Pierre, *Dark Matter candidates in a Type-II radiative neutrino mass model*, 2011.08195.

[113] M. Gustafsson, J. M. No and M. A. Rivera, *Predictive Model for Radiatively Induced Neutrino Masses and Mixings with Dark Matter*, *Phys. Rev. Lett.* **110** (2013), no. 21 211802 [1212.4806]. [Erratum: Phys. Rev. Lett.112,no.25,259902(2014)].

[114] O. Buchmueller, S. A. Malik, C. McCabe and B. Penning, *Constraining Dark Matter Interactions with Pseudoscalar and Scalar Mediators Using Collider Searches for Multijets plus Missing Transverse Energy*, *Phys. Rev. Lett.* **115** (2015), no. 18 181802 [1505.07826].

[115] N. F. Bell, G. Busoni and I. W. Sanderson, *Self-consistent Dark Matter Simplified Models with an s-channel scalar mediator*, *JCAP* **1703** (2017) 015 [1612.03475].

[116] A. Belyaev, G. Cacciapaglia and D. Locke, *Minimal consistent dark matter models for collider an direct detection characterisation: scalar dark matter*, *paper in progress* (2020).

[117] D. A. Ross and M. J. G. Veltman, *Neutral Currents in Neutrino Experiments*, *Nucl. Phys.* **B95** (1975) 135–147.

[118] **Particle Data Group** Collaboration, J. Beringer *et. al.*, *Review of Particle Physics (RPP)*, *Phys. Rev.* **D86** (2012) 010001.

[119] J. Hisano and K. Tsumura, *Higgs boson mixes with an SU(2) septet representation*, *Phys. Rev.* **D87** (2013) 053004 [1301.6455].

[120] H. Georgi and M. Machacek, *DOUBLY CHARGED HIGGS BOSONS*, *Nucl. Phys.* **B262** (1985) 463–477.

[121] M. Garny, A. Ibarra, S. Rydbeck and S. Vogl, *Majorana Dark Matter with a Coloured Mediator: Collider vs Direct and Indirect Searches*, *JHEP* **06** (2014) 169 [1403.4634].

[122] K. Fukushima, C. Kelso, J. Kumar, P. Sandick and T. Yamamoto, *MSSM dark matter and a light slepton sector: The incredible bulk*, *Phys. Rev. D* **90** (2014), no. 9 095007 [1406.4903].

[123] **NA64** Collaboration, D. Banerjee *et. al.*, *Search for vector mediator of Dark Matter production in invisible decay mode*, *Phys. Rev. D* **97** (2018), no. 7 072002 [1710.00971].

[124] E. Bagnaschi *et. al.*, *Global Analysis of Dark Matter Simplified Models with Leptophobic Spin-One Mediators using MasterCode*, *Eur. Phys. J. C* **79** (2019), no. 11 895 [1905.00892].

[125] B. D. Sáez, F. Rojas-Abatte and A. R. Zerwekh, *Dark Matter from a Vector Field in the Fundamental Representation of $SU(2)_L$*, *Phys. Rev. D* **99** (2019), no. 7 075026 [1810.06375].

[126] A. Belyaev, G. Cacciapaglia, J. Mckay, D. Marin and A. R. Zerwekh, *Minimal Spin-one Isotriplet Dark Matter*, *Phys. Rev. D* **99** (2019), no. 11 115003 [1808.10464].

[127] T. Hahn, *Automatic loop calculations with FeynArts, FormCalc, and LoopTools*, *Nucl. Phys. Proc. Suppl.* **89** (2000) 231–236 [hep-ph/0005029].

[128] G. Bélanger, F. Boudjema, A. Pukhov and A. Semenov, *micrOMEGAs4.1: two dark matter candidates*, *Comput. Phys. Commun.* **192** (2015) 322–329 [1407.6129].

[129] **XENON** Collaboration, E. Aprile *et. al.*, *First Dark Matter Search Results from the XENON1T Experiment*, *Phys. Rev. Lett.* **119** (2017), no. 18 181301 [1705.06655].

[130] **XENON** Collaboration, E. Aprile *et. al.*, *Dark Matter Search Results from a One Ton-Year Exposure of XENON1T*, *Phys. Rev. Lett.* **121** (2018), no. 11 111302 [1805.12562].

[131] **ATLAS** Collaboration, *Combination of searches for invisible Higgs boson decays with the ATLAS experiment*, .

[132] **ATLAS, CMS** Collaboration, ATLAS and C. Collaborations, *Report on the Physics at the HL-LHC and Perspectives for the HE-LHC*, in *HL/HE-LHC Physics Workshop: final jamboree Geneva, CERN, March 1, 2019*, 2019. 1902.10229.

[133] D. M. Asner *et. al.*, *ILC Higgs White Paper*, in *Proceedings, 2013 Community Summer Study on the Future of U.S. Particle Physics: Snowmass on the Mississippi (CSS2013): Minneapolis, MN, USA, July 29-August 6, 2013*, 2013. 1310.0763.

[134] H. Abramowicz *et. al.*, *The International Linear Collider Technical Design Report - Volume 4: Detectors*, 1306.6329.

[135] G. Jungman, M. Kamionkowski and K. Griest, *Supersymmetric dark matter*, *Phys. Rept.* **267** (1996) 195–373 [hep-ph/9506380].

[136] U. Ellwanger, C. Hugonie and A. M. Teixeira, *The Next-to-Minimal Supersymmetric Standard Model*, *Phys. Rept.* **496** (2010) 1–77 [0910.1785].

[137] G. Giudice and A. Romanino, *Split supersymmetry*, *Nucl. Phys. B* **699** (2004) 65–89 [hep-ph/0406088]. [Erratum: Nucl.Phys.B 706, 487–487 (2005)].

[138] M. Pospelov, A. Ritz and M. B. Voloshin, *Secluded WIMP Dark Matter*, *Phys. Lett. B* **662** (2008) 53–61 [0711.4866].

[139] S. Dodelson and L. M. Widrow, *Sterile-neutrinos as dark matter*, *Phys. Rev. Lett.* **72** (1994) 17–20 [hep-ph/9303287].

[140] J. E. Kim and G. Carosi, *Axions and the Strong CP Problem*, *Rev. Mod. Phys.* **82** (2010) 557–602 [0807.3125]. [Erratum: Rev.Mod.Phys. 91, 049902 (2019)].

[141] H.-C. Cheng, J. L. Feng and K. T. Matchev, *Kaluza-Klein dark matter*, *Phys. Rev. Lett.* **89** (2002) 211301 [hep-ph/0207125].

[142] D. Hooper and S. Profumo, *Dark Matter and Collider Phenomenology of Universal Extra Dimensions*, *Phys. Rept.* **453** (2007) 29–115 [hep-ph/0701197].

[143] C. Boehm and P. Fayet, *Scalar dark matter candidates*, *Nucl. Phys. B* **683** (2004) 219–263 [hep-ph/0305261].

[144] G. Branco, P. Ferreira, L. Lavoura, M. Rebelo, M. Sher and J. P. Silva, *Theory and phenomenology of two-Higgs-doublet models*, *Phys. Rept.* **516** (2012) 1–102 [1106.0034].

[145] A. Belyaev, G. Cacciapaglia, I. P. Ivanov, F. Rojas-Abatte and M. Thomas, *Anatomy of the Inert Two Higgs Doublet Model in the light of the LHC and non-LHC Dark Matter Searches*, *Phys. Rev.* **D97** (2018), no. 3 035011 [1612.00511].

[146] A. Belyaev, L. Panizzi, A. Pukhov and M. Thomas, *Dark Matter characterization at the LHC in the Effective Field Theory approach*, 1610.07545.

[147] M. Asano, T. Saito, T. Suehara, K. Fujii, R. S. Hundi, H. Itoh, S. Matsumoto, N. Okada, Y. Takubo and H. Yamamoto, *Discrimination of New Physics Models with the International Linear Collider*, *Phys. Rev.* **D84** (2011) 115003 [1106.1932].

[148] **CMS** Collaboration, A. M. Sirunyan *et. al.*, *Search for new physics in final states with an energetic jet or a hadronically decaying W or Z boson and transverse momentum imbalance at* $\sqrt{s} = 13$ TeV, *Phys. Rev.* **D97** (2018), no. 9 092005 [1712.02345].

[149] **ATLAS** Collaboration, M. Aaboud *et. al.*, *Search for dark matter and other new phenomena in events with an energetic jet and large missing transverse momentum using the ATLAS detector*, *JHEP* **01** (2018) 126 [1711.03301].

[150] **CMS** Collaboration, A. M. Sirunyan *et. al.*, *Search for dark matter produced with an energetic jet or a hadronically decaying W or Z boson at* $\sqrt{s} = 13$ *TeV*, *JHEP* **07** (2017) 014 [1703.01651].

[151] **CMS** Collaboration, A. M. Sirunyan *et. al.*, *Search for dark matter and unparticles in events with a Z boson and missing transverse momentum in proton-proton collisions at* $\sqrt{s} = 13$ *TeV*, *JHEP* **03** (2017) 061 [1701.02042]. [Erratum: JHEP09,106(2017)].

[152] **ATLAS** Collaboration, M. Aaboud *et. al.*, *Search for dark matter in events with a hadronically decaying vector boson and missing transverse momentum in pp collisions at $\sqrt{s} = 13$ TeV with the ATLAS detector*, *JHEP* **10** (2018) 180 [1807.11471].

[153] **ATLAS** Collaboration, A. Basalaev, *Search for dark matter particle candidates produced in association with a Z boson in pp collisions at a center-of-mass energy of 13 TeV with the ATLAS detector*, *J. Phys. Conf. Ser.* **934** (2017), no. 1 012024.

[154] **ATLAS** Collaboration, M. Aaboud *et. al.*, *Search for an invisibly decaying Higgs boson or dark matter candidates produced in association with a Z boson in pp collisions at $\sqrt{s} = 13$ TeV with the ATLAS detector*, *Phys. Lett.* **B776** (2018) 318–337 [1708.09624].

[155] **ATLAS** Collaboration, M. Aaboud *et. al.*, *Search for dark matter at $\sqrt{s} = 13$ TeV in final states containing an energetic photon and large missing transverse momentum with the ATLAS detector*, *Eur. Phys. J.* **C77** (2017), no. 6 393 [1704.03848].

[156] **CMS** Collaboration, A. M. Sirunyan *et. al.*, *Search for dark matter produced in association with a Higgs boson decaying to $\gamma\gamma$ or $\tau^+\tau^-$ at $\sqrt{s} = 13$ TeV*, *Submitted to: JHEP* (2018) [1806.04771].

[157] **CMS** Collaboration, A. M. Sirunyan *et. al.*, *Search for associated production of dark matter with a Higgs boson decaying to $b\bar{b}$ or $\gamma\gamma$ at $\sqrt{s} = 13$ TeV*, *JHEP* **10** (2017) 180 [1703.05236].

[158] **ATLAS** Collaboration, T. A. collaboration, *Search for Dark Matter Produced in Association with a Higgs Boson decaying to $b\bar{b}$ at $\sqrt{s} = 13$ TeV with the ATLAS Detector using 79.8 fb^{-1} of proton-proton collision data*, .

[159] **ATLAS** Collaboration, M. Aaboud *et. al.*, *Search for dark matter in association with a Higgs boson decaying to two photons at $\sqrt{s}$ = 13 TeV with the ATLAS detector*, *Phys. Rev.* **D96** (2017), no. 11 112004 [1706.03948].

[160] **ATLAS** Collaboration, G. Aad *et. al.*, *Search for Dark Matter in Events with Missing Transverse Momentum and a Higgs Boson Decaying to Two Photons in pp Collisions at $\sqrt{s} = 8$ TeV with the ATLAS Detector*, *Phys. Rev. Lett.* **115** (2015), no. 13 131801 [1506.01081].

[161] **CMS** Collaboration, A. M. Sirunyan *et. al.*, *Search for dark matter particles produced in association with a top quark pair at $\sqrt{s} = 13$ TeV*, *Submitted to: Phys. Rev. Lett.* (2018) [1807.06522].

[162] **CMS** Collaboration, A. M. Sirunyan *et. al.*, *Search for dark matter in events with energetic, hadronically decaying top quarks and missing transverse momentum at $\sqrt{s} = 13$ TeV*, *JHEP* **06** (2018) 027 [1801.08427].

[163] **ATLAS** Collaboration, M. Aaboud *et. al.*, *Search for dark matter produced in association with bottom or top quarks in $\sqrt{s} = 13$ TeV pp collisions with the ATLAS detector*, *Eur. Phys. J.* **C78** (2018), no. 1 18 [1710.11412].

[164] **CMS** Collaboration, A. M. Sirunyan *et. al.*, *Search for invisible decays of a Higgs boson produced through vector boson fusion in proton-proton collisions at* $\sqrt{s} = 13$ *TeV*, *Phys. Lett. B* **793** (2019) 520–551 [1809.05937].

[165] **ATLAS** Collaboration, M. Aaboud *et. al.*, *Combination of searches for invisible Higgs boson decays with the ATLAS experiment*, *Phys. Rev. Lett.* **122** (2019), no. 23 231801 [1904.05105].

[166] **CMS** Collaboration, A. M. Sirunyan *et. al.*, *Search for narrow and broad dijet resonances in proton-proton collisions at* $\sqrt{s} = 13$ *TeV and constraints on dark matter mediators and other new particles*, 1806.00843.

[167] **CMS** Collaboration, A. M. Sirunyan *et. al.*, *Search for new physics in dijet angular distributions using proton-proton collisions at* $\sqrt{s} = 13$ *TeV and constraints on dark matter and other models*, 1803.08030.

[168] **CMS** Collaboration, A. M. Sirunyan *et. al.*, *Search for dijet resonances in proton–proton collisions at* $\sqrt{s} = 13$ *TeV and constraints on dark matter and other models*, *Phys. Lett.* **B769** (2017) 520–542 [1611.03568]. [Erratum: Phys. Lett.B772,882(2017)].

[169] J. R. Ellis, T. Falk, K. A. Olive and M. Schmitt, *Constraints on neutralino dark matter from LEP-2 and cosmology*, *Phys. Lett. B* **413** (1997) 355–364 [hep-ph/9705444].

[170] **ATLAS** Collaboration, M. Aaboud *et. al.*, *Search for long-lived charginos based on a disappearing-track signature in pp collisions at* $\sqrt{s} = 13$ *TeV with the ATLAS detector*, *JHEP* **06** (2018) 022 [1712.02118].

[171] **CMS** Collaboration, A. M. Sirunyan *et. al.*, *Search for disappearing tracks as a signature of new long-lived particles in proton-proton collisions at* $\sqrt{s} = 13$ *TeV*, *JHEP* **08** (2018) 016 [1804.07321].

[172] **ATLAS** Collaboration, M. Aaboud *et. al.*, *Search for long-lived, massive particles in events with displaced vertices and missing transverse momentum in* $\sqrt{s} = 13$ *TeV* pp *collisions with the ATLAS detector*, *Phys. Rev. D* **97** (2018), no. 5 052012 [1710.04901].

[173] **CMS** Collaboration, A. M. Sirunyan *et. al.*, *Search for long-lived particles with displaced vertices in multijet events in proton-proton collisions at* $\sqrt{s} = 13$ *TeV*, *Phys. Rev. D* **98** (2018), no. 9 092011 [1808.03078].

[174] D. Barducci, A. Belyaev, A. K. M. Bharucha, W. Porod and V. Sanz, *Uncovering Natural Supersymmetry via the interplay between the LHC and Direct Dark Matter Detection*, *JHEP* **07** (2015) 066 [1504.02472].

[175] **GAMBIT** Collaboration, P. Athron *et. al.*, *A global fit of the MSSM with GAMBIT*, *Eur. Phys. J.* **C77** (2017), no. 12 879 [1705.07917].

[176] **GAMBIT** Collaboration, P. Athron *et. al.*, *Combined collider constraints on neutralinos and charginos*, 1809.02097.

[177] N. G. Deshpande and E. Ma, *Pattern of symmetry breaking with two higgs doublets*, *Phys. Rev. D* **18** (Oct, 1978) 2574–2576.

[178] R. Barbieri, L. J. Hall and V. S. Rychkov, *Improved naturalness with a heavy higgs: An alternative road to lhc physics*, arXiv:hep-ph/0603188.

[179] I. F. Ginzburg, K. A. Kanishev, M. Krawczyk and D. Sokolowska, *Evolution of universe to the present inert phase*, arXiv:1009.4593.

[180] M. Gustafsson, S. Rydbeck, L. Lopez-Honorez and E. Lundstrom, *Status of the inert doublet model and the role of multileptons at the lhc*, arXiv:1206.6316.

[181] M. Espírito-Santo, K. Hultqvist, P. Johansson and A. Lipniacka, *Search for neutralino pair production at sqrts from 192 to 208 gev*, .

[182] E. Lundstrom, M. Gustafsson and J. Edsjo, *Inert doublet model and lep ii limits*, arXiv:0810.3924.

[183] M. Aoki, S. Kanemura and H. Yokoya, *Reconstruction of inert doublet scalars at the international linear collider*, arXiv:1303.6191.

[184] E. Ma, *Verifiable radiative seesaw mechanism of neutrino mass and dark matter*, *Phys.Rev.* **D73** (2006) 077301 [hep-ph/0601225].

[185] R. Barbieri, L. J. Hall and V. S. Rychkov, *Improved naturalness with a heavy Higgs: An Alternative road to LHC physics*, *Phys.Rev.* **D74** (2006) 015007 [hep-ph/0603188].

[186] L. Lopez Honorez, E. Nezri, J. F. Oliver and M. H. Tytgat, *The Inert Doublet Model: An Archetype for Dark Matter*, *JCAP* **0702** (2007) 028 [hep-ph/0612275].

[187] C. Arina, F.-S. Ling and M. H. G. Tytgat, *IDM and iDM or The Inert Doublet Model and Inelastic Dark Matter*, *JCAP* **0910** (2009) 018 [0907.0430].

[188] E. Nezri, M. H. G. Tytgat and G. Vertongen, *e+ and anti-p from inert doublet model dark matter*, *JCAP* **0904** (2009) 014 [0901.2556].

[189] X. Miao, S. Su and B. Thomas, *Trilepton Signals in the Inert Doublet Model*, *Phys. Rev.* **D82** (2010) 035009 [1005.0090].

[190] M. Gustafsson, S. Rydbeck, L. Lopez-Honorez and E. Lundstrom, *Status of the Inert Doublet Model and the Role of multileptons at the LHC*, *Phys. Rev.* **D86** (2012) 075019 [1206.6316].

[191] A. Arhrib, R. Benbrik and N. Gaur, $H \to \gamma\gamma$ *in Inert Higgs Doublet Model*, *Phys. Rev.* **D85** (2012) 095021 [1201.2644].

[192] B. Swiezewska and M. Krawczyk, *Diphoton rate in the inert doublet model with a 125 GeV Higgs boson*, *Phys. Rev.* **D88** (2013), no. 3 035019 [1212.4100].

[193] A. Goudelis, B. Herrmann and O. StÃl, *Dark matter in the Inert Doublet Model after the discovery of a Higgs-like boson at the LHC*, *JHEP* **1309** (2013) 106 [1303.3010].

[194] A. Arhrib, Y.-L. S. Tsai, Q. Yuan and T.-C. Yuan, *An Updated Analysis of Inert Higgs Doublet Model in light of the Recent Results from LUX, PLANCK, AMS-02 and LHC*, *JCAP* **1406** (2014) 030 [1310.0358].

[195] M. Krawczyk, D. Sokolowska, P. Swaczyna and B. Swiezewska, *Constraining Inert Dark Matter by $R_{\gamma\gamma}$ and WMAP data*, *JHEP* **09** (2013) 055 [1305.6266].

[196] M. Krawczyk, D. Sokolowska, P. Swaczyna and B. Swiezewska, *Higgs $\to \gamma\gamma$, $Z\gamma$ in the Inert Doublet Model*, *Acta Phys. Polon.* **B44** (2013), no. 11 2163–2170 [1309.7880].

[197] A. Ilnicka, M. Krawczyk and T. Robens, *Inert Doublet Model in light of LHC Run I and astrophysical data*, *Phys. Rev.* **D93** (2016), no. 5 055026 [1508.01671].

[198] M. A. DÃaz, B. Koch and S. Urrutia-Quiroga, *Constraints to Dark Matter from Inert Higgs Doublet Model*, *Adv. High Energy Phys.* **2016** (2016) 8278375 [1511.04429].

[199] K. P. Modak and D. Majumdar, *Confronting Galactic and Extragalactic γ-rays Observed by Fermi-lat With Annihilating Dark Matter in an Inert Higgs Doublet Model*, *Astrophys. J. Suppl.* **219** (2015), no. 2 37 [1502.05682].

[200] F. S. Queiroz and C. E. Yaguna, *The CTA aims at the Inert Doublet Model*, *JCAP* **1602** (2016), no. 02 038 [1511.05967].

[201] C. Garcia-Cely, M. Gustafsson and A. Ibarra, *Probing the Inert Doublet Dark Matter Model with Cherenkov Telescopes*, *JCAP* **1602** (2016), no. 02 043 [1512.02801].

[202] M. Hashemi and S. Najjari, *Observability of Inert Scalars at the LHC*, *Eur. Phys. J.* **C77** (2017), no. 9 592 [1611.07827].

[203] P. Poulose, S. Sahoo and K. Sridhar, *Exploring the Inert Doublet Model through the dijet plus missing transverse energy channel at the LHC*, *Phys. Lett.* **B765** (2017) 300–306 [1604.03045].

[204] A. Alves, D. A. Camargo, A. G. Dias, R. Longas, C. C. Nishi and F. S. Queiroz, *Collider and Dark Matter Searches in the Inert Doublet Model from Peccei-Quinn Symmetry*, *JHEP* **10** (2016) 015 [1606.07086].

[205] A. Datta, N. Ganguly, N. Khan and S. Rakshit, *Exploring collider signatures of the inert Higgs doublet model*, *Phys. Rev.* **D95** (2017), no. 1 015017 [1610.00648].

[206] R. Enberg, P. J. Fox, L. J. Hall, A. Y. Papaioannou and M. Papucci, *LHC and dark matter signals of improved naturalness*, *JHEP* **11** (2007) 014 [0706.0918].

[207] T. Cohen, J. Kearney, A. Pierce and D. Tucker-Smith, *Singlet-Doublet Dark Matter*, *Phys. Rev.* **D85** (2012) 075003 [1109.2604].

[208] M. Drees, H. Dreiner, D. Schmeier, J. Tattersall and J. S. Kim, *CheckMATE: Confronting your Favourite New Physics Model with LHC Data*, *Comput. Phys. Commun.* **187** (2014) 227–265 [1312.2591].

[209] **CMS** Collaboration, C. Collaboration, *Search for electroweak production of charginos and neutralinos in multilepton final states in pp collision data at* $\sqrt{s} = 13$ TeV, .

[210] T. Sjöstrand, S. Ask, J. R. Christiansen, R. Corke, N. Desai, P. Ilten, S. Mrenna, S. Prestel, C. O. Rasmussen and P. Z. Skands, *An Introduction to PYTHIA 8.2*, *Comput. Phys. Commun.* **191** (2015) 159–177 [1410.3012].

[211] **DELPHES 3** Collaboration, J. de Favereau, C. Delaere, P. Demin, A. Giammanco, V. Lemaître, A. Mertens and M. Selvaggi, *DELPHES 3, A modular framework for fast simulation of a generic collider experiment*, *JHEP* **02** (2014) 057 [1307.6346].

[212] **Linear Collider ILD Concept Group -** Collaboration, T. Abe *et. al.*, *The International Large Detector: Letter of Intent*, 1006.3396.

[213] **ECFA/DESY LC Physics Working Group** Collaboration, J. A. Aguilar-Saavedra *et. al.*, *TESLA: The Superconducting electron positron linear collider with an integrated x-ray laser laboratory. Technical design report. Part 3. Physics at an e+ e- linear collider*, hep-ph/0106315.

[214] H. Baer, T. Barklow, K. Fujii, Y. Gao, A. Hoang, S. Kanemura, J. List, H. E. Logan, A. Nomerotski, M. Perelstein, M. E. Peskin, R. Pöschl, J. Reuter, S. Riemann, A. Savoy-Navarro, G. Servant, T. M. P. Tait and J. Yu, *The international linear collider technical design report - volume 2: Physics*, 2013.

[215] Y. Li and A. Nomerotski, *Chargino and neutralino masses at ilc*, 2010.

[216] M. Asano, T. Saito, T. Suehara, K. Fujii, R. S. Hundi, H. Itoh, S. Matsumoto, N. Okada, Y. Takubo and H. Yamamoto, *Discrimination of new physics models with the international linear collider*, arXiv:1106.1932.

[217] G. Moortgat-Pick, *Lhc/ilc interplay in susy searches*, arXiv:0801.2414.

[218] A. Freitas, H. U. Martyn, U. Nauenberg and P. M. Zerwas, *Sleptons: Masses, mixings, couplings*, 2004.

[219] J. A. Conley, H. K. Dreiner and P. Wienemann, *Measuring a light neutralino mass at the ilc: Testing the mssm neutralino cold dark matter model*, arXiv:1012.1035.

[220] **Particle Data Group** Collaboration, C. Patrignani *et. al.*, *Review of Particle Physics*, *Chin. Phys.* **C40** (2016), no. 10 100001.

[221] M. Skrzypek and S. Jadach, *Exact and approximate solutions for the electron nonsinglet structure function in QED*, *Zeitschrift fuer Physik C* **49(4)** (1991) 577–584.

[222] P. Chen, *Differential luminosity under multi - photon beamstrahlung*, *Phys. Rev. D* **46** (1992) 1186–1191.

[223] A. Belyaev, R. Foadi, M. T. Frandsen, M. Jarvinen, F. Sannino and A. Pukhov, *Technicolor Walks at the LHC*, *Phys. Rev. D* **79** (2009) 035006 [0809.0793].

[224] A. Belyaev, M. S. Brown, R. Foadi and M. T. Frandsen, *The Technicolor Higgs in the Light of LHC Data*, *Phys. Rev. D* **90** (2014) 035012 [1309.2097].

[225] A. Belyaev, A. Coupe, M. Frandsen, E. Olaiya and C. Shepherd-Themistocleous, *Walking technicolor in light of Z′ searches at the LHC*, *Phys. Rev. D* **99** (2019), no. 5 055004 [1805.10867].

[226] M. E. Peskin and T. Takeuchi, *A New constraint on a strongly interacting Higgs sector*, *Phys. Rev. Lett.* **65** (1990) 964–967.

[227] B. Holdom, *Raising the Sideways Scale*, *Phys. Rev. D* **24** (1981) 1441.

[228] T. Appelquist and F. Sannino, *The Physical spectrum of conformal SU(N) gauge theories*, *Phys. Rev. D* **59** (1999) 067702 [hep-ph/9806409].

[229] K. Yamawaki, M. Bando and K.-i. Matumoto, *Scale Invariant Technicolor Model and a Technidilaton*, *Phys. Rev. Lett.* **56** (1986) 1335.

[230] M. Bando, K.-i. Matumoto and K. Yamawaki, *TECHNIDILATON*, *Phys. Lett. B* **178** (1986) 308–312.

[231] D. K. Hong, S. D. H. Hsu and F. Sannino, *Composite Higgs from higher representations*, *Phys. Lett. B* **597** (2004) 89–93 [hep-ph/0406200].

[232] D. D. Dietrich, F. Sannino and K. Tuominen, *Light composite Higgs from higher representations versus electroweak precision measurements: Predictions for CERN LHC*, *Phys. Rev. D* **72** (2005) 055001 [hep-ph/0505059].

[233] M. E. Peskin and T. Takeuchi, *New constraint on a strongly interacting higgs sector*, *Phys. Rev. Lett.* **65** (Aug, 1990) 964–967.

[234] J. Gasser and G. R. S. Zarnauskas, *On the pion decay constant*, *Phys. Lett. B* **693** (2010) 122–128 [1008.3479].

[235] T. DeGrand, *Lattice tests of beyond Standard Model dynamics*, *Rev. Mod. Phys.* **88** (2016) 015001 [1510.05018].

[236] C. Pica, *Beyond the Standard Model: Charting Fundamental Interactions via Lattice Simulations*, *PoS* **LATTICE2016** (2016) 015 [1701.07782].

[237] J. M. Maldacena, *The Large N limit of superconformal field theories and supergravity*, *Adv. Theor. Math. Phys.* **2** (1998) 231–252 [hep-th/9711200].

[238] E. Witten, *Anti-de Sitter space and holography*, *Adv. Theor. Math. Phys.* **2** (1998) 253–291 [hep-th/9802150].

[239] S. S. Gubser, I. R. Klebanov and A. M. Polyakov, *Gauge theory correlators from noncritical string theory*, *Phys. Lett. B* **428** (1998) 105–114 [hep-th/9802109].

[240] A. Karch and E. Katz, *Adding flavor to AdS / CFT*, *JHEP* **06** (2002) 043 [hep-th/0205236].

[241] M. Kruczenski, D. Mateos, R. C. Myers and D. J. Winters, *Meson spectroscopy in AdS / CFT with flavor*, *JHEP* **07** (2003) 049 [hep-th/0304032].

[242] J. Babington, J. Erdmenger, N. J. Evans, Z. Guralnik and I. Kirsch, *Chiral symmetry breaking and pions in nonsupersymmetric gauge / gravity duals*, *Phys. Rev. D* **69** (2004) 066007 [hep-th/0306018].

[243] J. Erdmenger, N. Evans, I. Kirsch and E. Threlfall, *Mesons in Gauge/Gravity Duals - A Review*, *Eur. Phys. J. A* **35** (2008) 81–133 [0711.4467].

[244] D. Kutasov, J. Lin and A. Parnachev, *Conformal Phase Transitions at Weak and Strong Coupling*, *Nucl. Phys. B* **858** (2012) 155–195 [1107.2324].

[245] R. Alvares, N. Evans and K.-Y. Kim, *Holography of the Conformal Window*, *Phys. Rev. D* **86** (2012) 026008 [1204.2474].

[246] T. Alho, N. Evans and K. Tuominen, *Dynamic AdS/QCD and the Spectrum of Walking Gauge Theories*, *Phys. Rev. D* **88** (2013) 105016 [1307.4896].

[247] N. Evans and K. Tuominen, *Holographic modelling of a light technidilaton*, *Phys. Rev. D* **87** (2013), no. 8 086003 [1302.4553].

[248] T. Appelquist, P. S. Rodrigues da Silva and F. Sannino, *Enhanced global symmetries and the chiral phase transition*, *Phys. Rev. D* **60** (1999) 116007 [hep-ph/9906555].

[249] M. Bando, T. Kugo, S. Uehara, K. Yamawaki and T. Yanagida, *Is rho Meson a Dynamical Gauge Boson of Hidden Local Symmetry?*, *Phys. Rev. Lett.* **54** (1985) 1215.

[250] M. Bando, T. Kugo and K. Yamawaki, *Nonlinear Realization and Hidden Local Symmetries*, *Phys. Rept.* **164** (1988) 217–314.

[251] R. Casalbuoni, A. Deandrea, S. De Curtis, D. Dominici, R. Gatto and M. Grazzini, *Degenerate BESS model: The Possibility of a low-energy strong electroweak sector*, *Phys. Rev. D* **53** (1996) 5201–5221 [hep-ph/9510431].

[252] **CMS** Collaboration, A. M. Sirunyan *et. al.*, *Search for high-mass resonances in dilepton final states in proton-proton collisions at* $\sqrt{s} = 13$ *TeV*, *JHEP* **06** (2018) 120 [1803.06292].

[253] A. Belyaev, N. D. Christensen and A. Pukhov, *CalcHEP 3.4 for collider physics within and beyond the Standard Model*, *Comput. Phys. Commun.* **184** (2013) 1729–1769 [1207.6082].

[254] A. Semenov, *LanHEP — A package for automatic generation of Feynman rules from the Lagrangian. Version 3.2*, *Comput. Phys. Commun.* **201** (2016) 167–170 [1412.5016].

[255] E. Accomando, A. Belyaev, L. Fedeli, S. F. King and C. Shepherd-Themistocleous, *Z' physics with early LHC data*, *Phys. Rev. D* **83** (2011) 075012 [1010.6058].

[256] M. Jarvinen and E. Kiritsis, *Holographic Models for QCD in the Veneziano Limit*, *JHEP* **03** (2012) 002 [1112.1261].

[257] D. Arean, I. Iatrakis, M. Järvinen and E. Kiritsis, *V-QCD: Spectra, the dilaton and the S-parameter*, *Phys. Lett. B* **720** (2013) 219–223 [1211.6125].

[258] N. Evans, P. Jones and M. Scott, *Soft walls in dynamic AdS/QCD and the technidilaton*, *Phys. Rev. D* **92** (2015), no. 10 106003 [1508.06540].

[259] C. Degrande, C. Duhr, B. Fuks, D. Grellscheid, O. Mattelaer *et. al.*, *UFO - The Universal FeynRules Output*, *Comput.Phys.Commun.* **183** (2012) 1201–1214 [1108.2040].

[260] T. Stelzer and W. Long, *Automatic generation of tree level helicity amplitudes*, *Phys. Commun.* **81** (2004) 357–371 [hep-ph/9401258].

[261] A. Pukhov, *CalcHEP 2.3: MSSM, structure functions, event generation, batchs, and generation of matrix elements for other packages*, hep-ph/0412191.

[262] A. Pukhov *et. al.*, *CompHEP: A package for evaluation of Feynman diagrams and integration over multi-particle phase space. User's manual for version 33*, 1999.

[263] **CompHEP** Collaboration, E. Boos *et. al.*, *CompHEP 4.4: Automatic computations from Lagrangians to events*, *Nucl. Instrum. Meth.* **A534** (2004) 250–259 [hep-ph/0403113].

[264] J. Kublbeck, H. Eck and R. Mertig, *Computeralgebraic generation and calculation of Feynman graphs using FeynArts and FeynCalc*, *Nucl. Phys. Proc. Suppl.* **29A** (1992) 204–208.

[265] T. Hahn, *Generating Feynman diagrams and amplitudes with FeynArts 3*, *Comput. Phys. Commun.* **140** (2001) 418–431 [hep-ph/0012260].

[266] F. Maltoni and T. Stelzer, *MadEvent: Automatic event generation with MadGraph*, *JHEP* **02** (2003) 027 [hep-ph/0208156].

[267] P. de Aquino, W. Link, F. Maltoni, O. Mattelaer and T. Stelzer, *ALOHA: Automatic Libraries Of Helicity Amplitudes for Feynman Diagram Computations*, *Comput.Phys.Commun.* **183** (2012) 2254–2263 [1108.2041].

[268] T. Gleisberg *et. al.*, *SHERPA 1.alpha, a proof-of-concept version*, *JHEP* **02** (2004) 056 [hep-ph/0311263].

[269] T. Gleisberg *et. al.*, *Event generation with SHERPA 1.1*, *JHEP* **02** (2009) 007 [0811.4622].

[270] W. Kilian, T. Ohl and J. Reuter, *WHIZARD: Simulating Multi-Particle Processes at LHC and ILC*, 2007.

[271] A. Semenov, *LanHEP - a package for the automatic generation of Feynman rules in field theory. Version 3.0*, *Comput. Phys. Commun.* **180** (2009) 431–454 [0805.0555].

[272] G. Cullen, N. Greiner, G. Heinrich, G. Luisoni, P. Mastrolia, G. Ossola, T. Reiter and F. Tramontano, *Automated One-Loop Calculations with GoSam*, (2011) [1111.2034].

[273] N. D. Christensen, C. Duhr, B. Fuks, J. Reuter and C. Speckner, *Exploring the golden channel for HEIDI models using an interface between WHIZARD and FeynRules*, 1010.3251.

[274] G. 't Hooft and M. J. G. Veltman, *Scalar One Loop Integrals*, *Nucl. Phys.* **B153** (1979) 365–401.

[275] H. H. Patel, *Package-X: A Mathematica package for the analytic calculation of one-loop integrals*, *Comput. Phys. Commun.* **197** (2015) 276–290 [1503.01469].

[276] G. Passarino and M. Veltman, *One Loop Corrections for e+ e- Annihilation Into mu+ mu- in the Weinberg Model*, *Nucl. Phys. B* **160** (1979) 151–207.

[277] I. F. Ginzburg, *Simple and robust method for search dark matter particles and measuring their properties at ilc in various models of dm*, arXiv:1010.5579.